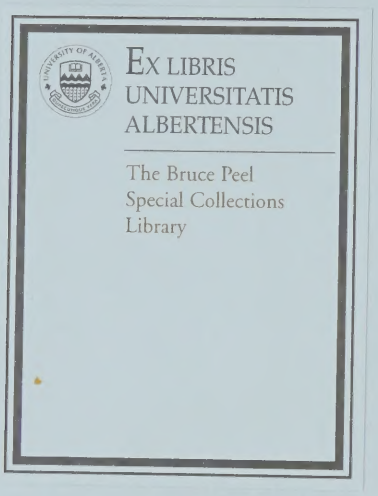
EX LIBRIS
UNIVERSITATIS
ALBERTENSIS
The Bruce Peel
Special Collections
Library

University of Alberta

Library Release Form

Name of Author:	Vyllinniskii Cameron
Title of Thesis:	Prospecting for Microbes: Microbial Imprint in Terrestrial Basalts with Implications in the Search for Past and Present Life on Mars.
Degree:	Master of Science
Year this Degree Granted:	2003

Permission is hereby granted to the University of Alberta Library to reproduce single copies of this thesis and to lend or sell such copies for private, scholarly or scientific research purposes only.

The author reserves all other publication and other rights in association with the copyright in the thesis, and except as herein before provided, neither the thesis nor any substantial portion thereof may be printed or otherwise reproduced in any material form whatever without the author's prior written permission.

Digitized by the Internet Archive
in 2025 with funding from
University of Alberta Library

https://archive.org/details/162017202191

Quote

"A broad and flexible background is the best insurance against premature scientific obsolescence."

Atlas and Bartha, 1998.

University of Alberta

Prospecting for Microbes: Microbial Imprint in Terrestrial Basalts with Implications in the Search for Past and Present Life on Mars.

By

Vyllinniskii Cameron

A thesis submitted to the Faculty of Graduate Studies and Research in partial fulfillment

of the requirements for the degree of Master of Science

Department of Earth and Atmospheric Sciences

Edmonton, Alberta

Spring 2003

University of Alberta

Faculty of Graduate Studies and Research

The undersigned certify that they have read, and recommend to the Faculty of Graduate Studies and Research for acceptance, a thesis entitled **Prospecting for Microbes: Microbial Imprint in Terrestrial Basalts with Implications in the Search for Past and Present Life on Mars** submitted by Vyllinniskii Cameron in partial fulfillment of the requirements for the degree of Master of Science.

Abstract

Examination of two terrestrial desert basalt samples from the San Francisco Volcanic Field in Arizona has been conducted in order to find and document evidence of microbial life. Remnants of organic material are suspected within three channels of a 900,000 year-old pedogenic sample and microorganisms were found inside fractured rock chips of a younger, 900 year-old subaerial sample. Within these chips, rods and cocci morphologies are attached to minerals via substantial amounts of biofilm material. The cells also display various life stages including cell division, lysis and desiccation. Scanning electron microscopy, electron microprobe and confocal microscopy with fluorescence staining were utilized for this task and proved to be effective biosignature tools. Also, a novel technique involving iridium-coated, fluorescence-stained samples was evaluated and shown to work. Results from this study suggest the hot endolithic environment may be a suitable model in the search for life on Mars.

Acknowledgements

This thesis is a representation of not only my research but also the contribution and help of many others. Many thanks to Lang Shi and Sergi Matveev, the individuals who taught me everything I now know about the electron microprobe. Don Resultay and Mark Labbe will forever be in my debt for the numerous times they 'squeezed' in my request to do just one or two thin sections. George Braybrook is the only SEM operator I know but I have no doubt he's the best. This thesis would be severely lacking if it weren't for George's extensive knowledge and capabilities and I will miss the many hours we spent (especially on Friday afternoons!) working with my samples. Michael Fisher and Randy Pakan's help in the Digital Imaging Facility was invaluable.

Thanks also to Dr. L. Paul Knauth of the Department of Geological Science, Arizona State University for sharing his samples, which were used in this research. Much thanks to Neil Banerjee for the friendly advice and words of wisdom.

Most of all, I would like to extend a mountain of thanks and gratitude to my supervisor, Dr. Karlis Muehlenbachs. Karlis gave me the opportunity that all graduate students desire: to explore and find answers unhindered. He was always willing to listen to my questions and concerns, deal with my tantrums and bouts of irritability and pushed me to look outside of that little box which sometimes obscures the view of so many of us up-and-coming young scientists. The many talks, which would have started with a question about my research but would progress to philosophy and life, will be missed. Dr. Muehlenbachs was a remarkable mentor and I will be a better scientist for having known him.

Lastly, I would like to thank Brian, my better half, for his support and encouragement. You kept me smiling through the worst times and you put up with me through the good and the bad. For this and so many other things, you have my eternal thanks.

Table of Contents

Introduction

Overview of Geomicrobiology 1

Thesis Objective 3

Samples **5**

Geologic Setting – The San Francisco Volcanic Field 5

Sample Description 5

Caliche 8

Materials and Analytical Procedures **12**

New Adaptations

Rock Chips 12

Iridium-coated samples 13

Scanning Electron Microscopy (SEM) 13

Electron Microprobe

Methodology 14

Element x-ray mapping 14

Limitations 16

Confocal Microscopy

Methodology 18

Confocal microscopy and fluorescent stains 18

Limitations 20

Novel Technique 20

Results and Discussion **21**

Sample 687 22

Sample 754 32

Chip #1 34

Instrument limitations noted from Chip #1 49

Chip #2 50

Future Work

Geomicrobiology 60

Instrumentation 62

Conclusions **64**

References **66**

Appendix A: Sample 741A **72**

Appendix B: Carbon and oxygen isotope analysis **75**

List of Tables

Table		Page number
1	Major element abundances and probable mineral phases for sample 687.	9
2	Major element abundances and probable mineral phases for sample 754.	10
3	Standards used for major element analysis and element maps.	15
A	Major element abundances and probable mineral phases for sample 741A.	73

List of Figures

Figure		Page Number
1	Map of Arizona showing location of three volcanic fields.	6
2	Schematic cross section of the sampling site.	7
3	Petrological photomicrographs of samples 687 and 754.	11
4	SEM photomicrographs of channel A with associated EDX spectrum.	24
5	SEM photomicrographs of channel F with associated EDX spectrum.	25
6	SEM photomicrographs of channel C with associated EDX spectrum.	26
7	Electron microprobe element x-ray maps for channel A.	27
8	Electron microprobe element x-ray maps for channel F.	28 & 29
9	Electron microprobe element x-ray maps for channel C.	30
10	Fluorescence-stained, confocal images of channels A, F and C.	33
11	SEM photomicrographs of cocci, rods, tracks and biofilms in rock chip #1.	35
12	SEM photomicrograph and associated EDX spectrum of the cryptocrystalline material.	36
13	SEM images showing some characteristic features of a biofilm in chip #1: attached cells, layering, cavities and EPS.	39
14	SEM images of the primary vesicle on chip #1 containing minerals C, E, F and G.	40
15	Electron microprobe element x-ray maps for mineral C.	41 & 42
16	Electron microprobe element x-ray maps for mineral E.	43 & 44
17	SEM photomicrographs of minerals C and E after undergoing element x-ray mapping.	46
18	SEM images of corresponding fluorescing sites, cells-#1 and cells-#2, on mineral G.	47

19	Confocal fluorescence-stained photomicrographs showing cells-#1 and cells-#2 sites on mineral G.	48
20	SEM overview of rock chip #2 with 'A' and 'B' sites where microbes were found.	51
21	Magnified SEM images of sites 'A' and 'B'.	52
22	SEM images of cells occupying spaces between minerals	53
23	SEM photomicrographs of dividing rods and cocci attached to mineral surfaces in chip #2.	54
24	SEM images of a colony of dividing rods and cocci in chip #2.	55
25	SEM photomicrographs of a tunnel feature possibly produced by microorganisms.	57
26	Confocal fluorescence-stained images of dividing cells from site 'A'.	58
27	Magnified confocal fluorescence-stained images of dividing cells from site 'A'.	59
28	Confocal fluorescence-stained images of microorganisms in another area of site 'A'.	61
A	SEM images of globular features within vesicles of a thin section of sample 741A.	74
B	Plot of carbon and oxygen isotope analysis of caliche from various SFVF desert samples and sample 754.	76

Glossary of Abbreviations

Å	Angstrom (10^{-10} m)
ATP	adenosine triphosphate
°C	degrees Celcius
cm	centimeter
CP	composition or backscatter map
CRB	Columbia River Basalt
DAPI	4',6-diamidino-2-phenylindole
EDS	Energy Dispersive Spectrometry
EDX	Energy Dispersive X-ray
EPS	extracellular polymeric substances
g	gram
hr	hour
km	kilometer
kV	kilovolts
LSCM	Laser Scanning Confocal Microscope
m	meter
M	Molarity
Ma	Mega anos (10^6 years)
min	minute
ml	milliliter
mm	millimeter
nm	nanometer (10^{-9} m)
PDB	Pee Dee Belemnite
PI	propidium iodide
sec	second
SEM	Scanning Electron Microscope
SFVF	San Francisco Volcanic Field
SLiME	Subsurface Lithoautotrophic Microbial Ecosystem
SMOW	Standard Mean Ocean Water

TES	Thermal Emission Spectrometer
TP	topography map
μg	microgram (10^{-6} g)
μm	micrometer (10^{-6} m)
wt.%	weight percent
WDS	Wavelength Dispersive Spectrometry
y	year
Z	atomic number

Introduction

Overview of Geomicrobiology:

More than three hundred years have passed since Antonie van Leeuwenhoek created the microscope and first looked at the world of microorganisms. One would think then, that our understanding of the variety and complexity of microbes and their effect and contributions to the biosphere would be substantial. However, in my humble opinion, this does not seem to be the case and in fact, only 1-10% of all existing microbial species are known (Atlas and Bartha, 1998a). It is true that many advances have been made in microbiology but most have been for the benefit of humans, to accommodate their needs or to fix the problems they have created: medicine, agriculture, food preservation and biodegradation of synthetic pollutants, to name a few. As such, much of the work has been relegated to a few specific and easily cultured organisms, such as *Escherichia coli*. Of growing importance are studies of the evolutionary relationships among microorganisms and their interaction with the inorganic world in which they exist. Microbes have been found - thriving in many cases - in virtually every environment on Earth, including extreme environments where conditions such as high and low temperatures, high pressure, salinity and acidity were once thought too hostile to support even microbial life (Stetter, 1999).

The multi-disciplinary field of geomicrobiology examines the involvement of microbes in past and present geological processes. It began in the early 1800's with important contributions by scientists such as Ehrenberg, Winogradsky, Beijerinck, Harder, Waksman, Zobell, Muentz and Merrill (Ehrlich, 1990a). Since then, significant and important discoveries have been made concerning novel varieties of microbes, their habitats and the types of processes they carry out, in both terrestrial and marine settings. In the marine environment, recently discovered organisms living in the vicinity of deep ocean hydrothermal vents (black smoker communities) and those occupying seafloor sediments have become the subjects of a variety of studies (e.g. Summit and Baross, 1998; Holden et al., 1998; Delaney, 1998; Baross, 1998; D'Hondt et al., 2000). Even more remarkable and perhaps, just as promising a habitat for life, is the ocean crust. Weathering of ocean crust was thought to be a result of abiogenic, chemical and physical

processes. However, recent studies show microorganisms, possibly hyperthermophilic Archaea, carrying out biogenic alteration of 6 and 110 Ma volcanic glasses (e.g. Thorseth et al., 1995; Torsvik et al., 1998; Fisk et al., 1998; Furnes and Staudigel, 1999; Furnes et al., 2001a). One of the main components of basalt in oceanic crust, volcanic glass is chemically unstable in water and its alteration thus leads to important and significant geochemical fluxes between oceanic crust and seawater (Staudigel et al., 1998). It is estimated that this bioalteration occurs to about 550m in the crust and may be ongoing at present. The same collaborators have also presented evidence that suggests bioalteration has been preserved in metamorphosed and deformed, Ordovician age ophiolites (H. Furnes et al., Bio-signatures in metabasaltic glass of a Caledonian ophiolite, West Norway, submitted to *Journal of the Geological Society, London*, 2001).

In the terrestrial environment, microbes are found inhabiting many places. Soils of course, contain the greatest concentration and assortment of microbial life (10^5-10^8 per gram), with lakes and streams containing smaller numbers (10^2-10^6 per gram) but similar diversity of organisms. Groundwaters from the vadose zone and shallow aquifers may have as many as 10^6 bacteria per gram but generally lacks eukaryotic microbes as depth increases (Ehrlich, 1990b). Hot springs offer a dynamic array of 'nutrients' and geochemical conditions to which a plethora of thermophilic Bacteria and Archaea have adapted. Many are novel lineages but nonetheless, it is estimated that this is a small percentage of the amount of microbial diversity yet to be found in such high temperature environments (Reysenbach and Shock, 2002). Two other terrestrial settings with a direct bearing on this thesis are deep subsurface ecosystems and cold and hot deserts. Both involve microbes living within the lithic environment.

Interest in deep subsurface microorganisms was originally focused on the microbiology of petroleum deposits. Subsequent searches eventually found a multitude of other subsurface microbes, living at depths to 2.8 km below the surface. Theoretically, this limit could extend to 4 km since temperatures increase by about 25°C per kilometer (Fredrickson and Onstott, 1996) and the upper temperature limit for life, at present, is 113°C. For many of these microorganisms, important nutrients such as organic carbon are obtained from buried sediments. Therefore, most subsurface microbes are indirectly dependent on photosynthesis to acquire energy. This was the general belief until

SLiMEs, subsurface lithoautotrophic microbial ecosystems, were discovered by Stevens and McKinley (1995). These researchers found the first SLiME within deep aquifers of the Columbia River Basalt Group (CRB), which consisted primarily of autotrophic bacteria that synthesized organic compounds using hydrogen (H_2) produced from the abiogenic reaction of anaerobic groundwaters and iron minerals in the basalt. Other researchers (Pedersen et al., 1997; Chapelle et al., 2002) have since found similar subsurface lithoautotrophic communities. All subsurface ecosystems have one thing in common: they are intimately tied to an aquifer or have routine access to groundwater flow. Endolithic communities in hot and cold desert environments do not have this luxury. Microbes living inside the rocks of the Antarctic dry valleys or the Sonoran desert for example, endure a variety of harsh conditions: limited water availability, low humidity, extreme temperatures including large fluctuations in daily temperatures and possibly high levels of solar radiation. These extreme conditions in turn, accounts for the distinctive difference in the type of microbial flora found in hot and cold deserts. The interior of rocks in hot deserts contain only prokaryotic organisms, whereas eukaryotes predominate in cold deserts (Friedmann, 1980).

Thesis Objective:

The goal of this study is to search for evidence of biogenicity in two samples of young terrestrial basalts from an arid volcanic field in Arizona; in essence, a hot desert environment. The thesis will expand on and add to ongoing work so far accomplished in the field of geomicrobiology and life in extreme environments. Its importance to this area of research cannot be overstated given continued discoveries of new, previously unknown organisms like nanosized hyperthermophilic Archaea (Huber et al., 2002) and current controversies, for example questions of biogenicity regarding Earth's oldest fossils (Fedo and Whitehouse, 2002; Brasier et al., 2002; Schopf et al., 2002) or the type of process involved in sustaining life within subsurface lithotrophic microbial communities (Anderson et al., 1998), all of which until recently, had been accepted by the majority in the scientific community as being generally conclusive. Relatively few investigations have been made of microbial life in the rocks of desert regions and this is especially true for the hot desert areas.

Another important goal and primary application of the work in this thesis is the search for life or evidence of past life on Mars. The basaltic samples obtained for this study contain caliche, which is not investigated here but which shows evidence of calcite biomineralization. Knauth et al. (in review, 2002) are in the process of studying the caliche layer in these same samples and others with three objectives in mind: understanding the process and environment of caliche formation, particularly from a biogenic perspective; assessing whether caliche formed on Mars and hence, the possibility that microbial life was once present, especially given that the same conditions required for the formation of caliche on Earth may have once existed on Mars; and, as a result of the first two points, evaluating the prospect of searching for early life in the Precambrian and on Mars. Dust storms and wind abrasion processes are prominent on Mars so the existence of caliche is, at this time, questionable. However, thermal emission spectrometer (TES) data obtained by the Mars Global Surveyor spacecraft presently orbiting Mars indicate basalts are one of the most common rock types on the planet's surface (Mittlefehldt, 2000). This fact coupled to the results shown from previously mentioned studies involving biogenicity and basalts, as well as the promising results of this work and the similarity of environments of the basalt samples and present-day Mars, suggests basalts from Mars might be the ideal candidates in the search for evidence of extraterrestrial microbial life.

Previous and ongoing studies show that thus far, no single geochemical technique is considered, *a priori*, a biogenic indicator. The determination of biogenicity in geological materials, young or old, consequently relies on the application of multiple tools, several of which are employed here. In addition, a new technique not previously utilized by past or current researchers is described. The interaction of microorganisms with igneous materials is a fairly novel area of research that may have major implications for studies involving the origin and mechanism of early life on Earth, determination of biosignatures in terrestrial and extraterrestrial geological materials and the search for life on other planets, such as Mars.

Samples

Samples were provided by Dr. L. Paul Knauth of the Department of Geological Science, Arizona State University. Dr. Knauth and colleagues are currently examining the caliche layer of a suite of basaltic samples from three separate volcanic fields in Arizona (Figure 1).

Geologic Setting – The San Francisco Volcanic Field

Three samples from the San Francisco Volcanic Field (SFVF) were obtained for this study but only two were used and information about the third is contained in Appendix A. The SFVF covers approximately 5000 km^2 in the transition zone between the Colorado Plateau and the Basin and Range Province. The field was created during the last 5 Ma and recent activity within it occurred about 900-750 years ago (Arculus and Gust, 1995). The SFVF is representative of intracontinental volcanism, where basaltic magmas from the mantle travels through the continental crust, ponding and subsequently interacting with the surrounding country rocks. In contrast to the bimodal (basalt and rhyolite) lavas produced in most intracontinental systems, the SFVF displays a spectrum of variable compositions and a substantial quantity of andesite. Rock types include alkali and tholeiitic basalts; high-K andesites, dacites and rhyolites; silicic trachytes and high-Na andesites and dacites. Crustal melting, assimilation and magma mixing, coupled to the source of basalt and location of ponding, and density differences between the basalt, fractionated basalt and continental rocks possibly accounts for the silicic and andesitic lavas. Fractional crystallization is also an important process but it is generally agreed that on a field-wide basis, no single petrogenic model is applicable (Bloomfield, 1990; Arculus and Gust, 1995).

Sample Description

The two samples used in this study are identified as samples 687 and 754 and the general sampling sites are shown in Figure 2. Both are Pleistocene in age. Sample 687 is ~ 900,000 years old (American stage "Woodhouse": 800,000-2 Ma) and was taken from a roadcut. It is a pedogenic (subsurface) sample from the underside of a vug in highly

Figure 1: Map of Arizona State showing the location of three basalt volcanic fields (Uinkaret & Vulcan's Throne, San Francisco and Sentinal) from which samples were collected. Map modified from Knauth et al., in review (2002).

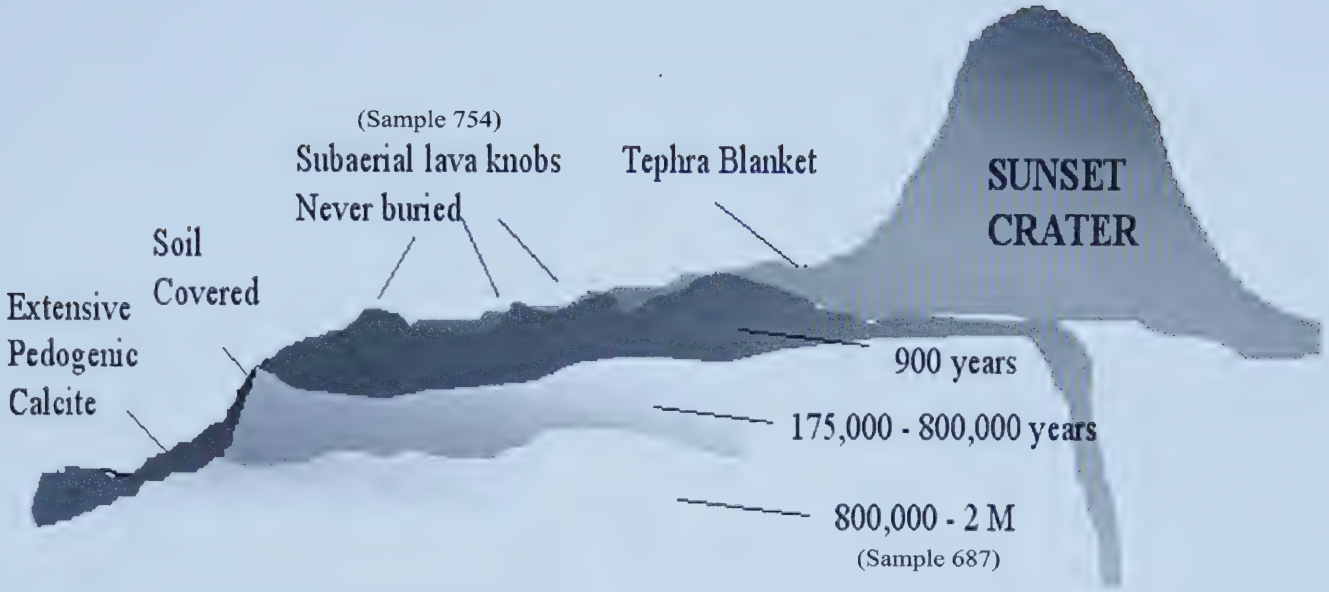

Figure 2: Schematic cross section running northeast from Sunset Crater cinder cone. The Kanana lava flow emerges from the base of Sunset Crater and flows over older lava flows from other vent areas. Pinnacles, above tephra covering the Kanana flow, were sampled. Map modified from Knauth et al., in review (2002).

weathered basalt and is believed to have developed primarily in a soil environment. Sample 754 is 900 years old (American stage "Sunset") and was found on the underside of a fracture on a large, exposed flow knob known as the Kanana lava flow. The knob is subaerial; it has never been buried by soil and has been in contact with air for its entire history. All samples are originally from large hand samples that were physically quarried out and from which, smaller pieces were broken off and given to Dr. Karlis Muehlenbachs (L. P. Knauth, Arizona State University, personal communication, 2002). These pieces, weighing approximately 150 – 500g, were subsequently passed on to me.

The older basalt sample (687) is overlain by a thick carbonate caliche layer which, on the younger sample, is not developed and therefore, noticeably absent. Both basalt samples are highly porphyritic and have relatively the same mineral phases (Table 1 & 2). Primary phenocrysts are olivine, plagioclase and orthopyroxene, up to 30 mm in size. These same phases occur in the groundmass, which also includes abundant magnetite (many of which are titaniferous) and lesser amounts of ilmenite, spinel and glass. Olivine is the dominant phase with a modal abundance of approximately 35-40%. Xenocrysts of quartz and possibly garnet were found. Some pyroxenes have cooling rims, inclusions of spinel and in general, do not appear to be much altered. Iddingsite alteration and color zonation is seen in the vast majority of olivine crystals and cooling rims are absent. Carlsbad twinning and oscillatory zonation is commonly observed in plagioclase. In sample 754, most phenocrysts are euhedral and textures, such as arrowhead stacks of magnetite, indicate a rapid rate of cooling (Arculus and Gust, 1995). Vesicles are also prominent in this sample. The majority of crystals within sample 687 appear weathered and most are sub- to anhedral. Carbonate veins are common in sample 687 but absent in sample 754 and vesicles are rare. Some of the petrological characteristics of the samples are shown in Figure 3.

Caliche

Caliche, also known as calcrete, is typically precipitated calcium carbonate in the lower soil horizons of arid and semi-arid regions. The deposited layers are classified as calcic or petrocalcic depending on the level of induration. Calcic layers are more than 1.5 cm thick and contain greater than 15 and 5 wt.% calcium carbonate in the layer and

Table 1: Major element abundances (wt. %) and probable mineral phases for sample 687

No.	Na_2O	SiO_2	SO_3	FeO	MgO	Al_2O_3	K_2O	MnO	P_2O_5	Cr_2O_3	CaO	TiO_2		Mineral Phase
1	2.617	39.497	0.026	10.240	12.594	14.794	1.993	0.057	0.033	0.005	10.351	4.474	96.68	amphibole (core)
2	0.002	36.779	0.000	21.819	39.527	0.021	0.019	0.262	0.017	0.018	0.193	0.039	98.70	olivine (core)
3	0.033	37.677	0.000	21.814	39.279	0.020	0.048	0.326	0.109	0.012	0.197	0.019	99.53	olivine (core)
4	0.010	37.328	0.000	21.740	39.324	0.034	0.015	0.310	0.047	0.020	0.239	0.001	99.07	olivine (core)
5	0.019	37.506	0.000	21.767	39.805	0.023	0.009	0.278	0.071	0.022	0.214	0.021	99.74	olivine (core)
6	0.000	37.652	0.000	21.215	39.911	0.048	0.004	0.314	0.211	0.016	0.184	0.017	99.57	olivine (core)
7	0.045	37.714	0.000	21.337	39.832	0.058	0.016	0.287	0.102	0.011	0.174	0.050	99.63	olivine (core)
8	0.026	37.360	0.000	21.549	39.486	0.000	0.025	0.321	0.062	0.035	0.197	0.007	99.07	olivine (core)
9	0.017	37.679	0.000	22.177	39.126	0.000	0.027	0.345	0.050	0.010	0.335	0.008	99.77	olivine (core)
10	0.127	35.460	0.007	36.944	25.943	0.204	0.051	0.748	0.084	0.049	0.678	0.083	100.38	olivine (rim)
11	0.047	36.341	0.000	34.104	28.856	0.231	0.068	0.595	0.035	0.023	0.582	0.077	100.96	olivine (rim)
12	0.055	35.362	0.000	37.506	26.334	0.159	0.039	0.691	0.100	0.038	0.611	0.081	100.98	olivine (rim)
13	0.008	35.608	0.000	33.423	29.535	0.000	0.059	0.567	0.000	0.015	0.588	0.152	99.96	olivine (rim)
14	0.029	35.592	0.000	33.154	29.964	0.000	0.043	0.534	0.000	0.011	0.454	0.080	99.86	olivine (rim)
15	0.032	33.800	0.014	41.808	21.949	0.048	0.069	0.835	0.060	0.023	0.669	0.193	99.50	olivine (rim)
16	4.296	51.604	0.000	0.796	0.089	29.923	0.285	0.000	0.000	0.000	12.753	0.155	99.90	plagioclase
17	4.027	51.114	0.000	0.829	0.087	30.279	0.256	0.000	0.000	0.000	13.157	0.094	99.84	plagioclase
18	4.037	51.390	0.000	0.748	0.079	30.088	0.231	0.000	0.000	0.000	13.180	0.127	99.88	plagioclase
19	5.265	51.903	0.000	1.349	0.078	28.989	0.520	0.000	0.000	0.000	11.952	0.219	100.28	plagioclase
20	4.157	51.536	0.000	0.848	0.072	30.107	0.232	0.000	0.000	0.000	12.934	0.114	100.00	plagioclase
21	4.136	51.377	0.000	0.848	0.039	30.188	0.211	0.000	0.000	0.000	12.969	0.122	99.89	plagioclase
22	4.660	52.543	0.000	0.727	0.071	29.066	0.354	0.000	0.000	0.000	11.996	0.090	99.51	plagioclase
23	4.294	52.190	0.000	0.888	0.067	29.687	0.341	0.003	0.007	0.000	12.616	0.128	100.22	plagioclase
24	4.253	51.937	0.010	0.841	0.072	29.953	0.324	0.000	0.029	0.002	12.938	0.138	100.50	plagioclase
25	3.879	51.099	0.000	0.820	0.103	30.419	0.285	0.000	0.055	0.005	13.784	0.135	100.58	plagioclase
26	15.674	52.195	0.030	1.565	0.116	29.100	2.057	0.000	0.000	0.003	0.388	0.029	101.16	alkali feldspar
27	0.812	44.666	0.017	12.842	9.790	5.838	0.085	0.218	0.139	0.003	21.817	4.499	100.73	glass
28	0.772	44.362	0.036	12.333	10.007	6.114	0.083	0.197	0.145	0.041	22.429	4.678	101.20	glass
29	0.724	44.716	0.032	11.785	10.104	6.409	0.063	0.166	0.130	0.035	22.122	4.131	100.42	glass
30	0.721	45.042	0.042	12.015	10.083	6.197	0.085	0.212	0.087	0.027	21.993	4.402	100.91	glass
31	0.748	44.849	0.042	11.727	10.269	6.342	0.074	0.159	0.164	0.038	22.367	4.318	101.10	glass
32	0.675	44.670	0.024	11.358	10.180	6.750	0.062	0.169	0.121	0.057	22.448	4.100	100.61	glass
33	0.764	45.478	0.000	12.729	9.968	5.433	0.064	0.228	0.050	0.000	21.733	4.064	100.51	glass
34	0.793	42.439	0.000	12.663	9.400	7.393	0.044	0.178	0.082	0.006	21.840	4.997	99.84	glass
35	0.047	0.751	0.031	70.542	1.497	2.247	0.146	0.763	0.054	0.494	0.246	24.774	101.59	ilmenite/magnetite
36	0.101	0.719	0.019	68.142	1.285	1.976	0.164	0.802	0.039	0.087	0.251	27.000	100.59	ilmenite/magnetite
37	0.017	0.786	0.051	72.522	1.407	1.927	0.171	0.764	0.058	0.239	0.275	23.810	102.03	ilmenite/magnetite
38	0.145	0.689	0.041	66.834	1.534	1.739	0.151	0.885	0.040	0.086	0.282	25.661	98.09	ilmenite/magnetite
39	0.085	0.699	0.043	69.262	1.897	2.739	0.137	0.672	0.067	2.574	0.274	22.302	100.75	ilmenite/magnetite
40	0.112	0.758	0.033	70.715	2.007	2.284	0.142	0.679	0.048	0.328	0.399	24.088	101.59	ilmenite/magnetite
41	0.000	0.000	0.057	0.048	0.851	0.000	0.028	0.000	0.056	0.000	65.683	0.000	66.72	calcium carbonate
42	0.000	0.000	0.040	0.017	1.055	0.000	0.000	0.000	0.052	0.000	62.587	0.000	63.75	calcium carbonate
43	0.000	0.000	0.032	0.050	0.969	0.000	0.000	0.000	0.043	0.021	62.441	0.027	63.58	calcium carbonate
44	0.011	0.000	0.018	0.064	0.792	0.000	0.037	0.000	0.058	0.016	64.542	0.027	65.57	calcium carbonate
45	0.036	0.000	0.023	0.054	0.946	0.000	0.009	0.000	0.062	0.011	59.709	0.001	60.85	calcium carbonate
46	0.009	0.000	0.024	0.054	1.089	0.000	0.016	0.000	0.099	0.016	65.440	0.046	66.79	calcium carbonate
47	0.000	0.000	0.024	0.097	1.039	0.000	0.000	0.011	0.097	0.014	63.914	0.019	65.22	calcium carbonate

Table 2: Major element abundances (wt. %) and probable mineral phases for sample 754

No.	Na_2O	SiO_2	SO_3	FeO	MgO	Al_2O_3	K_2O	MnO	P_2O_5	Cr_2O_3	CaO	TiO_2	Total	Mineral Phase
48	0.021	38.759	0.000	16.240	44.300	0.000	0.037	0.202	0.048	0.066	0.113	0.076	99.86	opx (core)
49	0.021	38.042	0.000	16.349	44.129	0.000	0.006	0.205	0.005	0.059	0.140	0.034	98.99	opx (core)
50	0.024	38.792	0.000	16.219	44.028	0.000	0.030	0.191	0.005	0.075	0.117	0.020	99.50	opx (core)
51	0.034	38.821	0.000	16.477	43.951	0.000	0.000	0.219	0.029	0.057	0.122	0.076	99.79	opx (core)
52	0.000	38.904	0.000	16.813	43.866	0.000	0.015	0.206	0.000	0.005	0.132	0.046	99.99	opx (core)
53	0.028	38.590	0.000	16.528	43.735	0.017	0.029	0.214	0.026	0.025	0.183	0.052	99.43	opx (core)
54	0.018	38.673	0.000	16.463	43.962	0.044	0.057	0.217	0.012	0.019	0.209	0.031	99.71	opx (core)
55	0.026	38.512	0.000	16.518	43.824	0.075	0.038	0.228	0.019	0.078	0.206	0.021	99.55	opx (core)
56	0.287	35.192	0.029	39.040	21.623	1.349	0.418	0.798	1.293	0.052	2.172	0.269	102.52	opx (rim)
57	0.021	35.122	0.022	38.340	24.939	0.341	0.097	0.754	0.428	0.038	1.042	0.220	101.36	opx (rim)
58	0.095	34.100	0.041	40.831	22.902	0.416	0.194	0.778	0.141	0.066	0.765	0.839	101.17	opx (rim)
59	0.883	42.958	0.011	13.453	8.614	6.677	0.078	0.220	0.093	0.051	21.861	4.727	99.63	glass (rim)
60	0.061	35.263	0.019	36.684	26.714	0.248	0.093	0.635	0.047	0.033	0.741	0.143	100.68	opx (rim)
61	0.034	0.375	0.025	27.956	14.261	41.035	0.095	0.258	0.018	15.566	0.094	1.025	100.74	spinel series
62	0.706	9.845	0.068	45.619	17.354	17.540	0.260	0.306	0.065	0.784	0.531	10.770	103.85	spinel series
63	0.057	0.026	0.000	28.153	13.704	38.556	0.012	0.218	0.054	18.777	0.022	0.970	100.55	spinel series
64	0.059	0.000	0.000	32.352	12.414	37.888	0.006	0.247	0.011	16.769	0.044	1.199	100.99	spinel series
65	3.862	51.219	0.000	0.713	0.124	30.202	0.084	0.000	0.000	0.000	13.625	0.099	99.93	plagioclase
66	3.559	50.794	0.000	0.745	0.131	30.379	0.082	0.000	0.000	0.000	13.923	0.049	99.66	plagioclase
67	3.156	49.708	0.000	0.767	0.139	31.199	0.060	0.000	0.014	0.000	14.727	0.040	99.81	plagioclase
68	3.196	49.721	0.000	0.836	0.145	31.403	0.042	0.000	0.010	0.000	14.665	0.057	100.08	plagioclase
69	3.266	49.887	0.000	0.743	0.103	31.205	0.045	0.000	0.000	0.000	14.592	0.043	99.88	plagioclase
70	3.324	50.064	0.000	0.701	0.105	31.212	0.026	0.000	0.000	0.000	14.493	0.058	99.98	plagioclase
71	3.325	49.926	0.000	0.805	0.135	31.208	0.028	0.000	0.000	0.000	14.365	0.061	99.85	plagioclase
72	3.387	50.618	0.000	0.897	0.111	31.088	0.134	0.000	0.010	0.000	13.975	0.085	100.31	plagioclase
73	3.513	50.991	0.043	0.940	0.147	31.311	0.204	0.012	0.007	0.000	14.363	0.152	101.68	plagioclase
74	3.352	50.110	0.000	0.936	0.162	31.581	0.155	0.000	0.000	0.008	14.944	0.076	101.32	plagioclase
75	3.207	50.498	0.015	0.861	0.145	31.701	0.166	0.008	0.010	0.008	14.606	0.094	101.32	plagioclase
76	0.738	43.662	0.026	14.368	9.590	7.629	0.093	0.285	0.059	0.058	20.594	4.381	101.48	glass
77	0.359	49.001	0.027	10.102	14.362	4.255	0.044	0.249	0.072	0.193	20.243	1.807	100.71	glass
78	0.563	46.793	0.035	10.283	12.796	6.220	0.066	0.220	0.163	0.302	20.939	2.837	101.22	glass
79	5.588	58.328	0.036	10.442	0.792	15.979	4.445	0.219	0.440	0.012	2.454	0.978	99.71	glass
80	0.666	46.006	0.020	12.612	11.257	6.057	0.070	0.225	0.149	0.060	20.770	3.304	101.20	glass
81	0.650	45.615	0.042	10.678	11.774	6.902	0.049	0.202	0.272	0.206	21.255	3.626	101.27	glass
82	0.611	46.309	0.012	10.938	12.007	6.643	0.084	0.214	0.131	0.110	21.187	3.252	101.50	glass
83	0.612	45.551	0.020	11.780	11.132	6.686	0.030	0.170	0.114	0.025	21.203	3.510	100.83	glass
84	0.563	46.286	0.016	12.456	11.719	5.925	0.030	0.237	0.202	0.056	20.489	2.896	100.88	glass
85	0.461	3.880	0.034	69.605	1.449	2.896	0.386	0.708	0.157	0.086	0.647	21.965	102.27	magnetite
86	0.341	3.765	0.063	69.685	1.442	2.783	0.393	0.722	0.120	0.087	0.663	21.646	101.71	magnetite
87	0.393	3.888	0.050	69.391	1.454	3.200	0.288	0.711	0.124	0.096	0.823	22.423	102.84	magnetite
88	1.721	10.584	0.062	64.679	1.275	4.872	0.921	0.696	0.181	0.070	0.770	20.474	106.31	magnetite
89	0.503	3.575	0.066	68.961	1.677	2.806	0.312	0.746	0.130	0.099	0.930	22.576	102.38	magnetite
90	2.896	16.365	0.072	57.917	1.296	6.722	1.323	0.628	0.095	0.060	0.758	18.755	106.89	magnetite
91	1.026	4.368	0.056	64.600	1.387	2.714	0.421	0.666	2.071	0.082	3.038	21.844	102.27	magnetite
92	1.155	6.268	0.055	68.846	1.359	3.565	0.560	0.738	0.087	0.072	0.608	21.780	105.09	magnetite
93	0.005	37.044	0.032	23.234	38.046	0.000	0.024	0.332	0.123	0.000	0.552	0.078	99.47	opx.
94	0.502	46.288	0.014	10.685	12.885	5.952	0.039	0.202	0.101	0.000	20.353	2.567	99.59	cpx.
95	0.523	45.845	0.035	9.328	12.821	6.324	0.023	0.123	0.234	0.178	21.947	2.354	99.74	cpx.
96	0.585	44.200	0.018	10.548	11.817	6.716	0.036	0.160	0.224	0.046	20.954	3.472	98.78	cpx.
97	0.000	38.340	0.038	18.932	41.965	0.026	0.008	0.255	0.052	0.000	0.325	0.040	99.98	opx.
98	0.008	38.416	0.017	18.484	41.890	0.000	0.009	0.232	0.036	0.000	0.279	0.041	99.41	opx.
99	0.610	44.164	0.022	12.179	10.706	6.629	0.047	0.212	0.213	0.017	20.916	3.610	99.33	cpx.
100	0.003	37.556	0.032	22.559	38.441	0.020	0.032	0.331	0.147	0.014	0.512	0.055	99.70	opx.

Note: opx = orthopyroxene; cpx = clinopyroxene

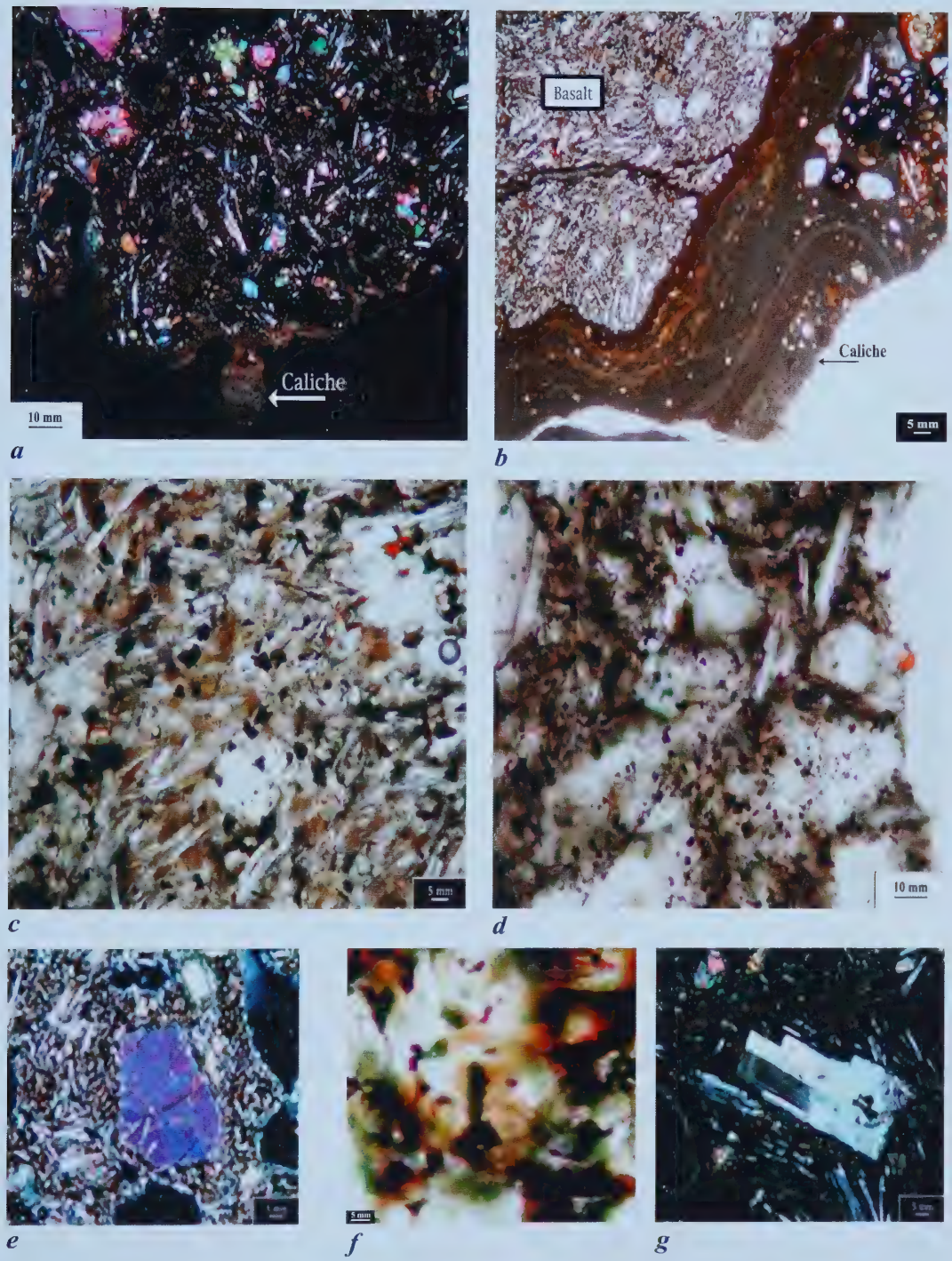

Figure 3: Photomicrographs of sample petrology in thin section. Overview of sample 754 (*a*) & sample 687 (*b*); large black crystals is magnetite in samples 687 (*c*) & 754 (*d*); olivine (zoned purple crystal) showing iddingsite alteration (*e*); arrowhead magnetite in center of image (*f*); Carlsbad twinning & oscillatory zoning in plagioclase (*g*). Crossed-polars in photographs *a*, *e*, *g*. Plane light in *b*, *c*, *d*, *f*. Scale bars for *c*, *e* & *g* is 5mm.

parent material respectively, while petrocalcic horizons have 40 wt.% calcium carbonate, are highly indurated, layered and impenetrable to plant roots (Allaby and Allaby, 1990). There are two sources of calcium for caliche: wind blown eolian dust and extraction from parent materials such as the basalt. It has been generally accepted that the dominant source of calcium is from the former (Schlesinger, 1985) however, this may not hold true for caliche developed on young basalts. Strontium (Sr) isotopic analysis of the caliche in an older lava flow in the Flagstaff area reveals that 55-67% of Sr came from the parent basalt (Knauth et al., in review, 2002).

Materials and Analytical Procedures

Thin sections of both samples were examined using reflected light microscopy. In addition, three other primary analytical methods were employed in examining thin sections and rock chips of each sample: scanning electron microscopy (SEM), electron microprobe and confocal microscopy. New adaptations, limitations and a novel technique concerning these methods were explored and are subsequently described. All work was performed at the University of Alberta, using facilities in the Departments of Earth & Atmospheric Sciences and Biological Sciences.

New Adaptations

Rock Chips

Geological samples for SEM and in particular, electron microprobe analysis, are routinely prepared as polished thin sections or grain mounts. Thin sections of biological samples are also often prepared for use in confocal microscopy. For these techniques, thin sections are appropriate and preferred, however the same cannot be said for geomicrobiological work. I believe that the cutting, grinding and polishing involved in preparing thin sections removes all or most microorganisms, or traces of such microbes from the sample. The preparation can also be a source of contamination. Investigations of sample thin sections are usually carried out first but if there is no suggestion of biogenic remains or activity, then examination of unprocessed, raw pieces of the samples may

prove productive. In various studies, I have commonly used fractured or broken pieces of rock chips and in many of these, have been rewarded with spectacular and surprising results. For example, in this thesis, thin sections of one sample displayed no evidence of biogenicity but on examination of two rock chips of the same sample, microorganisms were discovered. A survey of the literature suggests this method may be a novel approach in the search for biogenic indicators within geological materials.

Iridium-coated samples

Samples for SEM and electron microprobe analysis, requires the sample be coated with a conductive material. In geological work, coatings or thin films of carbon, chromium or gold are typically applied. Again, in various studies, I have explored the use of iridium (Ir) as a sample coating for both thin sections and rock chips. Iridium was suggested by NASA (Blake, et al., 1999) but, to my knowledge, its use has not been documented as a typical conductive coating for geomicrobiological work. Iridium is carbon-free, will not oxidize and degrade in the same period as chromium and once applied, has only a fraction of the standard thickness of a gold coat (100-150 Å). A thin film is desirable for high resolution and clarity of surface features (Gabriel, 1985). Also, I have used samples that had been coated with iridium for more than a year; these samples had minimal amounts of film degradation and therefore, did not require secondary coatings of iridium. In short, iridium has thus far proven to be a superior coating for geological materials in geomicrobiological investigations.

Scanning Electron Microscopy (SEM)

Rock chips between 0.5-1.5 cm in size, from the interior of the main hand specimens, were broken off and cleaned with high-pressure air to remove any extraneous debris. The chips were then affixed to 1/2" aluminum stubs using colloidal silver liquid (Ted Pella, Inc.; Lot # 000511810). The adhesion required 24 hours, after which they were coated with iridium. Thin sections were ~ 30 μm thick and in the interest of keeping contamination to a minimum, gloves were worn and an ultrasonic cleaner was not used. The epoxy used for thin sections was a combination of Buehler Epo-Thin Resin and

Hardener. Thin sections and chips were sputter coated with iridium for 40 sec at 100 milliamps and 10 microns ($10x10^{-1}$ torr) of pressure in a xenon atmosphere. The resulting film of iridium was approximately 40 Å thick. The samples were examined on a JEOL-JSM 6301 FXV scanning electron microscope coupled to a PGT–IMIX energy dispersive x-ray analyzer (EDX-A). Accelerating voltages were 5 and 20 kV.

Electron Microprobe

Methodology

The same samples, thin sections and rock chips, used for SEM work were also utilized in the electron microprobe. Major element analyses and element maps were done on various iridium coated thin sections and rock chips. Instrument is a JEOL – JXA 8900 with five wavelength dispersive spectrometers (WDS) and an energy dispersive spectrometer (EDS). Accelerating voltage was 15 kV with a probe current of $1.5x10^{-8}$ A. Standards used are listed in Table 3.

Element x-ray mapping

The concentration or deficiency of certain elements in geological materials is an important tool as an initial gauge of biogenicity. Simply put, rocks are composed of a variety of elements that span the spectrum of the periodic table. However, certain types of rocks such as basalts, will contain specific major elements (see Table 1 & 2) and some minor components in essentially the same amounts throughout the sample. Conversely, all microorganisms are comprised primarily of the elements required to make organic molecules: carbon (C), oxygen (O), hydrogen (H) and nitrogen (N). In addition, a select number of 'heavier' elements are also required: phosphorus (P), potassium (K), sulfur (S), magnesium (Mg), calcium (Ca) and iron (Fe). All of these elements, termed macronutrients, are obtained from the environment to create and continually support, the growth of a microorganism and are therefore needed in substantial quantities and are of utmost importance to microorganisms. Carbon and nitrogen are essential for synthesizing cellular material like proteins, nucleic acids, amino acids, fatty acids and sugars and on a

Table 3: Standards used for major element analysis and element maps

Element	Element Notation	Standard
C	C	silicon carbide
Na	Na_2O	kaersuitite
N	N	boron nitride
Cl	Cl	tugtupite
Mn	MnO	willemite
Mg	MgO	kaersuitite, Fo90*
S	SO_3	barite, sphalerite*
Fe	FeO	kaersuitite, Fo90*
Si	SiO_2	Fo93, Fo90*
Ca	CaO	rvgar1, kaersuitite*
Al	Al_2O_3	augite, kaersuitite*
K	K_2O	orthoclase, kaersuitite*
P	P_2O_5	apatite
Cr	Cr_2O_3	chromite
Ti	TiO_2	ilmenite

Note: * indicates alternative standards used for olivine analysis

dry weight basis, are ~ 50% and 12% respectively, of a cell. The other macronutrients also occupy many different roles in diverse cellular processes, including synthesis of cellular material, structure and stability of assorted cell components, enzyme activity and respiration (i.e. energy production and transportation). Nutrients only required in small amounts, called micronutrients, are a range of metallic elements such as copper (Cu), molybdenum (Mo), nickel (Ni) and tungsten (W) which are used by an assortment of organisms (Madigan et al., 1997a).

In a given habitat, organisms will therefore remove, transform if necessary and subsequently concentrate, all elements needed for their survival. The result will be a decrease or absence of these elements in the surrounding environment and corresponding increase within the organism. Elements not required may also be removed and deposited outside of the zone occupied by an organism. This principal forms the basis for using element (x-ray) maps as a method for investigating the biogenic nature of geological materials. The method works particularly well for igneous rocks, which do not contain any appreciable amounts of carbon, nitrogen, phosphorus and sulfur. Analyses are typically carried out for fifteen different elements, which are also listed in Table 3.

In regards to the actual element mapping process, mention should be made of a noticeable dark, 'burned' feature that results on an area of a sample that has undergone mapping. This discoloration is due to deposition of carbonaceous material, produced from the polymerization of vacuum pump oils through interaction of the electron beam (Mathez and Delaney, 1981; Cox, 1983). There is evidence that the deposition can be a critical problem, especially if trying to detect low carbon concentrations. Without additional experimentation it is difficult to know the extent to which this affects the features being analyzed in the basalt samples but based on previous studies using the same experimental parameters, the amount of carbon deposited is considered within background levels and is not thought to contribute significant levels of carbon contamination. However, this is not the case for nitrogen, which is discussed below.

Limitations

The analysis of lighter elements in the microprobe can sometimes be problematic but this is particularly true of nitrogen. It is uncertain whether instrumental factors such

as the choice of spectrometer (of the available five) or its location and distance from the detector in the microprobe are reasons for the poor, inconsistent or negative results typically obtained from nitrogen analysis. However, one factor that might be the primary source of the problem and which definitely affects the nitrogen analysis is the 'burned' feature mentioned previously, that results from the buildup of carbonaceous material during element mapping. Apparently, this deposited material and carbon in particular, strongly absorbs nitrogen and oxygen x-rays, severely decreasing the intensity of the x-rays the longer the electron beam stays on a point (Cox, 1983). Another suggestion concerns the window of the gas-filled counter, which is the x-ray detector in the microprobe (Scott, 1983). The window prevents gas leaking into the vacuum chamber while transmitting x-rays of a sample being analyzed and is designed to be very thin (3-125μm). However, when analyzing light elements, specifically nitrogen, it is suggested that a much thinner window (~0.1μm) be used; for example, a high nitrogen plastic film that also reduces the absorption edges of its constituent elements, such as collodion ($C_{12}H_{11}O_{22}N_6$). There is always the possibility that nitrogen is not present in the object being analyzed however, it will be shown that this is unlikely in the case of two minerals with large amounts of cellular material that were mapped and gave discrepant nitrogen results. As stated earlier, nitrogen is an exceedingly important element in microbial cells and should have been present within the organisms on both minerals.

Another probable limitation concerns the samples. Thin sections are optimal for microprobe work since the relatively flat surface minimizes topographical errors. This becomes more of an issue when rock chips are used. Chip surfaces are rugged and uneven, increasing errors propagated by topography. The effect can be minimized by patiently and carefully orienting the chip to obtain, as flat as possible, the desired surface or feature to be analyzed. Specific minerals containing microbial material but which were also reasonably flat with few topographical features were targeted for examination in this study. Special sample holders and stages are available to accommodate this task and were used with the chips in this thesis.

Confocal Microscopy

Methodology

Autofluorescence and fluorescence after staining, for probable biological entities in an iridium coated thin section and two basalt chips, were checked on a single-photon Molecular Dynamics inverted laser scanning confocal microscope (LSCM) with green excitation at 568 nm. The excitation source is an argon-krypton laser and Multiprobe 2001–Image Space II scanning software was utilized. The stain used was propidium iodide (PI) but the staining technique employed, after Tobin et al., (1999), was slightly modified. All solution concentrations and staining times remained the same [30 min, 70% methanol; 1.5 hr., 5 μg/ml PI; 0.2M PBS (a solution of NaCl, KCl, Na_2HPO_4, KH_2PO_4) for rinsing] for the thin sections and one rock chip of both samples but the length of time of exposure to PI for a second chip of sample 754, was changed (5 min. instead of 1.5 hr.). Also, samples were not centrifuged and thin sections of the chips were not made following staining. Fluorescence emission for PI was 590 nm.

Confocal microscopy and fluorescent stains

Fluorescence staining in conjunction with confocal microscopy is the last technique employed in determining biogenicity within the basalt samples. Epi-illumination fluorescence microscopy has typically been used to image fluorescing entities in different types of materials however, due to the design of an epi-illumination microscope, images are produced which lack detail because of diminished contrast and sharpness. In a confocal microscope, a single point on the sample is illuminated by a focused beam of light and a pin-hole aperture allows only light from the plane of focus to pass through to the detector while excluding any light from out-of-focus planes. This set-up generates detailed images, increases resolution and creates digitized optical sections that can be used to construct three-dimensional images (Nomenclature Committee of the Royal Microscopical Society, 1989; Herman, 1998).

Just as, or perhaps more important than the form of imaging employed, is the selection of a stain. The types of stains (alternatively called fluorescent probes or fluorochromes) available for fluorescence work are vast and also serve different functions, primarily in biological applications. For example, stains can be obtained which

bind to organelles, molecules and ions in the cell; others can be used to evaluate cell viability, pH and membrane potentials (Karsten, 1999). DAPI (4',6-diamidino-2-phenylindole) and PI are two types of classic nucleic acid (DNA and RNA) stains. One of the ways in which stains are classified is according to cell membrane permeability. Variations in permeability can be significant and will depend on factors such as cell type, stain concentrations and staining conditions. PI is a membrane impermeant stain, which means it will not be taken up by viable cells and is typically used for detecting dead cells in which the membrane has been compromised (Molecular Probes Handbook at http://www.probes.com, 2002). However, the addition of cold methanol in the staining procedure allows for the cell membrane to become permeable and therefore, will allow passage of PI into living cells. DAPI is semi-permeant and can be used for living and dead cells but will typically require the addition of other materials to make cells permeable (Huber et al., 1985; Williams et al., 1998).

PI was chosen for this work over DAPI, which has typically been used in a variety of geomicrobiological studies involving fluorescence staining (e.g. Huber et al., 1985; Hirsch et al., 1995; Furnes et al., 2001a). While both require similar preparations and will work in an analogous manner, there seems to be some advantage to using PI instead of DAPI. DAPI binds specifically to consecutive A-T (adenine-thymine) rich nitrogen bases in the minor groove of double-stranded DNA (dsDNA). PI on the other hand, does not have a preference for any sequence; it will intercalate between any of the five bases and will also bind to both dsDNA and double or single-stranded RNA (ssRNA). DAPI can bind to other sequences but the fluorescence emission is much less (~20% of the dsDNA-DAPI bond). PI complexed to nucleic acids has an ~20-30 fold fluorescence enhancement, while that of DAPI to dsDNA is only ~20-fold (Kapuscinski, 1995; Molecular Probes Handbook at http://www.probes.com, 2002). Another advantage concerns the medium in which the microorganism is found, a factor that might have a direct bearing on the properties of the individual stains. A negative and unavoidable aspect of fluorescence staining is that inorganic, abiogenic materials such as clay particles or debris from the preparation of samples may also be stained. Burde et al. (1999a, 1999b) conducted a study involving staining of known terrestrial microfossils (ages of 100y - 3Ma) with PI, at the conclusion of which they surmised the technique,

"may provide unequivocal verification of the presence of microfossils....."

The authors had experimented with various stains and found that, depending on the properties of the matrix materials, stains such as DAPI tended to be absorbed and retained within micropores in the sample, giving false positives; PI minimized this problem (J. D. Farmer, Arizona State University, personal communication, 2002).

Limitations

An important lesson was learned while experimenting with the staining procedure. Initial staining of a thin section and rock chip, each from a different sample, made abundantly clear that the length of time of these samples in the staining solution (1.5hr., as outlined in the methodology) was far greater than required. Prolonged staining with PI only served to oversaturate the samples, causing background fluorescence to be extremely high and making differentiation of the much smaller signals from any cells on the chip, unnecessarily difficult. This could also have been a factor in the negative results obtained for the stained thin section. The procedure probably worked well for Tobin et al., (1999) who proceeded to make thin sections of their samples after staining, thereby removing much of the background signal but was not optimal for my non-sectioned basalt chips or previously made thin sections. It is suggested that if following a particular staining procedure from published literature, modifications of staining times may be required depending on the nature and type of sample, as well as the stain being used.

Novel Technique

Confocal microscopy is ubiquitous in microbiological work and has only been used, minimally, in geological studies such as the analysis of sandstone porosity, weathering and assessing the orientation of fission tracks in minerals (Barker et al., 1998). Few geomicrobiological applications to date, have been documented (e.g. Tobin et al., 1999). Ideally, a flat surface is one criterion generally required in order to obtain high-resolution images with the inverted confocal microscope, regardless of the nature of the sample. This is typically met by preparing thin sections of the sample to be imaged. Thin sections may be of no consequence in biological work but as alluded to previously, it is potentially, a significant problem in geomicrobiological studies involving rock

substrates where organisms are attached to minerals. Another issue is the process used in investigating biogenicity. Materials like the basalts in this study might have only one or two potential sites where microbial activity or remains are suspected. Geochemical or microbiological techniques are applied to these sites in a particular sequence so that any introduction of carbon not indigenous to the sample is avoided. In this study, the first tools used were SEM and the electron microprobe. Staining of the same samples was the last procedure carried out since the stain is a source of carbon.

The new and unique aspect of the above procedure is the staining of iridium-coated thin sections and rock chips. Fluorescence staining of any type of coated material has not been reported in the literature and as such, its application in this thesis is considered novel. The iridium coat presented no observed adverse effects to the staining: it did not interact or act as a barrier to the stain, nor did it increase autofluorescence or background levels of fluorescence. Studies reviewed in the literature involving confocal work has primarily been accomplished by using separate samples for geochemical and microbiological techniques, such as SEM and fluorescence microscopy. In one study (Tobin et al., 1999), staining was first carried out and was followed by carbon coating of the same section for microprobe work; in effect, the reverse of what was done in this study.

Another accomplishment in this thesis was the successful in situ, fluorescence imaging of microbial cells under iridium coated, non-sectioned, rock chips of the basalt. Again, published studies usually image fluorescence in thin sections of their samples (e.g. Thorseth et al., 1995; Tobin et al., 1999) and undoubtly, researchers have tried to do this with unprepared samples but at the time of writing of this thesis, it is not known if there has been any measure of success.

Results and Discussion

The focus of this research is to investigate and document the possibility of life existing within basaltic rocks of a hot desert environment. Knauth et al. (in review) have applied carbon and oxygen isotope analysis to carbonate caliche associated with the

basalt samples that are used in this study and have found preliminary evidence suggesting the caliche has been partially processed by microorganisms. The isotopic signature may therefore be a suitable analogue for finding evidence of past life on Mars or during the Precambrian on Earth. This thesis will show that a series of complementary techniques are also suitable for determining biosignatures and that basaltic rocks may be primary abodes for microorganisms and are, at the very least, of equal importance as primary life-containing targets, on Earth or Mars.

As is the case with many recent studies, the process involved in searching for life in environments considered uncommon or extreme requires meticulous testing with several lines of supporting evidence that will ultimately prove or disprove such notions. Important bioalteration studies of volcanic glass in ocean basalts by the Bergen Group (H. Furnes, K. Muehlenbachs, I. H. Thorseth, T. Torsvik, O. Tumyr), has provided a geochemical and microbiological framework for carrying out these geomicrobiological investigations. Techniques include: observation and differentiation of biogenic and abiogenic textures; element concentration and distribution patterns; carbon and oxygen isotope measurements; nucleic acid staining and hybridization with molecular probes to identify the organism domain (Bacteria or Archaea). Several of these methods were employed here, in addition to an imaging approach not previously explored by the Group or other researchers. Remnants of organic material were detected within three channels in a thin section of sample 687 and microorganisms were found in fractured rock chips of sample 754. It should also be noted that aforementioned studies by the Bergen Group and others primarily involved glassy material which, in the basalt samples examined in this thesis, is not abundant and very difficult to locate.

Sample 687

Since microorganisms are believed to inhabit the overlying, thick caliche layer on this sample, it was thought that this would be an obvious entry for organisms into the basalt matrix and hence, initial examinations of a thin section were concentrated at the interface between the caliche and the basalt. However, light microscopy and SEM analysis showed no textural evidence of biogenic alteration, which would indicate that microorganisms were present or had been present at some point in time. Such features

would include irregular alteration fronts developed adjacent to fractures and vesicle walls, as well as granular and tubular type textures, some of which are similar in size and shape to textures produced by microbes in laboratory experiments (Furnes and Staudigel, 1999; Furnes et al., 2001b). Searching for these textures was made particularly difficult by the degree of crystallization and the coarse grained nature of the sample. However, using SEM-EDS as a first approximation, three channels were targeted as potentially containing organic remains or microorganisms. Channels A and F (Figures 4 and 5, respectively) extend from the caliche into the basalt from the contact zone between caliche and basalt, and channel C (Figure 6) is located entirely within the basalt. All contain elevated and/or decreased amounts of elements, potassium and calcium specifically, relative to the surrounding material, signifying a possible discrimination tactic characteristic of microorganisms.

Element maps for channels A, F and C are presented in Figures 7, 8 and 9, respectively. With the exception of channel F, only maps that convey the possibility of organic materials being present are displayed. On the basis of average atomic number (Z), mineral phases in the area being mapped are shown in the composition or backscatter maps (CP). Dark gray areas usually represent low Z minerals such as plagioclase while olivine and other high Z, Fe-rich, mafic phases are much brighter in color or white. Pores or holes in the thin section were filled with epoxy and appear black in the CP images. Topography maps (TP) are also included for each channel. Carbon, one of the most essential of all biogenic elements, is present in all three channels but calcium and chlorine are absent. This distinction is important for determining the biogenic or abiogenic nature of carbon in the sample. Primary inorganic sources of carbon would be the calcium carbonate caliche, other carbonate minerals, contamination or the epoxy used for mounting the thin section. High carbon concentrations are, not surprisingly, associated with the carbonate caliche (as on the left side of the carbon and calcium maps for channel F; Figure 8*c* & *d*) or natural joints and cracks in the basalt that contain pockets of carbonate. However, since calcium and therefore carbonate, is absent from the channels, the carbon could not have been sourced from carbonate.

Another inorganic source of carbon may be from the basalt itself. Tingle et al., (1991) have shown that some basalts frequently contain carbonaceous matter, in the form

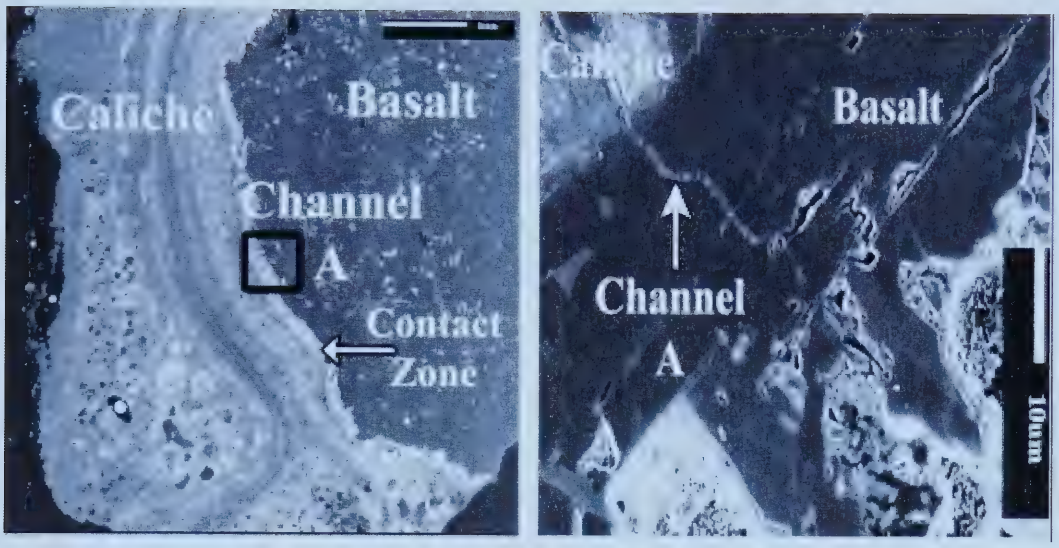

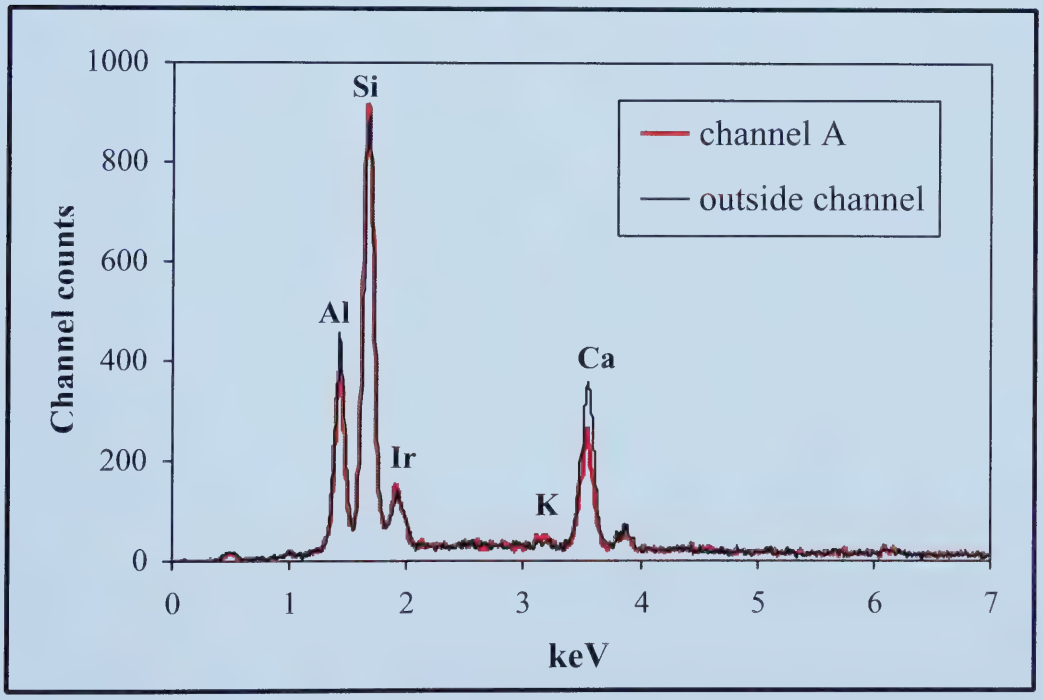

Figure 4: SEM photomicrographs of channel A in sample 687 and the associated EDX spectrum. The location of channel A as well as visible layering and inclusions of darker basalt material within the carbonate caliche are shown in the left image. A lighter colored band (contact zone) separating the caliche from the basalt is probably a reactionary front. The image on the right is a close-up of channel A. Slightly elevated and decreased amounts of K and Ca, respectively, are noticeable for the channel relative to the basalt. Scale bars are 1mm and 10μm, left and right photomicrographs, respectively.

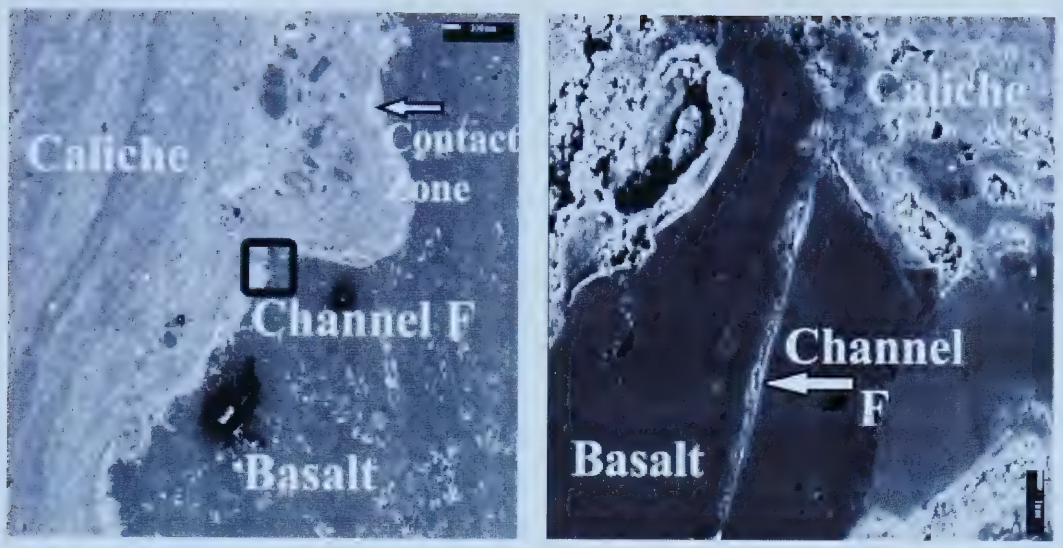

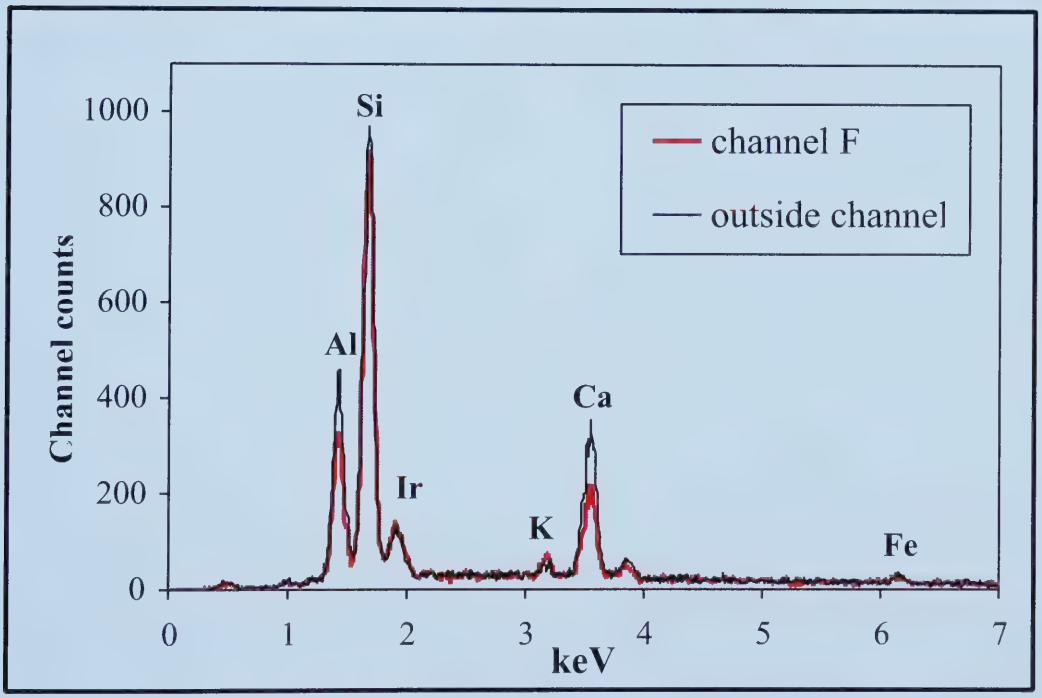

Figure 5: SEM photomicrographs of channel F in sample 687 and the associated EDX spectrum. The location of channel F as well as visible layering and inclusions of darker basalt material within the carbonate caliche are shown in the left image. The contact zone, separating the caliche from the basalt is also visible. The image on the right is a close-up of channel F, extending from the caliche into the basalt. Slightly elevated and decreased amounts of K and Ca, respectively, are noticeable for the channel relative to the basalt. Scale bars are 100μm and 1μm, left and right photomicrographs, respectively.

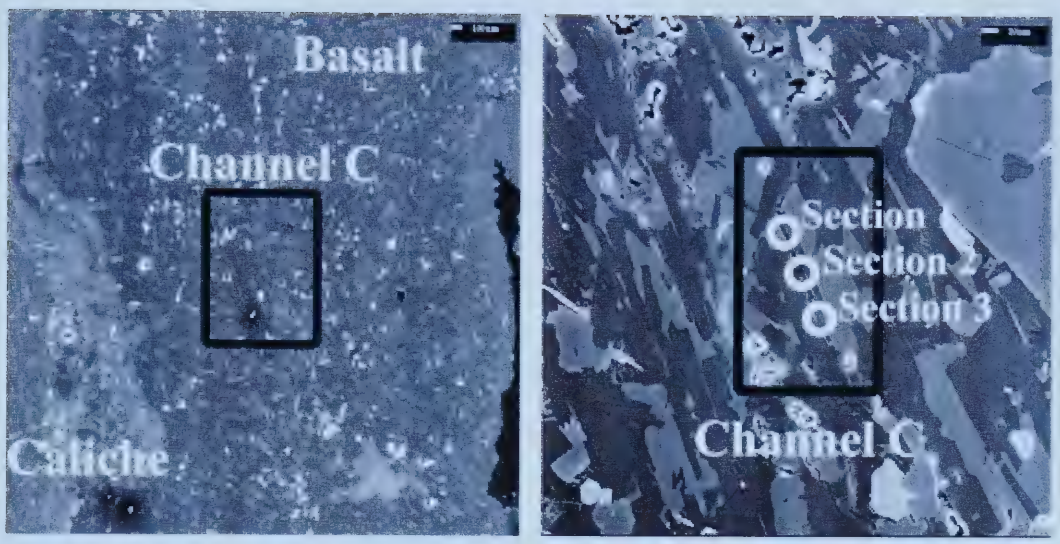

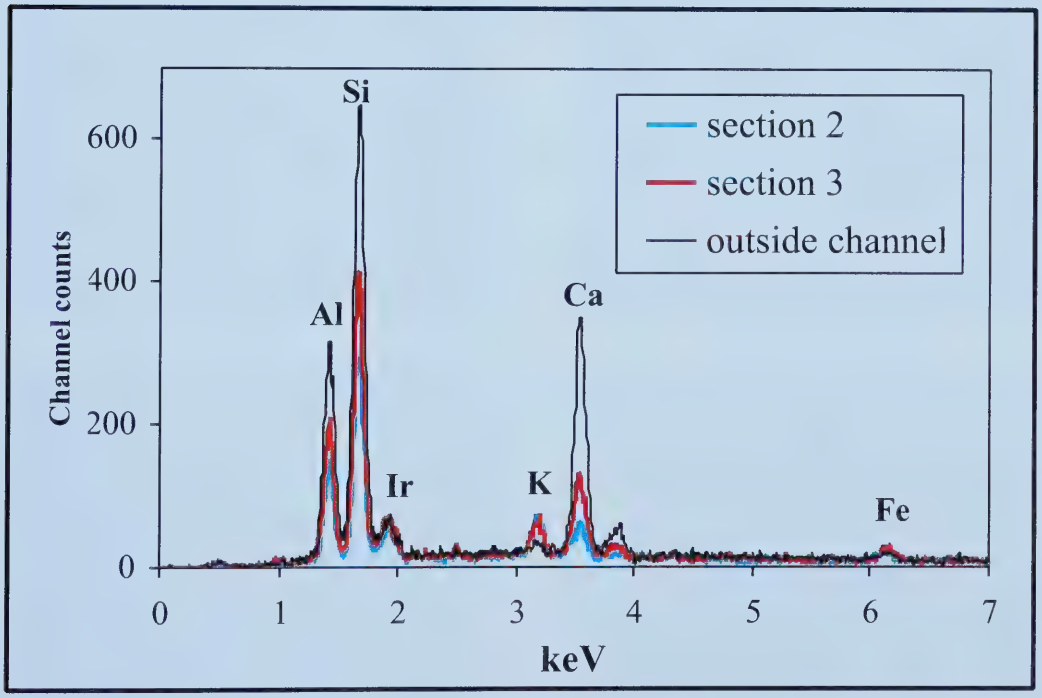

Figure 6: SEM photomicrographs of channel C in sample 687 and the associated EDX spectrum. The location of channel C within the basalt is shown in the left image. The image on the right is a close-up of channel C, displaying sections along which EDX analysis was conducted. Elevated amounts of K and much lower quantities of Ca, Si and Al are noticeable for the sections relative to the basalt. Scale bars are 100µm and 10µm, left and right photomicrographs, respectively.

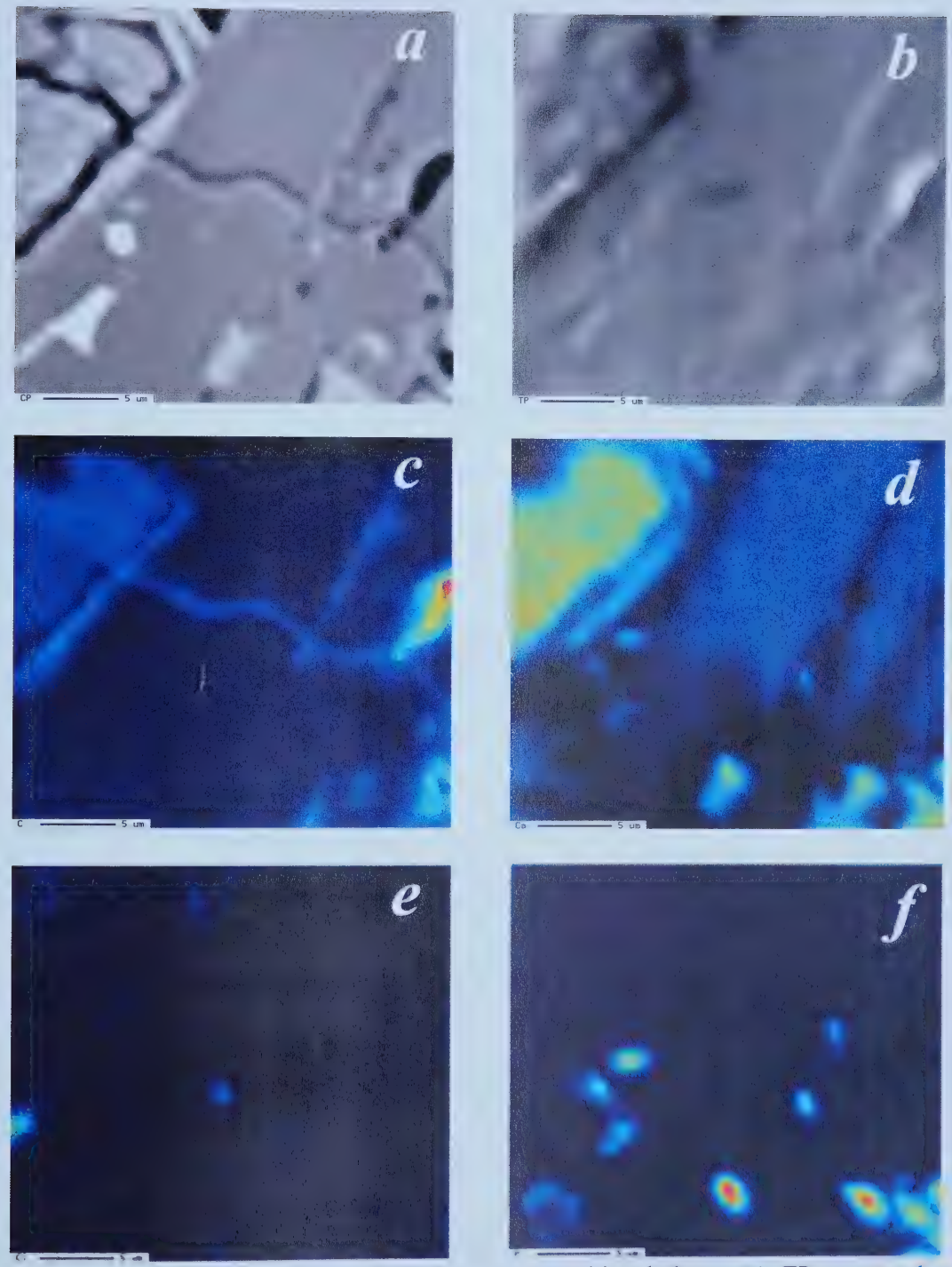

Figure 7: Element maps for channel A: CP or compositional phases (*a*); TP, topography map (*b*); carbon (*c*); calcium (*d*); chlorine (*e*); phosphorus (*f*). Relative concentration scale: lowest is black to blue-green-yellow-red (highest). Note the presence of carbon and absence of other elements within the channel. Scale bar (5µm) and orientation of the channel is the same in all images.

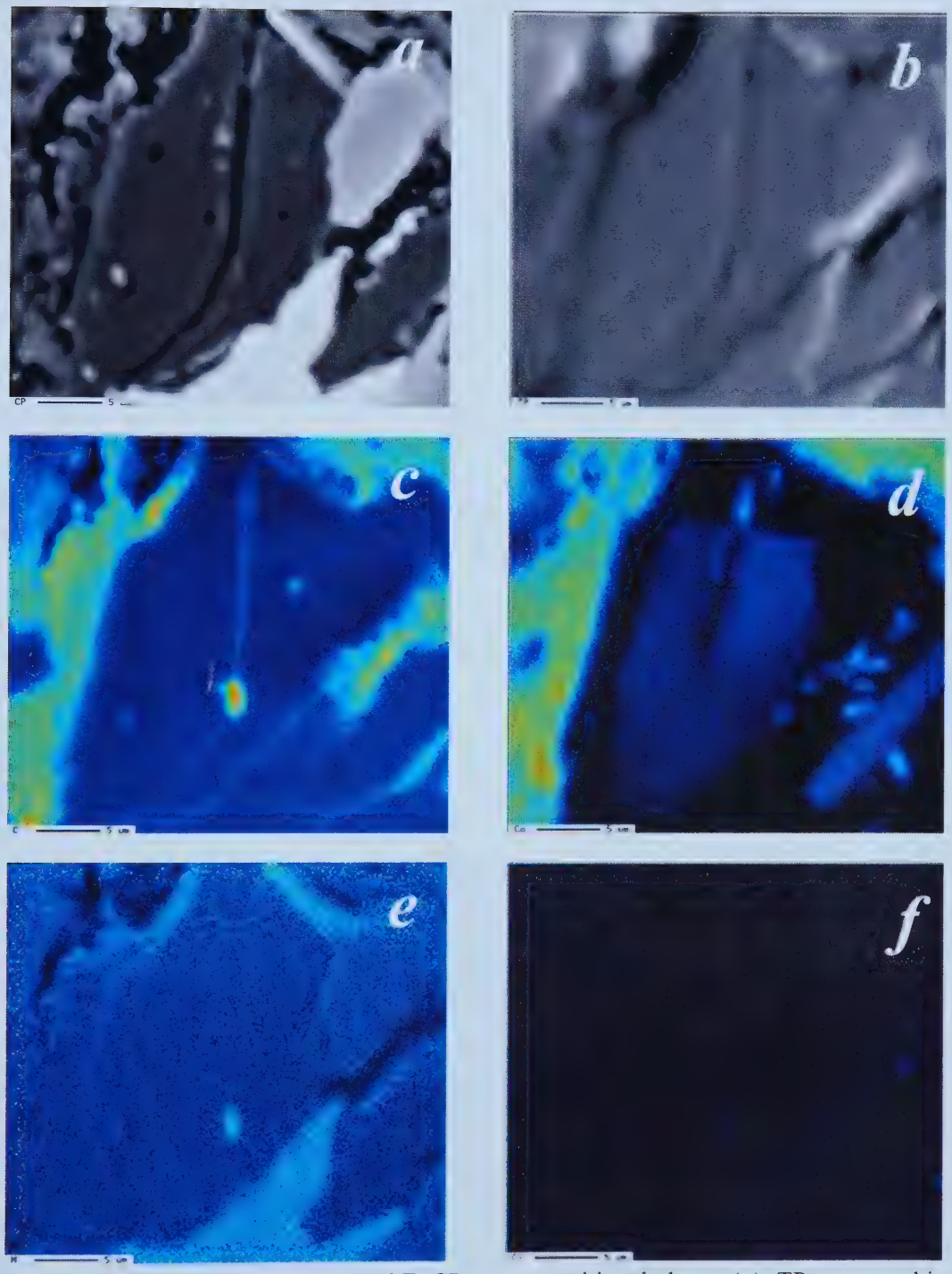

Figure 8: Element maps for channel F: CP or compositional phases (*a*); TP, topographic map (*b*); carbon (*c*); calcium (*d*); nitrogen (*e*); chlorine (*f*). Relative concentration scale: lowest is black to blue-green-yellow-red (highest). Carbon and a concentrated area of nitrogen are present within the channel but absent in the basalt. Scale bar (5µm) and orientation of the channel is the same in all images.

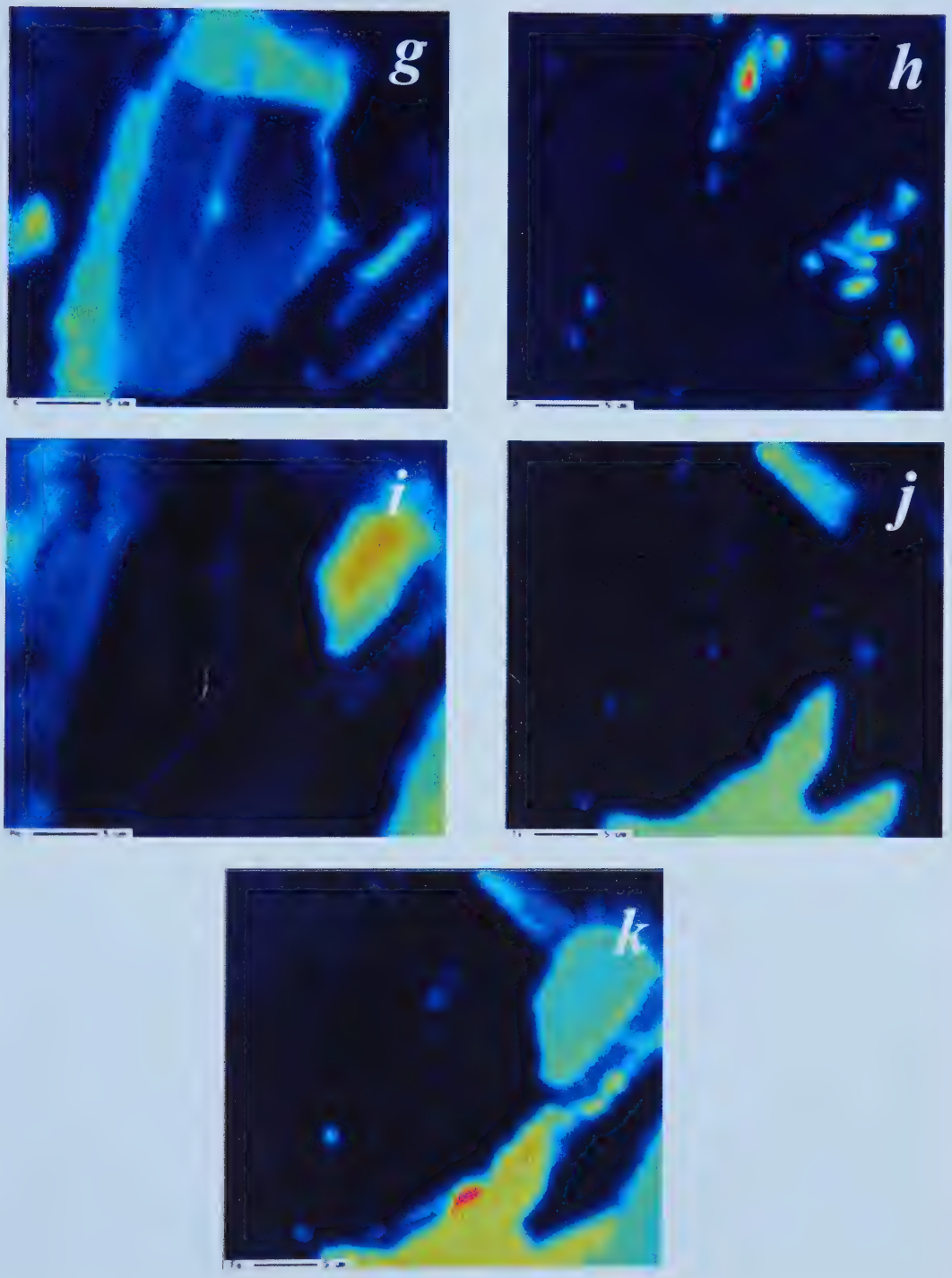

Figure 8: Continued. Some of these elements, such as potassium (*g*); phosphorus (*h*) and magnesium (*i*) are required by all organisms and are present within channel F. Other elements, titanium (*j*) and iron (*k*), are possibly needed by various types of organisms. These last two elements are not present throughout the channel and may be due to mineral phases.

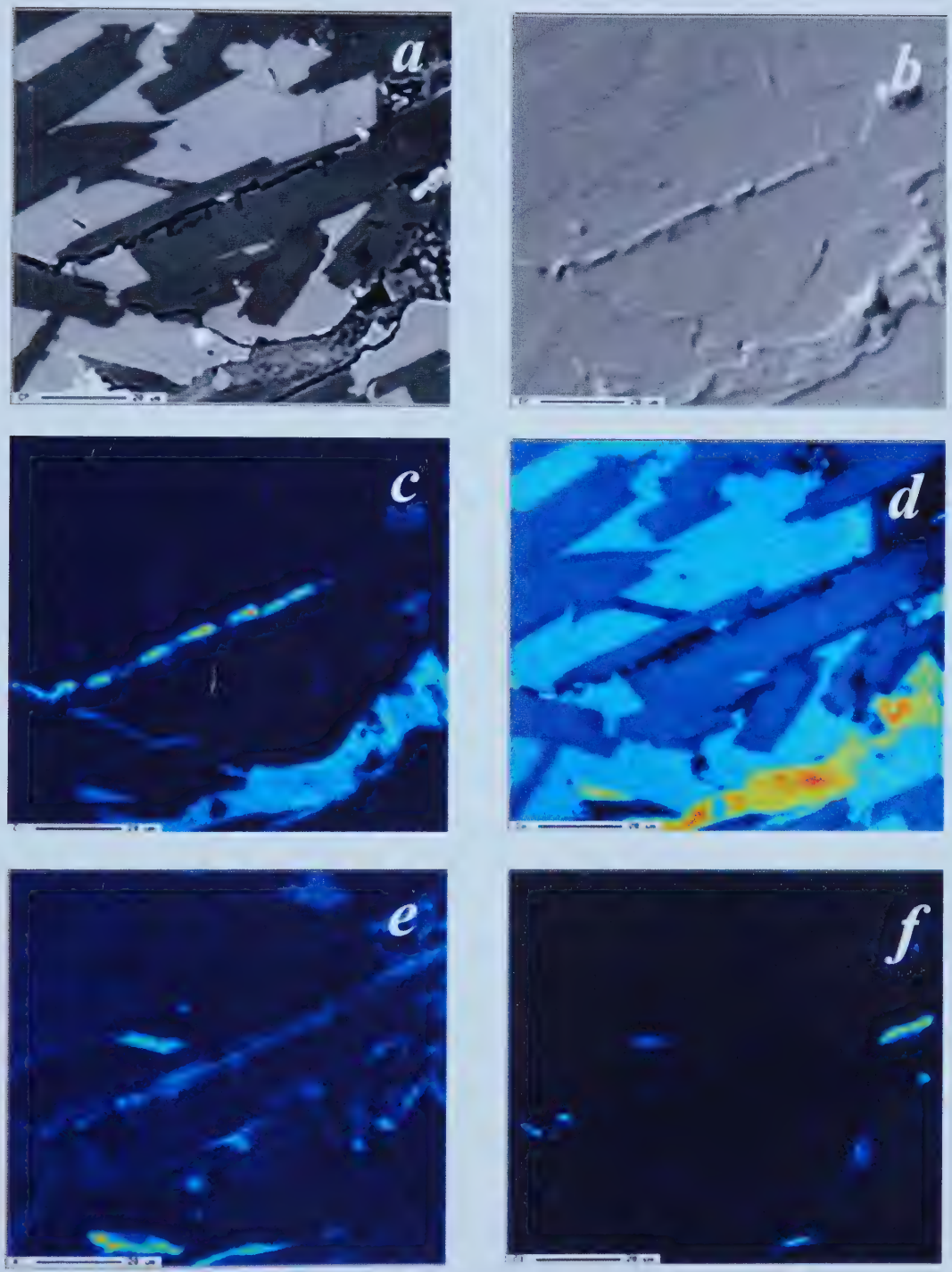

Figure 9: Element maps for channel C: CP or compositional phases (*a*); TP, topographic map (*b*); carbon (*c*); calcium (*d*); potassium (*e*); chlorine (*f*). Relative concentration scale: lowest is black to blue-green-yellow-red (highest). Carbon and potassium are present in the channel but absent in the basalt. Scale bar (20µm) and orientation of the channel is the same in all images.

of particles or films, believed to have been formed from Fischer-Tropsch reactions between volcanic gas and fresh fractures. This carbonaceous material has a bluish-purple coloration, is not greater than a few nanometers thick, amorphous and is chemically associated with silica, aluminum, alkalis, halogens and/or transition metals and organic compounds. These characteristics, however, were not found for the carbon signal in the channels. Also, Tingle et al. (1991) could not rule out the possibility of organic material in their study having a biogenic origin. Contamination was unlikely due to the great care taken while handling the section, which was also iridium and not carbon coated. The absence of epoxy was confirmed by analyzing for chlorine, which is not present in either the channels or the basalt. The calcium and chlorine maps verify the carbon signature is not from carbonate but is elemental in nature. It is suggested that remnants of organic material from biogenic activity accounts for the presence of carbon in these channels.

Other element maps, not necessarily of a biogenic nature, are also shown. In channel A (Figure 7), areas of phosphorus concentration do not coincide with any part of the channel but instead correspond to small, light gray phases that can be seen on the CP map. These areas also have elevated calcium concentration. All of this suggests the phosphorus highs are probably inorganic and related to some type of mineral, possibly apatite. A much better correlation of possible biogenic elements are seen in the additional maps for channel F (Figure 8), even though they do not all link to one another in the same places. For instance, the solitary nitrogen high within the mineral containing channel F, matches exactly and only with, the prominent carbon high that seems to end the channel on the carbon map. Both highs (located at the 'bend' in the channel on the CP map) are actually found just on the outer right edge of channel F, within a depression that can be seen on the CP and TP maps. On the other hand, some potassium, phosphorus, carbon and even magnesium highs all connect along the channel at various places but do not correlate with nitrogen. It is possible that the carbon and nitrogen spikes were caused by the depression itself since topographical features can give anomalous false positive concentrations but this is unlikely, as one would expect similar highs in the same area for some or all of the other elements. Iron and titanium (Ti) connect perfectly and show no relation to the other elements. They are most likely the representation of an iron-rich inorganic phase such as ilmenite, magnetite or spinel.

Potassium is the only other element that strongly correlates with carbon in channel C (Figure 9) and, of all three channels, the carbon concentration within this channel is much more pronounced. There is a hint of chlorine within the channel but all distinct chlorine concentrations correspond to epoxy filled holes. Other channels in the thin section of sample 687 showed no evidence of possible biosignatures and many turned out to be natural fractures or cracks.

Autofluorescence or primary fluorescence is fluorescence innate to different types of materials. Autofluorescence was checked before staining and is absent in the channels; it exists in the basalt but is not prominent. Confocal images of the PI-stained channels are presented in Figure 10. The characteristic red emission of PI is distinct, as is its absence from the channels. This would seem to indicate that entities of an organic nature, microbial cells specifically, are non-existent and hence, the carbon signals obtained from element mapping are false. I believe whole or partially decomposed cells are not present but remnants of organic material from microbial activity exist in the channels. DNA and RNA from microbes that at one time occupied the channels, may have decomposed or been altered to such a degree that the formation of the nucleic acid-fluorochrome complex may not be possible, thereby prohibiting any fluorescence emission. Another possibility is that if any nucleic acids were present in the channels prior to staining, the acids could have been denatured during microprobe mapping, by high temperatures generated as a result of the interaction between the microprobe electron beam and the mineral which houses the channel, preventing again, any possible binding of the stain. Oversaturation due to a prolonged staining period could also have contributed to disguising any signal that may have been apparent in the channels.

Sample 754

As with sample 687, light microscopy and SEM analysis of a couple of polished thin sections of this sample showed no textural evidence of biogenic activity or alteration. However, examination of two fractured rock chips proved to be quite fruitful, as microbes were found in both. The chips were fractured off the main hand specimen and extreme care was taken to avoid contamination. The chips were also processed as

Figure 10: Propidium iodide (PI) stained confocal images of channels A (top left), F (top right), & C (bottom). Areas outlined in black are the channel locations. Dark material covering the channels is due to deposition of carbonaceous material from x-ray mapping. The red coloration is the PI stain, which is absent within the channels. Circular spot analysis pits are evident in the close-up of channel C (bottom right). All scale bars are 20µm. An oil immersion lens, 40x, was used for all images.

quickly as possible: the time from fracturing to iridium coating was approximately 1.5 days. Chip #1 and chip #2 are both from sample 754.

Chip #1

SEM images in Figure 11 gives an overview of the types of organisms and features seen in chip #1. Two primary morphologies are observed: rod and cocci forms, with the former being more prevalent. Large and small cell sizes are seen and are generally within the range for average bacteria, 0.5-1μm in diameter and 1-3μm in length. Rods are ubiquitous, either in groups or as individuals but most cocci are found in groups or clusters. Cells also seem to display different life stages: some such as the cocci clusters in Figure 11*a* and *b* are possibly dead, dying or dessicated, taking on the appearance of deflated rubber balls; others appear viable and may be in the process of dividing, while some have possibly undergone cell lysis in which the cell has ruptured and the contents have been lost (Madigan et al., 1997b), leaving behind an outline of their membrane as the only evidence they once existed. Tracks or imprints of cells indicating areas they once occupied or from those cells that may have been motile, possibly as a response to chemotaxis, is evident (Figure 11*c* & *e*).

Other distinctive features include coarse-looking, fine-grained cryptocrystalline material either as inclusions or surrounding minerals and a relatively thick coating or film, covering some cells and minerals. A magnified image of relatively clean (i.e. does not contain many organisms) cryptocrystalline material and associated spectrum is presented in Figure 12. The material is interesting because its presence seems to attract and concentrate microorganisms in its vicinity. One reason for this might be the high levels of biogenic elements found within it: magnesium, phosphorus, potassium and iron. In Figure 12, plagioclase is the mineral with which the cryptocrystalline material is associated and as the spectrum shows, does not contain these elements. The presence of phosphorus is especially remarkable for two reasons: apatite, the most likely source of inorganic phosphorus, is rare in the sample and the only other source for phosphorus would be microorganisms. That the organisms themselves may account for the phosphorus is not surprising since many are observed embedded or maybe in the process

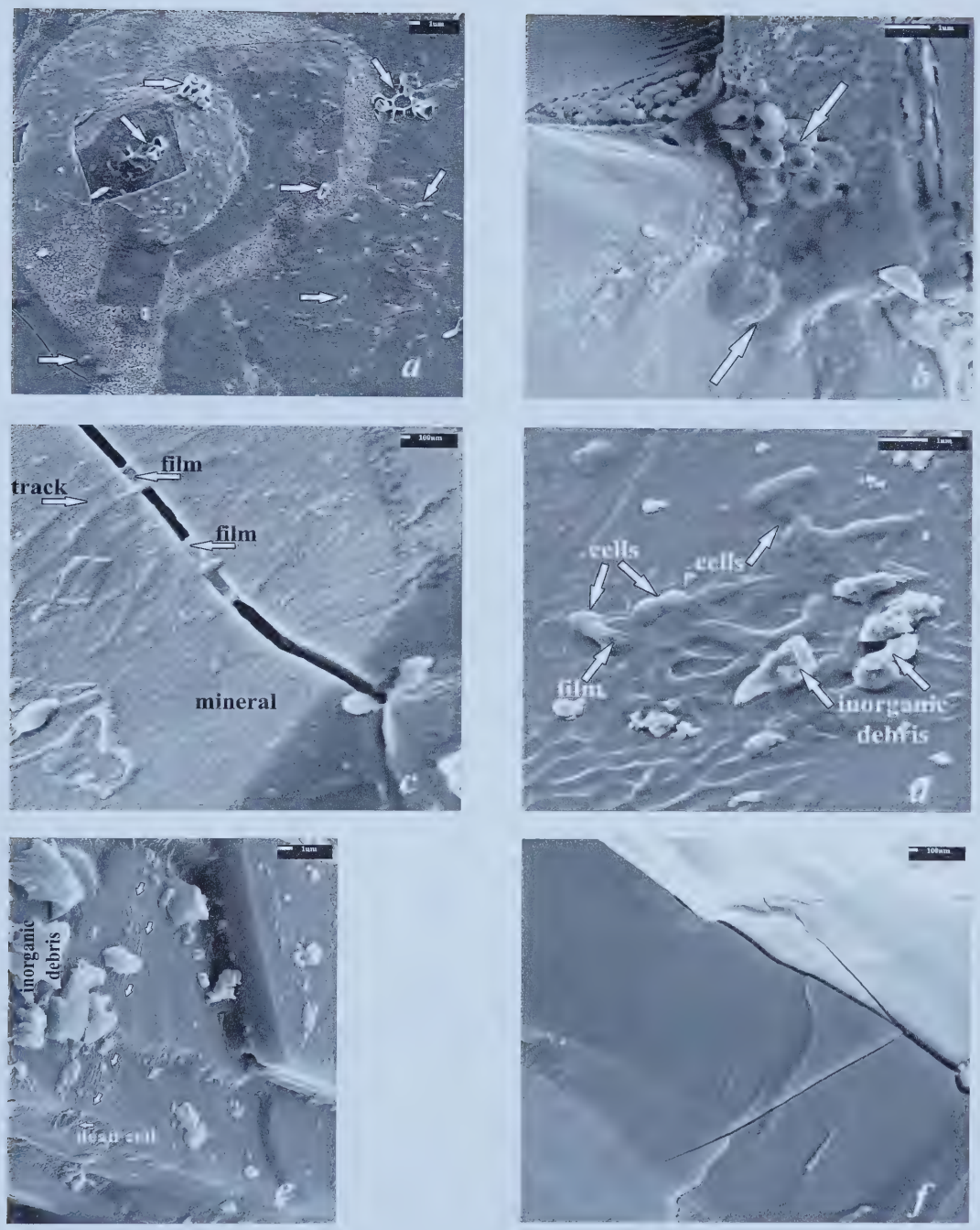

Figure 11: SEM images of features in chip #1. Cocci and rods possibly in various life stages (arrows: *a*, *b*, *d*). Grainy cryptocrystalline material can be seen in *a*. Tracks and biofilms are present in *c*, *d*, & *e*. In comparison to the film created by organisms, the surface of most minerals appear quite clean, as are any natural fractures and cracks (*f*). Scale bars: 1µm (*a, b, d, e*); 100nm (*c, f*).

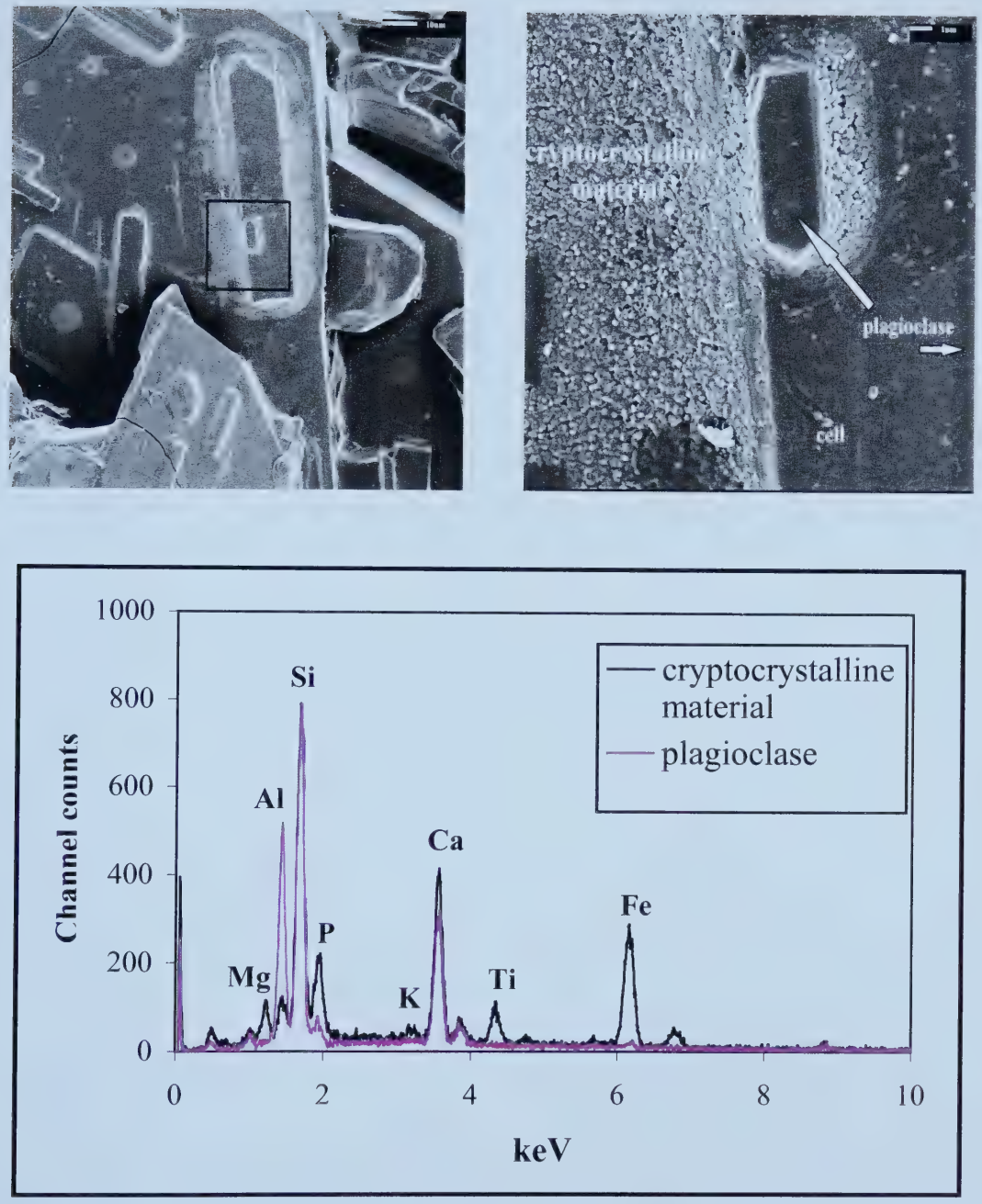

Figure 12: SEM images and spectrum for the cryptocrystalline material and associated crystal. Top left is plagioclase inclusion (outlined) within larger plagioclase crystal; both are engulfed by cryptocrystalline material. Top right is the magnified plagioclase inclusion and cryptocrystalline material on which the spectrum (bottom) is based. Cells are present nearby. Important biogenic elements (Mg, P, K, Fe) enriched in the material are noticeably lacking in the plagioclase crystal. Scale bars: 10µm (top left); 1µm (top right).

of dying within the cryptocrystalline material. Once dead, the cell and its contents such as phosphorus-concentrating adenosine triphosphate (ATP) would decay and potentially assimilate into the material, subsequently giving a high phosphorus signal when analyzed. Thus, the cryptocrystalline material may be analogous to a recycling depot, where some elements derived inorganically, like iron and magnesium, are already in a more accessible form as nutrients for the microorganisms; added to this are elements like phosphorus and potassium from decaying cells. The whole assortment of nutrients then becomes available for use by other microbes or growing cells.

The thick film covering some cells and minerals also attaches the majority of cells to the mineral surfaces they occupy. This film is most likely biogenic in nature and probably composed primarily of extracellular polymeric substances (EPS), a term that has also been referred to as extracellular polysaccharides, exopolysaccharides and exopolymers. EPS is a biopolymer produced by microorganisms and it encompasses a variety of organic macromolecules such as polysaccharides, proteins, nucleic acids, lipids and other polymeric compounds. EPS is found outside the cell wall and its formation, composition and deposition can be determined by different processes: active secretion by living cells, spontaneous release of cellular components due to normal growth processes, cell death or lysis and adsorption from the environment (Wingender et al., 1999; Wolfaardt et al., 1999). An abundance of hydrophilic sugar residues in polysaccharide molecules, one of the main components of EPS, allows EPS to be exceedingly hydrated. It is over 90% water (Christensen and Characklis, 1990), a factor that would be extremely beneficial to desert-dwelling organisms. Apart from facilitating the attachment of a microorganism to a surface, other roles of EPS include its structural and functional importance in biofilms, as a protective barrier to biotic and abiotic entities from the environment, preventing desiccation of cells, permitting continuous reactions across the cell membrane (Westall et al., 2000) and acquiring nutrients through the enzymatic action of proteins.

Additionally, an interesting function of EPS may be indirectly assisting the exchange of genetic material between cells. Some minerals like clays, quartz and feldspars form complexes with DNA and this fact, coupled to the high concentration and accumulation of cells made possible as a result of the binding property of EPS, increases

the opportunities for cell-to-cell contact and hence, the transfer of genetic material (Wingender et al., 1999; Wolfaardt et al., 1999). Figure 13 shows cells attached via EPS to a probable biofilm being created, involving mainly cocci but rods as well. Biofilms are individual clusters or microcolonies of organisms embedded and held together by EPS. In some biofilms, water channels exist within the EPS matrix and serves to separate the colonies, convey water and nutrients to the cells, remove waste and transport cells to other areas in the film (Stolz, 2000). The biofilm in Figure 13 displays typical characteristics seen in many types of films: different consortia of embedded cells, colonies of cells attached by EPS, incorporation of inorganic materials, layering and cavities that may act as potential water channels or channels for other transport activities.

The vesicle imaged by SEM in Figure 13*a* proved to be one of the primary areas on chip #1 containing many microorganisms. Two minerals, both plagioclase and labeled C and E, with attached cells were selected for element mapping (Figure 14). These minerals were among the few within the vesicle that once the chip was oriented, were flat enough to offset topography effects during analysis and at the same time, contained relatively large numbers of microorganisms. Figures 15 and 16 are the corresponding x-ray maps for minerals C and E, respectively. The same sets of elements are shown for each mineral. As expected, carbon highs are associated with the cells and other organic entities such as decaying cells and biofilms. The vesicle was thoroughly examined with the SEM, which showed carbonates are not present in the mapped region. Calcium is present in plagioclase but visibly absent in the areas that have carbon (Figures 15*d* & 16*d*). The lighter elements that have a greater probability of being biogenic in nature correlates with carbon as follows: phosphorus shows a very good correlation in both minerals; sulfur displays some patchy but good agreement, especially with phosphorus in the conspicuous group of cocci on mineral E (Figure 16*a*, *e* & *f*); nitrogen agrees extremely well with both carbon and phosphorus in mineral C but is virtually non-existent in mineral E.

The x-ray maps of the heavier elements on minerals C and E support the data already presented in Figure 12. Potassium, magnesium, iron and titanium all correlate and are concentrated within cryptocrystalline material present on both minerals. Iron, magnesium and titanium are essentially homogeneous throughout the material whereas

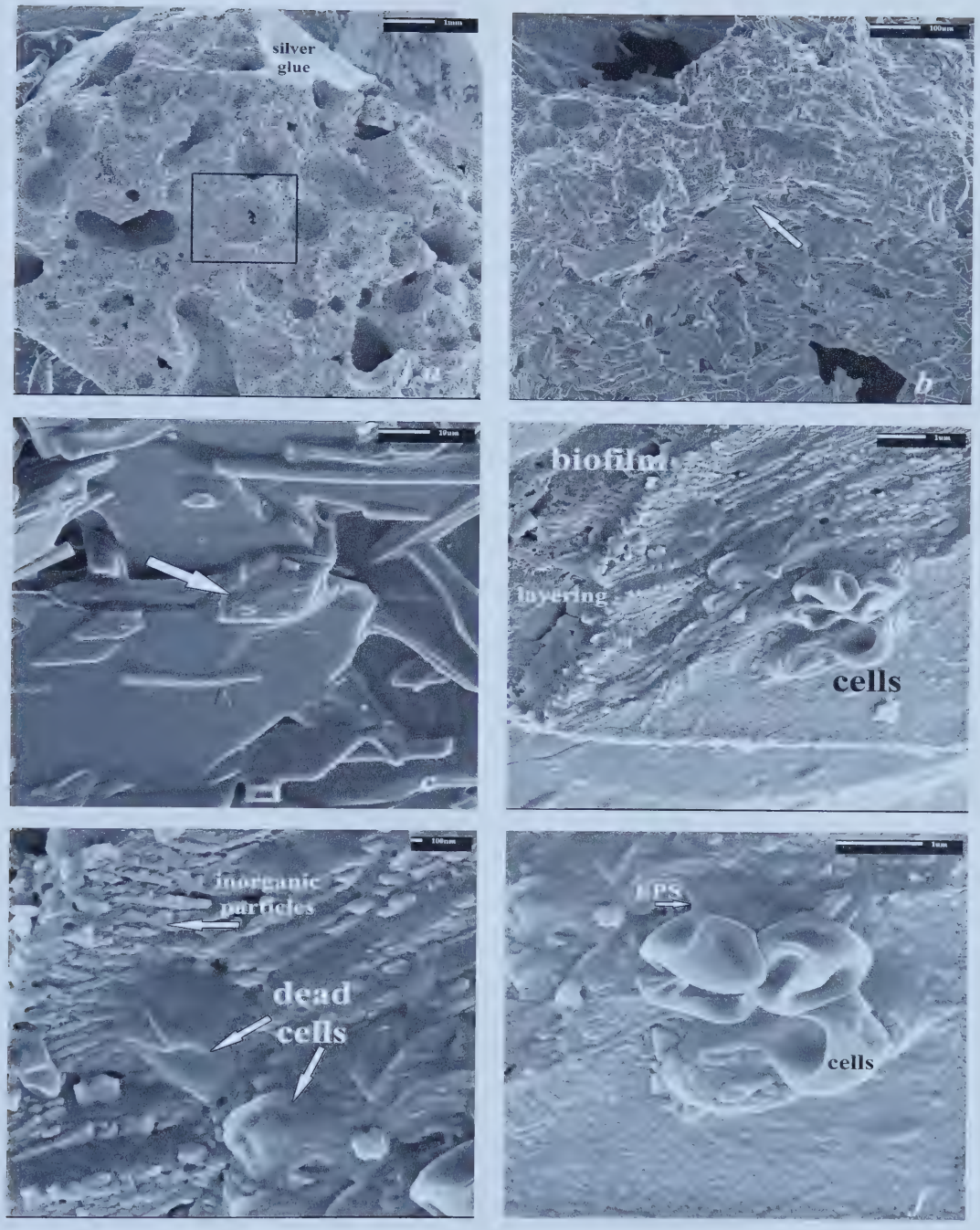

Figure 13: SEM images of a biofilm in chip #1. The vesicle housing the biofilm is outlined in *a*. Magnified view of the vesicle wall and the underside of the crystal to which the biofilm is attached (*b* and *c*, respectively). Cells and inorganic materials are attached and embedded via EPS. Other properties that characterize EPS such as layering and cavities are evident (*d*, *e*, *f*). Scale bars: 1mm (*a*); 100μm (*b*); 10μm (*c*); 1μm (*d*, *f*); 100nm (*e*).

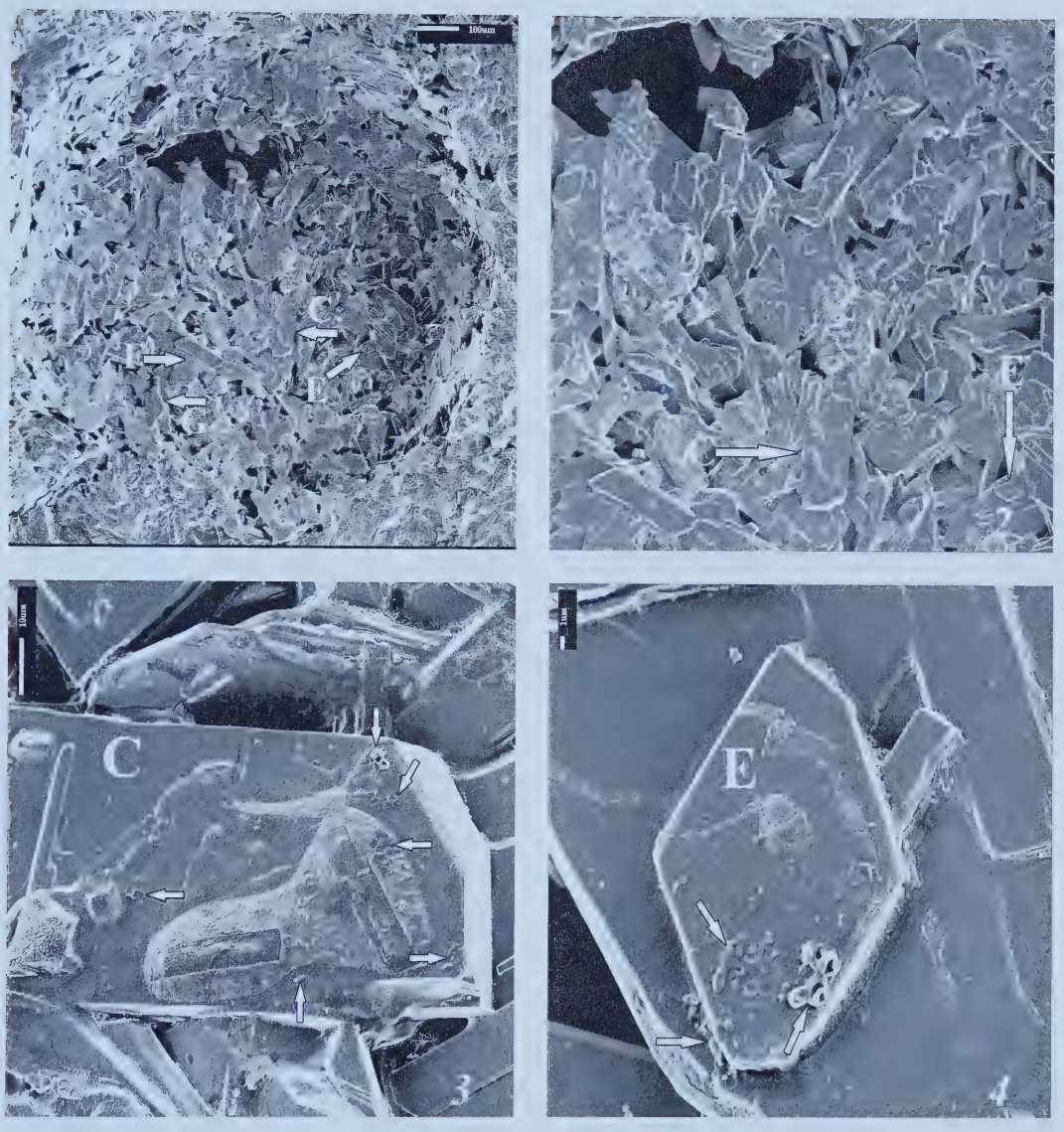

Figure 14: SEM images of the vesicle in chip #1 containing minerals C, E, F & G. Minerals C, E & G were subsequently investigated (*1* & *2*). Mineral F was only used as a marker to locate the nearby mineral G (see Figures 18 & 19). Minerals C and E were subsequently exposed to electron microprobe analysis. Arrows in images *3* & *4* points to individuals or clusters of cells in various life states. Minerals C and E are thought to be plagioclase crystals. Scale bars: 100µm (*1*); 10µm (*3*); 1µm (*4*).

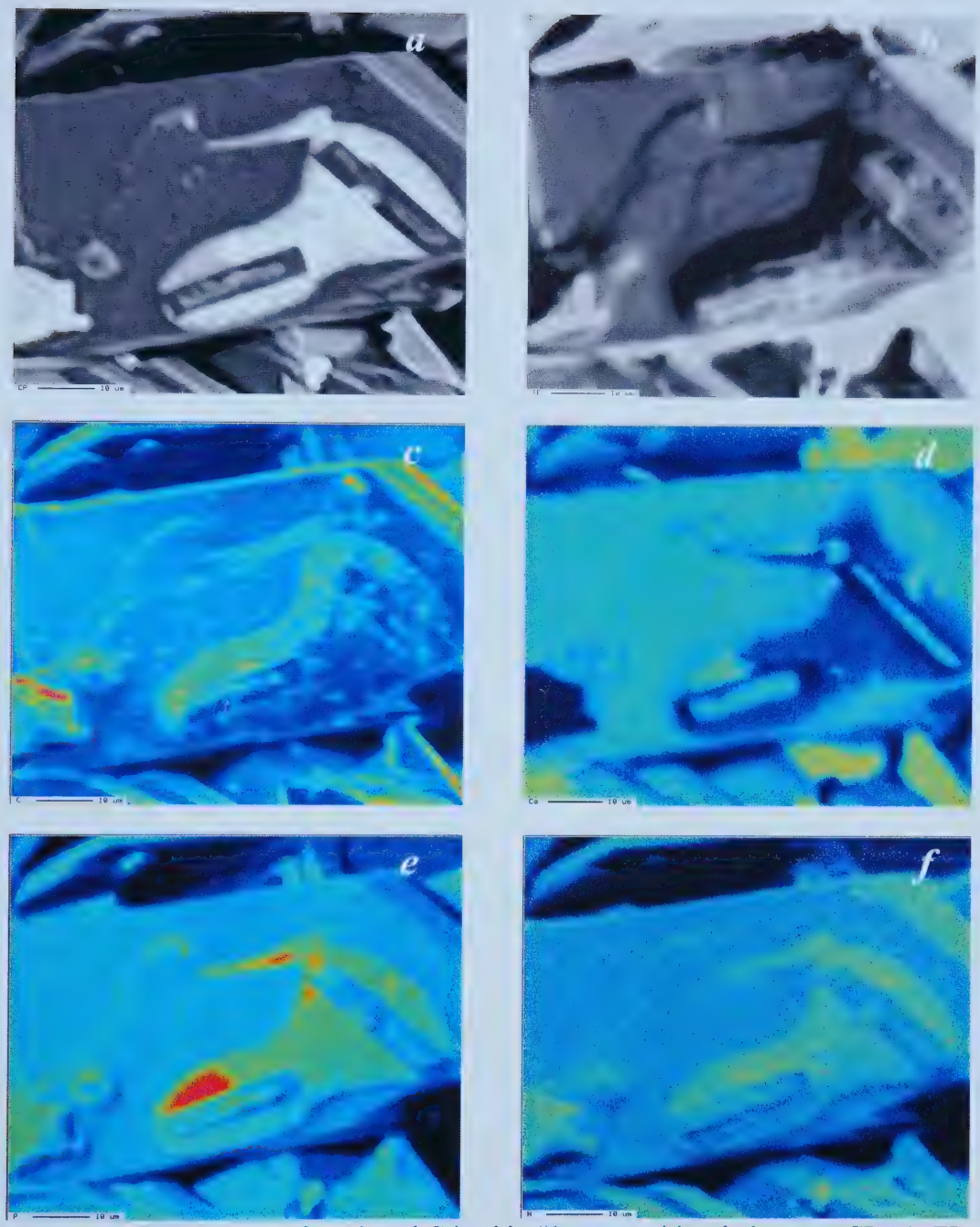

Figure 15: Element maps for mineral C in chip #1: compositional phases or CP (*a*); TP, topographic map (*b*); carbon (*c*); calcium (*d*); phosphorus (*e*); nitrogen (*f*). Relative concentration scale: lowest is black to blue-green-yellow-red (highest). Carbon, phosphorus & nitrogen correlate with each other and with the location of cells, cellular materials or cryptocrystalline material. These elements are absent in the crystal. Scale bar (10µm) and orientation of the channel is the same in all images.

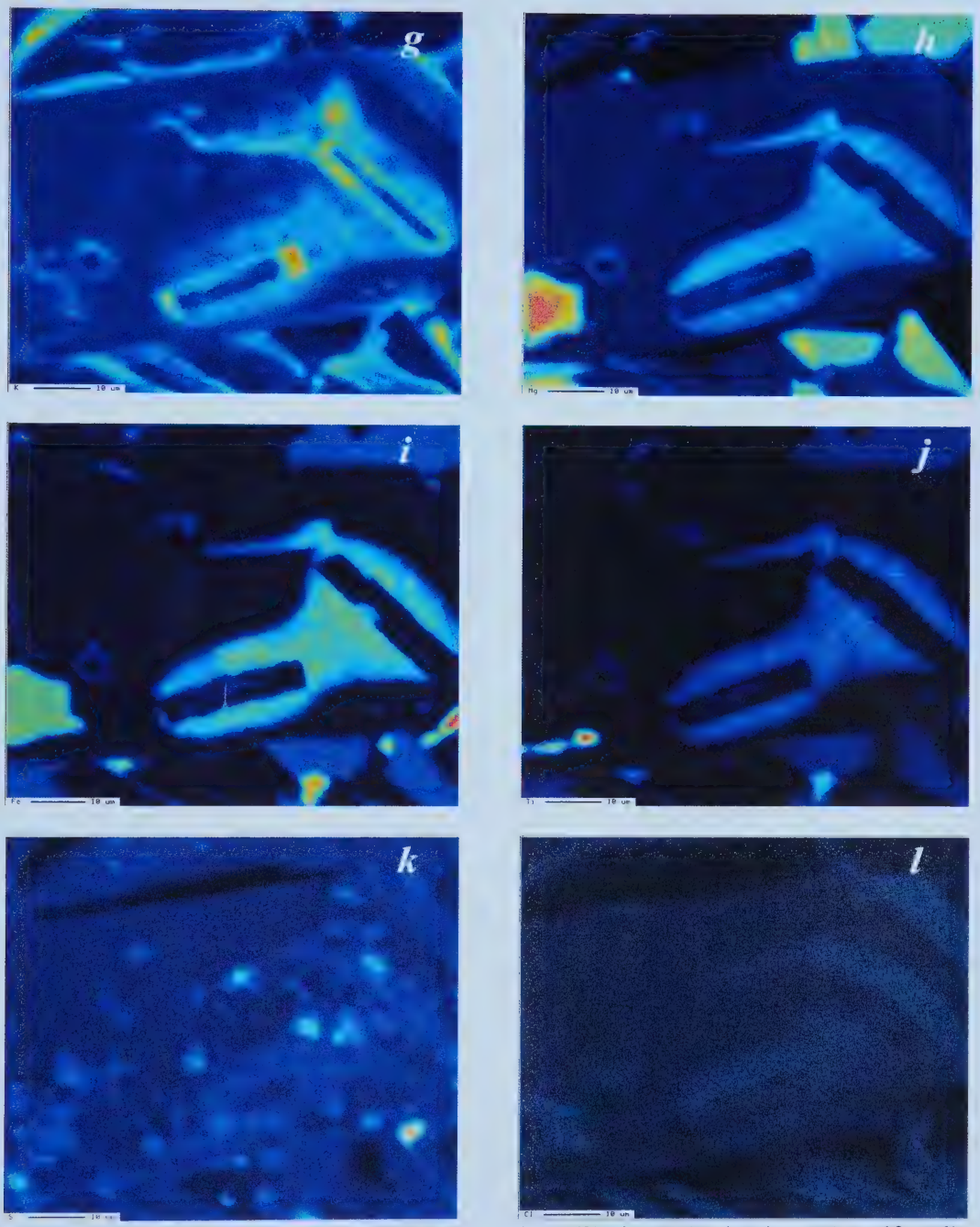

Figure 15: Continued. Potassium (*g*); magnesium (*h*); iron (*i*); titanium (*j*); sulfur (*k*); chlorine (*l*). Similar correlations are seen amongst other biogenic elements (potassium, magnesium and sulfur). The relatively strong iron and titanium signals are likely from degraded mafic minerals, such as magnetite or ilemenite, that make up the bulk of the cryptocrystalline material. The absence of chlorine confirms there is no contamination from epoxy. Scale bar (10µm) and orientation of the channel is the same in all images.

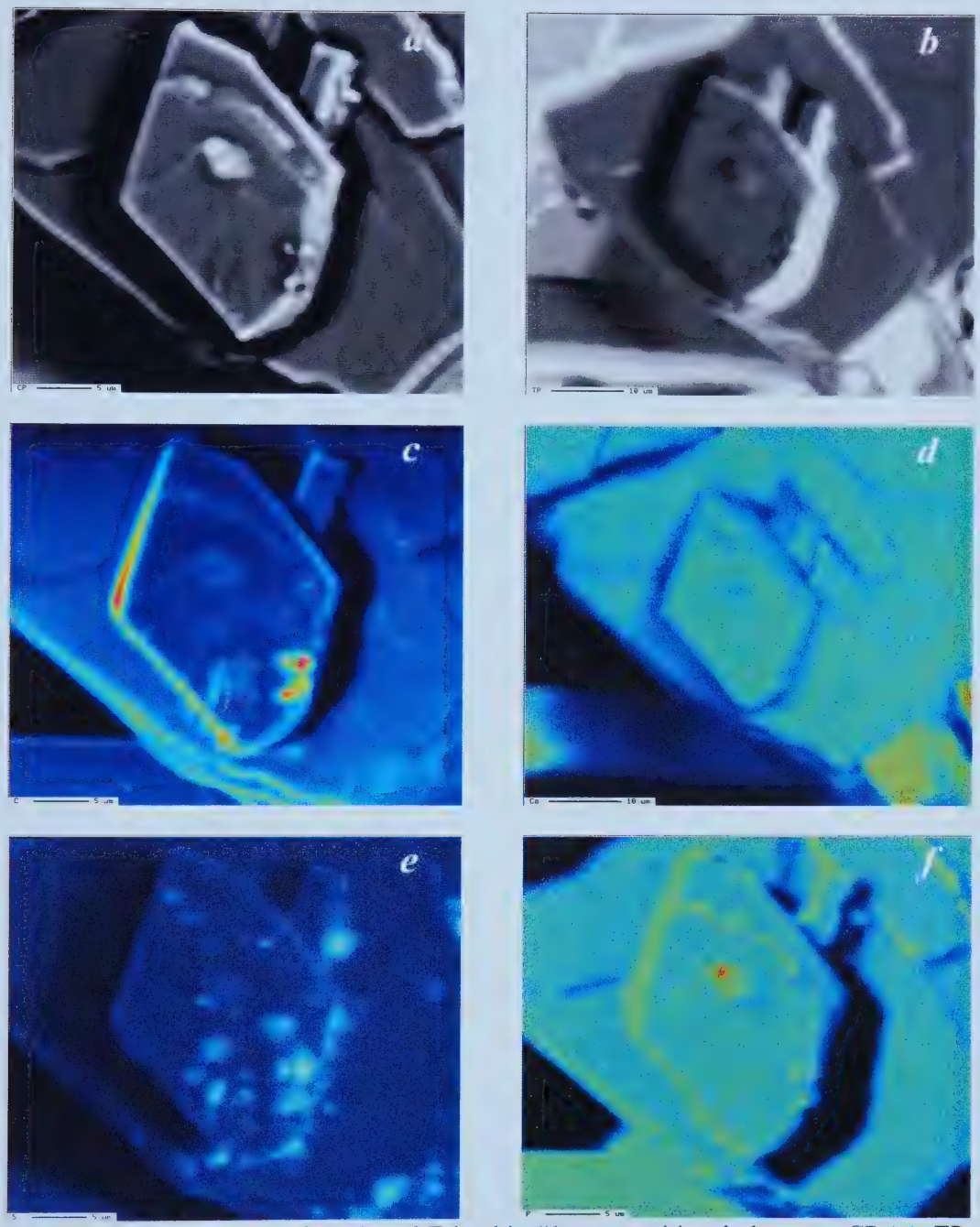

Figure 16: Element maps for mineral E in chip #1: compositional phases or CP (*a*); TP, topographic map (*b*); carbon (*c*); calcium (*d*); sulfur (*e*); phosphorus (*f*). Relative concentration scale: lowest is black to blue-green-yellow-red (highest). Orientation of the channel is the same in all images. Scale bars are all 5µm except for Ca and the TP map (10µm). Carbon, sulfur and phosphorus correlate well with the prominent group of cocci on the mineral (see the carbon high on image *c*). The strong carbon signal in the upper left edge of the mineral is due to topography effects.

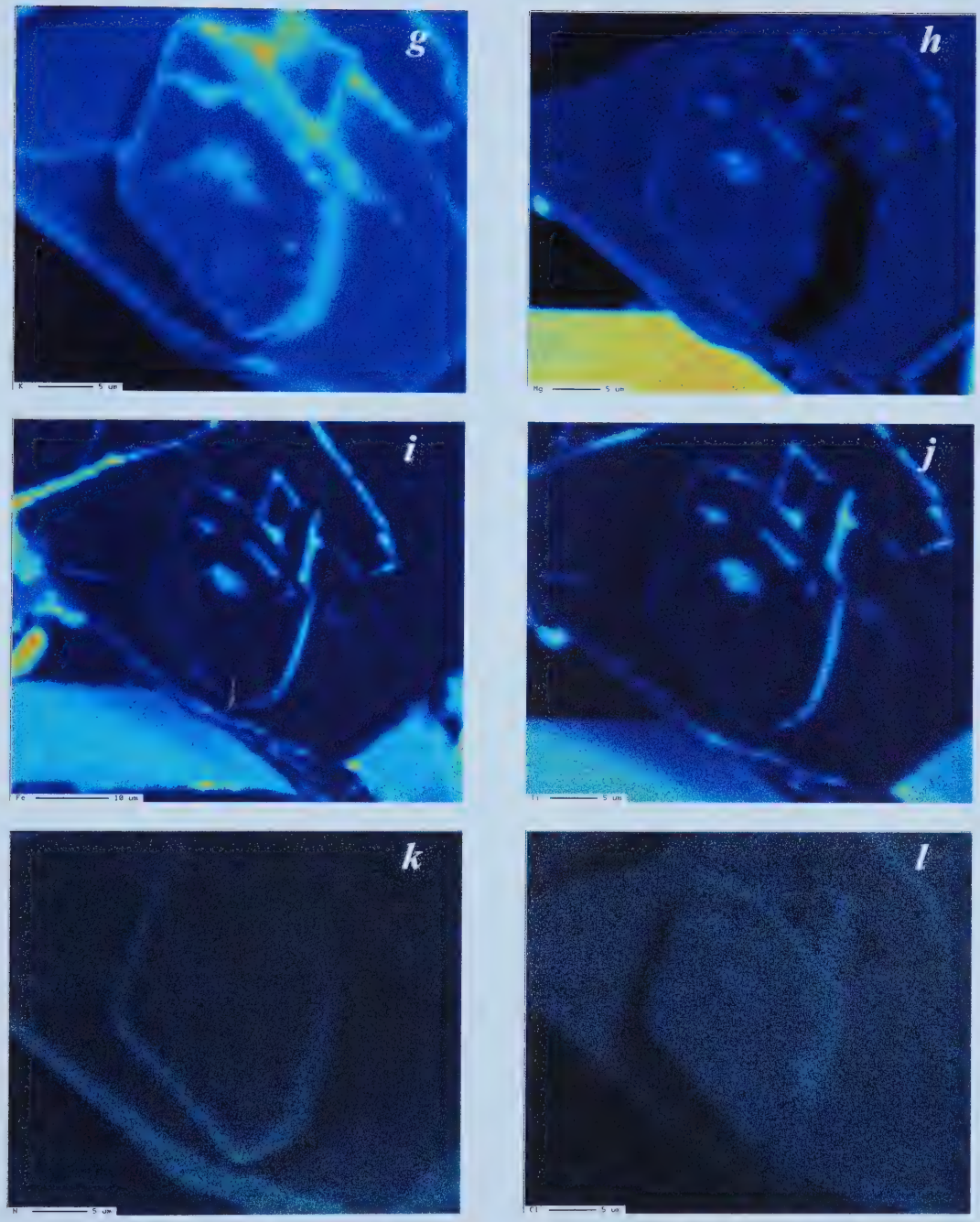

Figure 16: Continued. Potassium (*g*); magnesium (*h*); iron (*i*); titanium (*j*); nitrogen (*k*); chlorine (*l*). Some correlations are seen amongst other biogenic elements (potassium and magnesium). The iron and titanium signals are likely from degraded mafic minerals, such as magnetite or ilemenite, that make up the bulk of cryptocrystalline material or possibly due to edge effects. Nitrogen is not seen on this crystal. The absence of chlorine confirms there is no contamination from epoxy. Scale bar (5µm) is the same for all images except iron (10µm). The orientation of the channel is the same in all images.

potassium is scattered with some areas of higher concentrations, particularly on mineral C. This may be the effect of topography, which is slightly enhanced on mineral C. An overview of minerals C and E with magnification of the aforementioned conspicuous groups of cocci and rods, after x-ray element mapping has been carried out, are presented in Figure 17. At first glance, there seems to be no effect of the analysis on the cells. However, if one compares Figures 14-*4* and 17-*3,* a noticeable change of appearance is observed on the rods of mineral E, which look more degraded. A close inspection of the adjacent cocci group before and after mapping shows the cells looking surprisingly more 'plump' after the analysis! This does not seem to be a product of the imaging process and quite frankly, I can't think of any reasons to explain it.

Fluorescence staining of chip #1 was moderately successful but the process did provide some important lessons, which are outlined in the next section. Two minerals were found within the vesicle shown in Figure 13*a* and containing minerals C and E but only one could be imaged. The minerals are labeled F and G in Figures 18, 19 and 14-*1*. Mineral F, which is actually two connected minerals, could not be imaged at higher magnification (40x, oil) because of a lack of focus due to a deeper position in the vesicle but it was used as a marker to locate the nearby mineral G since it had a distinctive shape, could be seen in the confocal microscope at lower magnification (20x) and was easily identified in the SEM. Mineral G was the only mineral within the vesicle that could be imaged. It is also connected to another mineral but the appropriate individual with fluorescing entities is outlined in the figures and labeled mineral G. EDS spectrum from the SEM shows mineral G is a pyroxene.

Two fluorescing areas on mineral G are indicated on Figure 18*b* and both correlate with the presence of cells. The first area, labeled cells-#1 (Figure 18*c* & *d*), is a group of cocci displaying various stages of possible desiccation and cell lysis. A few rods looking much healthier are also in the vicinity, as is a plagioclase inclusion surrounded by cryptocrystalline material containing a large amount of embedded cellular and biofilm material and most likely, living cells. Since both the material and cocci are in such close proximity, the prominent fluorescence signal (Figure 19) in this area probably emanates from both, assuming all the nucleic acids in the cocci are not denatured. Cells-#2, the second fluorescing area on mineral G (Figure 18*e* & *f*), seem to be occupied

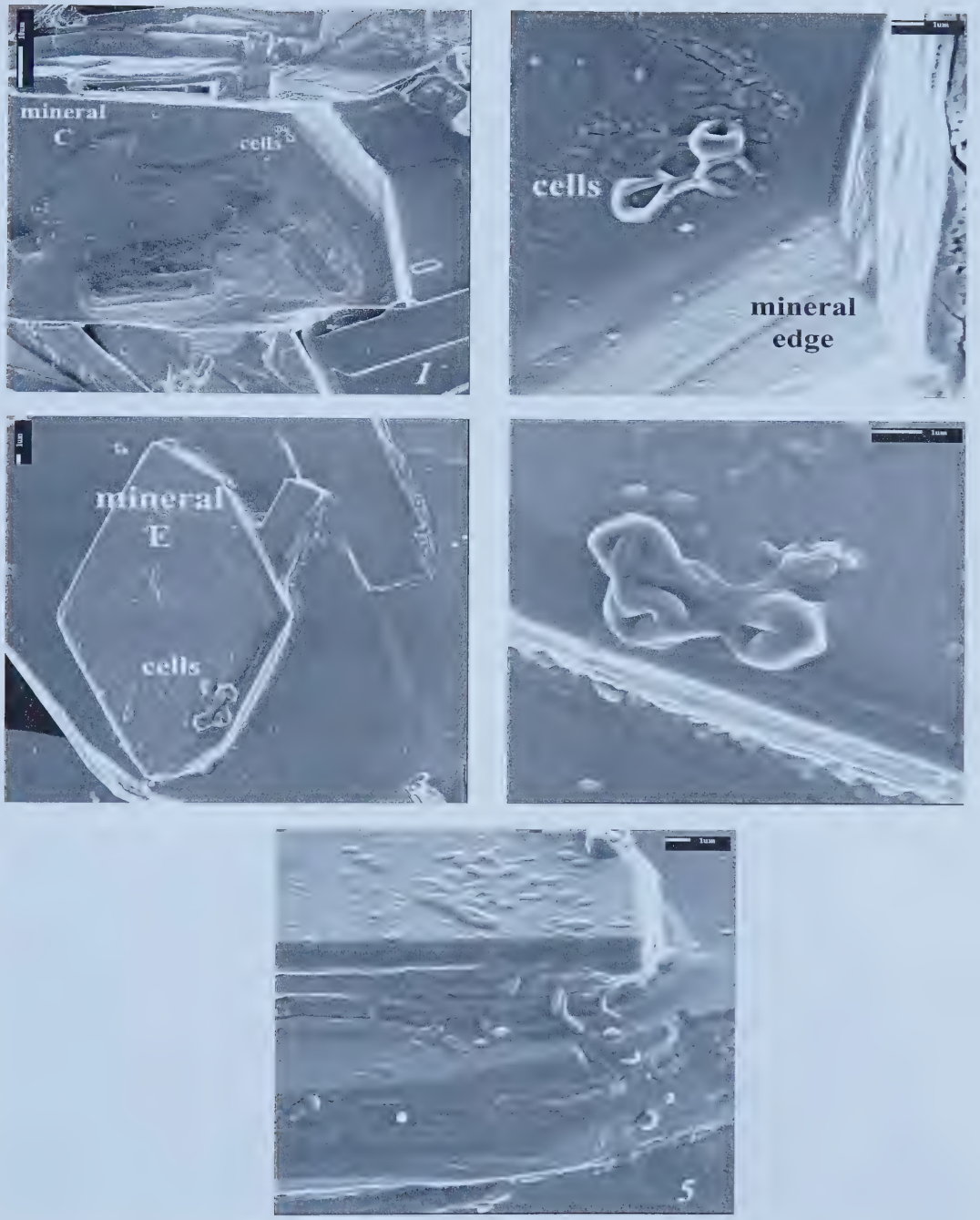

Figure 17: SEM images of minerals C (*1, 2*) and E (*3, 4, 5*) on chip #1, after undergoing x-ray mapping. Some cells were affected more than others; this might be a function of cell size and thickness. Cocci cells in *2* and *4* appear more plump after analysis. The group of rods, next to the cocci group in *3* and towards the top of image *5* is clearly degraded (compare to Figure 14-*4*). Image *5* is a magnified view of the lower left edge of mineral E; cellular material can be seen coating the underside. Scale bars: 10 μm (*1*); 1μm (*2, 3, 4, 5*).

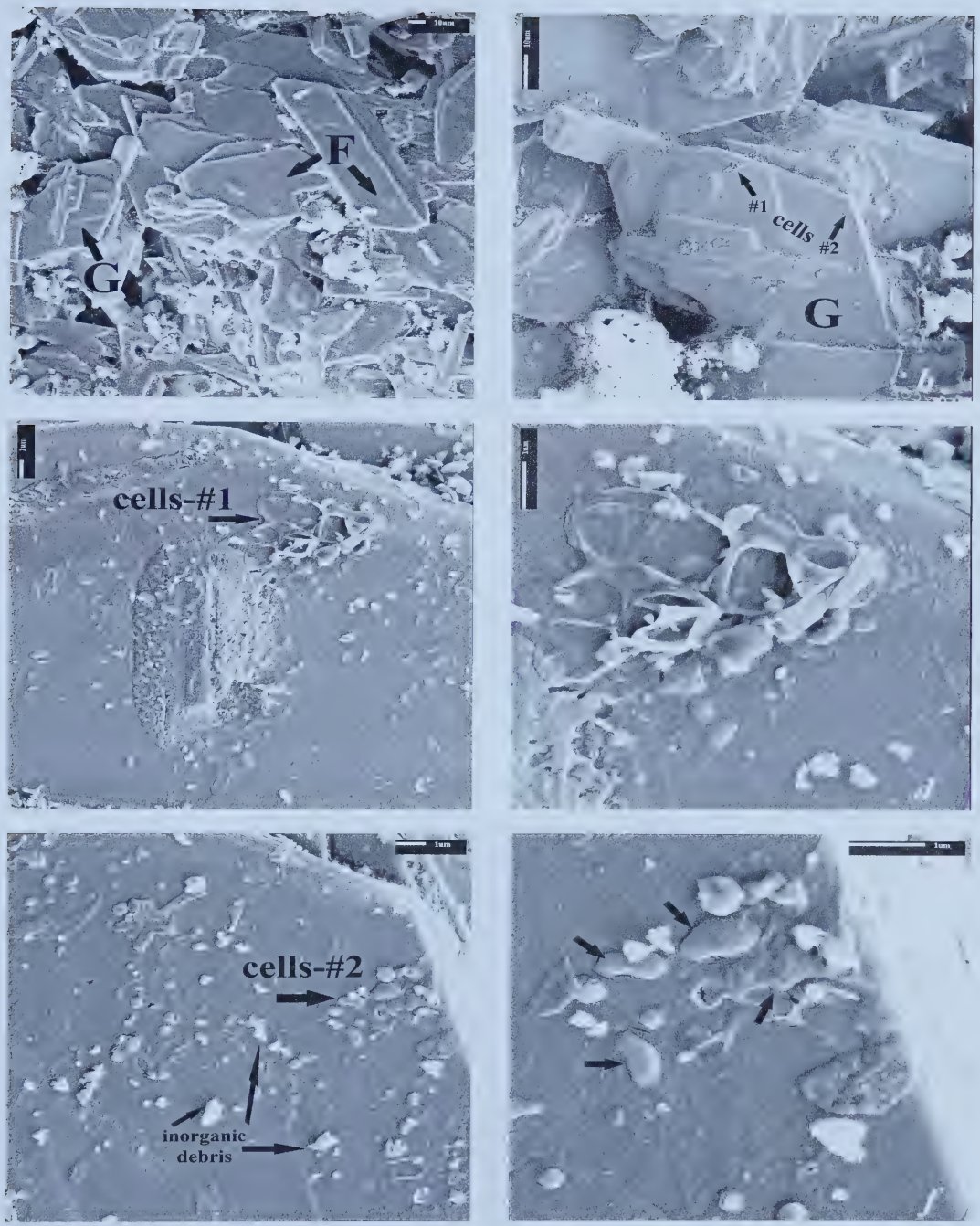

Figure 18: SEM images of minerals F and G in chip #1. Mineral F was used as a marker to locate mineral G. Two areas (seen in images *b*, *c*, *e*) on G containing cells that correspond to strong fluorescence signals in subsequent confocal images (Figure 19), are labeled cells-#1 and cells-#2. Images *d* and *f* are magnified views of both areas, which also contain a fair amount of inorganic debris. Arrows in *f* indicate cells. Plagioclase inclusion with surrounding cryptocrystalline material is in the center of *c*. Scale bars: 10μm (*a*, *b*); 1μm (*c*, *d*, *e*, *f*).

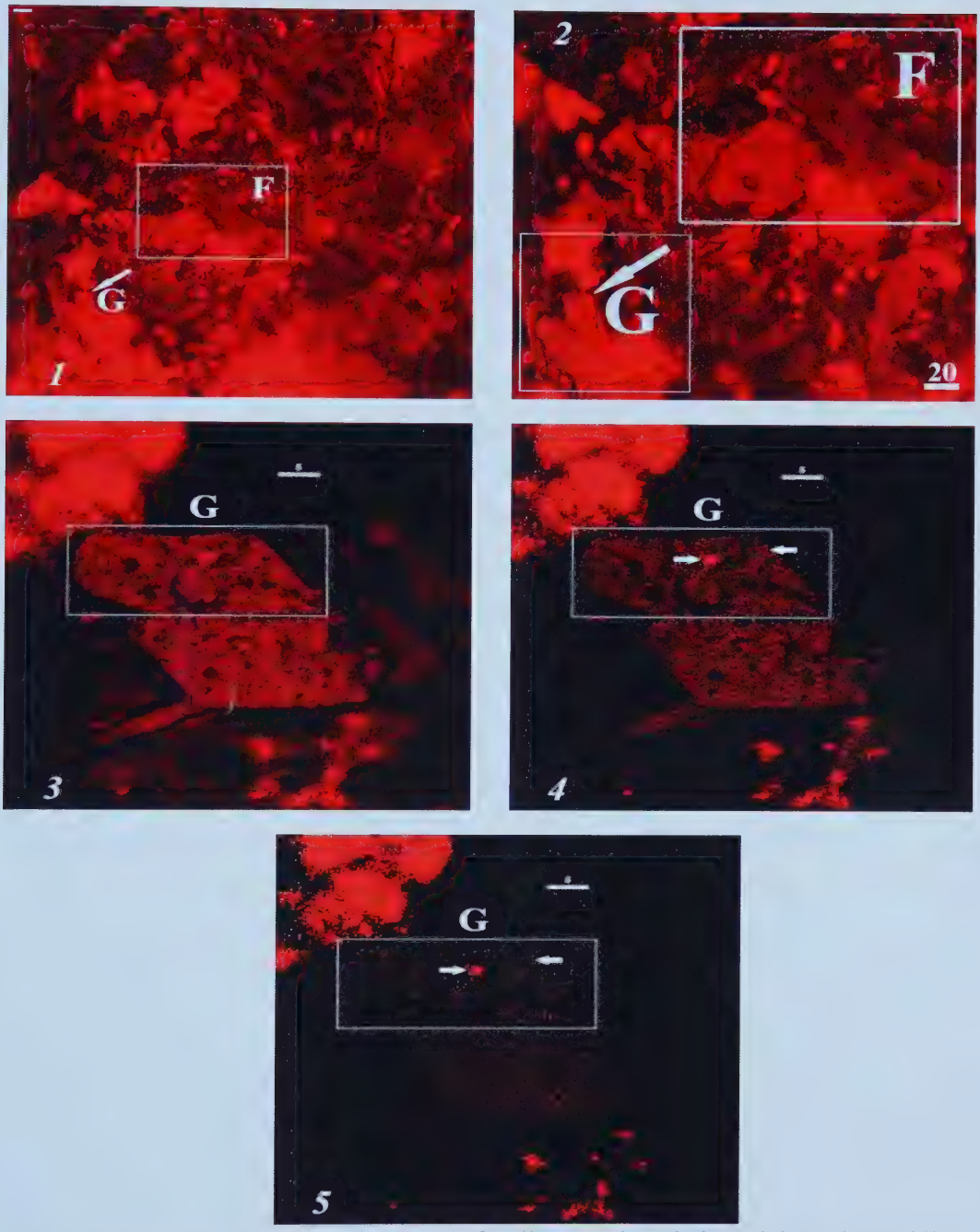

Figure 19: Confocal photomicrographs of cells on mineral G. Bright red propidium iodide signal is due to prolonged staining period (*1* & *2*). Cells-#1 area is indicated by left arrow (outlined section) in *4* and *5*, pointing to a bright, circular fluorescence signal; the second arrow to the right indicates cells-#2 area. The background is being progressively subtracted from images *3* to *5*. Intense red signal in the upper left hand corner of image *5* is due to oversaturation. Scale bar in *1* and *2* is 20µm; all other images are 5µm.

primarily by rods covered in a relatively thick biofilm. When the dark level or offset for the image is adjusted, thereby subtracting the background color of the stain, both areas and others on mineral G still give strong fluorescing signals (Figure 19-*5*). Some fluorescence might be associated with inorganic debris but the majority is believed to be from the many cells residing on mineral G. The correlation of the presence of cells in the above two areas lends support to this hypothesis.

Instrument limitations noted from Chip #1

The direct analysis of cellular or organic materials with the electron microprobe has highlighted an additional problem concerning the nature of the sample, which might also apply to difficulties observed with the analysis of nitrogen. Again, attention is brought to the cells on minerals C and E (Figures 14 & 17), which should have the highest concentrations of carbon. The cocci have the highest carbon concentrations but many of the rods give relatively weak signals, even the large group next to the cocci group on mineral E (Figure 14-*4*). There is a noticeable and sizeable difference in the thickness of the cells and it is believed that this is the reason for a discrepancy in the carbon signals. This is evident from looking at just the group of rods on mineral E (Figure 16*c*): a weak carbon signature emanates from the thickest outer edge of the group but the majority of cells give no signal. The electron beam penetrates to a certain depth in a sample (average of 3μm) and since the rods are less than 0.5μm in thickness, they are essentially invisible during analysis. The effect of size and the general nature of organic materials may not be a significant problem in young geological materials, especially if organisms are present and can be imaged or analyzed by means other than the electron microprobe but there might be larger implications using this particular technique for older materials where the original nature and concentrations of carbon and perhaps, other light elements, are not as optimal or as evident as it once was.

The second limitation applies to the confocal microscope. Almost immediately it was made clear that the working distance and depth of field at high magnification is quite limited in confocal microscopy, particularly with rock chips. Minerals, such as C and E, in the bottom of a vesicle are therefore, not ideal candidates for imaging. Minerals C and E could not be seen and focused on even with lower magnification objectives (20x),

which was disappointing since staining could have provided evidence as to any denaturing effects on DNA and RNA by the electron beam and mapping process. The last limitation, oversaturation due to an extensive staining period, has already been detailed.

Chip #2

This chip was, after thin sections, the first sample of 754 examined and consequently, the first of both chips in which microorganisms were found. SEM images were spectacular but element mapping was not deemed possible strictly due to extensive topography factors concerning the area in which the organisms were located. Figure 20 gives an overview of chip #2 and the areas where the main groups of microorganisms were found, are shown in Figure 21. Microbes were also located sporadically in other places on the sample but these two sites contained concentrated numbers. As was the case for chip #1, large pore spaces and areas of dense, tightly packed mineral grains within the basalt were bare of any organisms, which were confined to regions of smaller, well-connected porosity (site 'A') and spaces between minerals in vesicles that also contain pores (site 'B' and Figure 22). There seemed to be no preference for one mineral over another and access to porosity was probably a greater determinant for the organism's habitat.

The two morphologies, rods and cocci, observed in chip #1 are also found in chip #2 (Figure 23), however rods are even more prevalent. Cell sizes are, for the most part, comparable but there are differences. Cocci forms in this sample are smaller ($< / = 1\mu m$) than those in chip #1 (~$1.5\mu m$). The reverse holds true for the rods: sizes from <$0.5\mu m$ to $1\mu m$ are seen in chip #1 but the majority in chip #2 are > $1\mu m$. A marked contrast in the state of the cells of both chips is also observed. The cocci groups in chip #1 are possibly dessicated, in the process of dying or dead while the majority of rods are seemingly viable. On the contrary, both types of cells in chip #2 are plump, numerous and may be viable and where they are found, exists in substantial groups or clusters. As shown in Figures 23 and 24, copious amounts of cells throughout the sample are in the process of dividing and accordingly display prominent division bridges, a feature that forms during

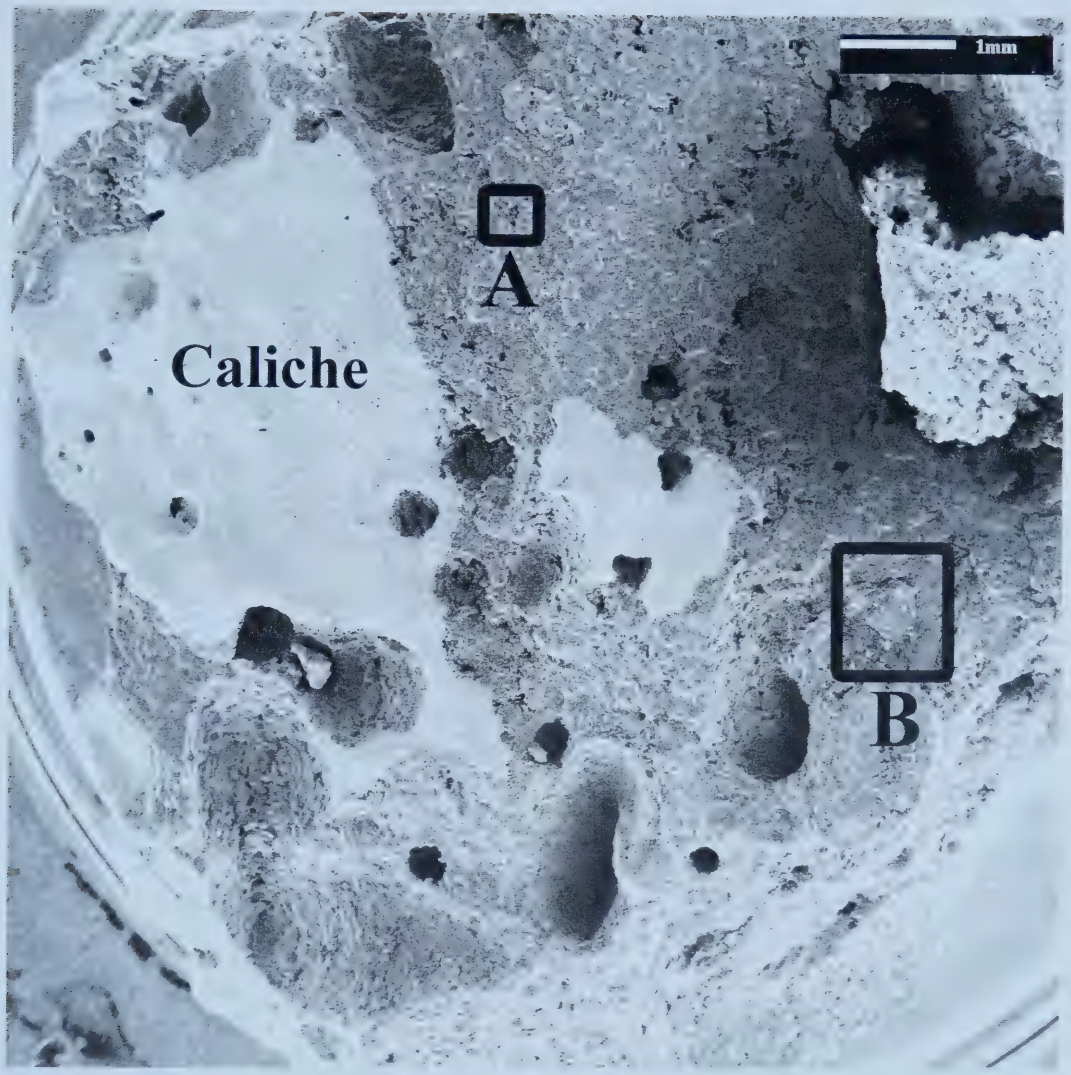

Figure 20: SEM photomicrograph showing overview of basalt chip #2. Microbes were found in the sites outlined and labeled as 'A' and 'B'. Large openings are vesicles. White coating is caliche, which is sparsely present on this specimen. The sample is coated with iridium. Scale bar is 1 mm.

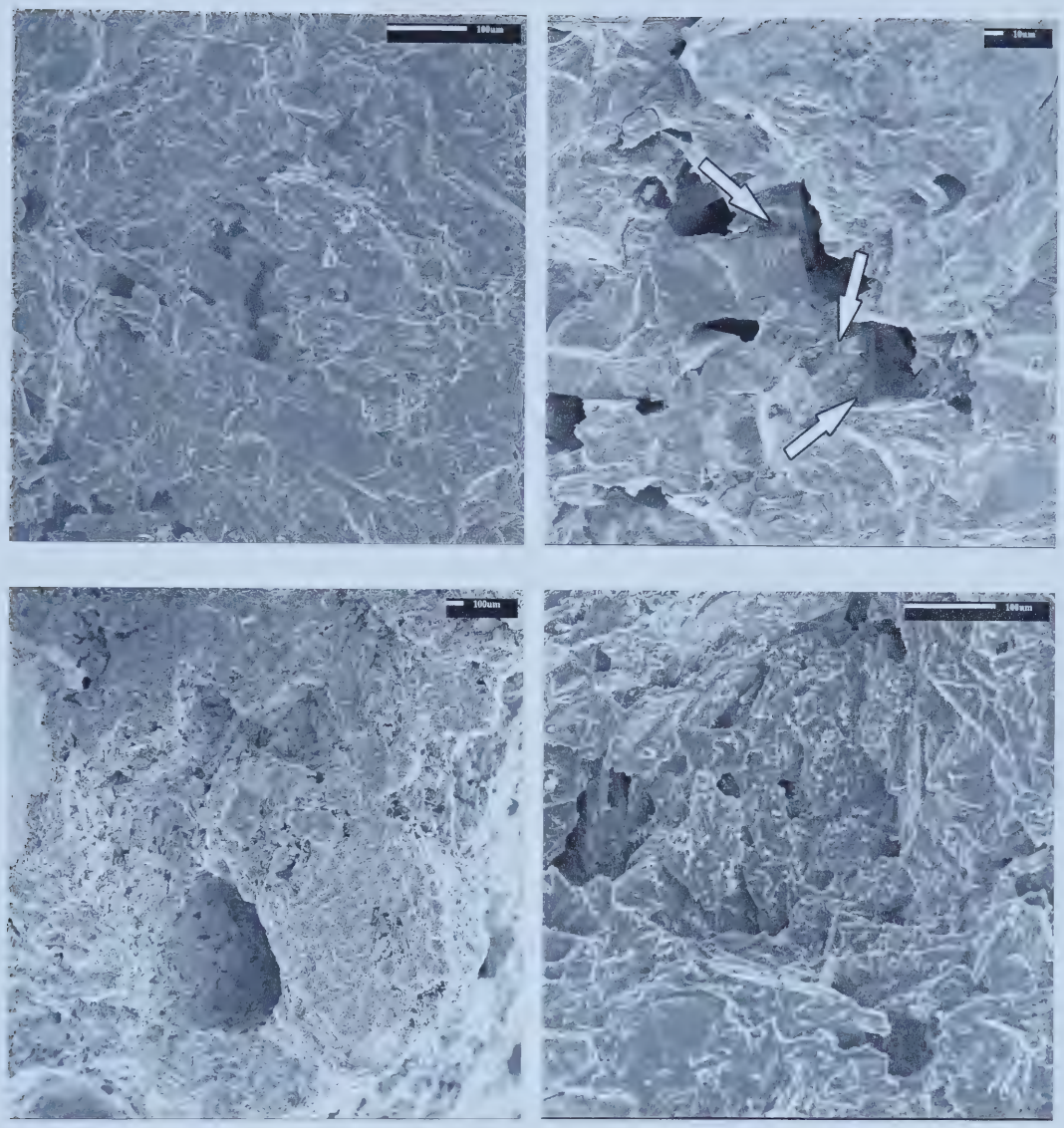

Figure 21: Magnified SEM images of 'A' (top) and 'B' (bottom) sites from Figure 20. Arrows indicate some areas in 'A' where microbes were found. Microorganisms were also found occupying spaces between crystals in 'B'. Scale bars are 100μm (top left); 10μm (top right); 100μm (bottom left and right).

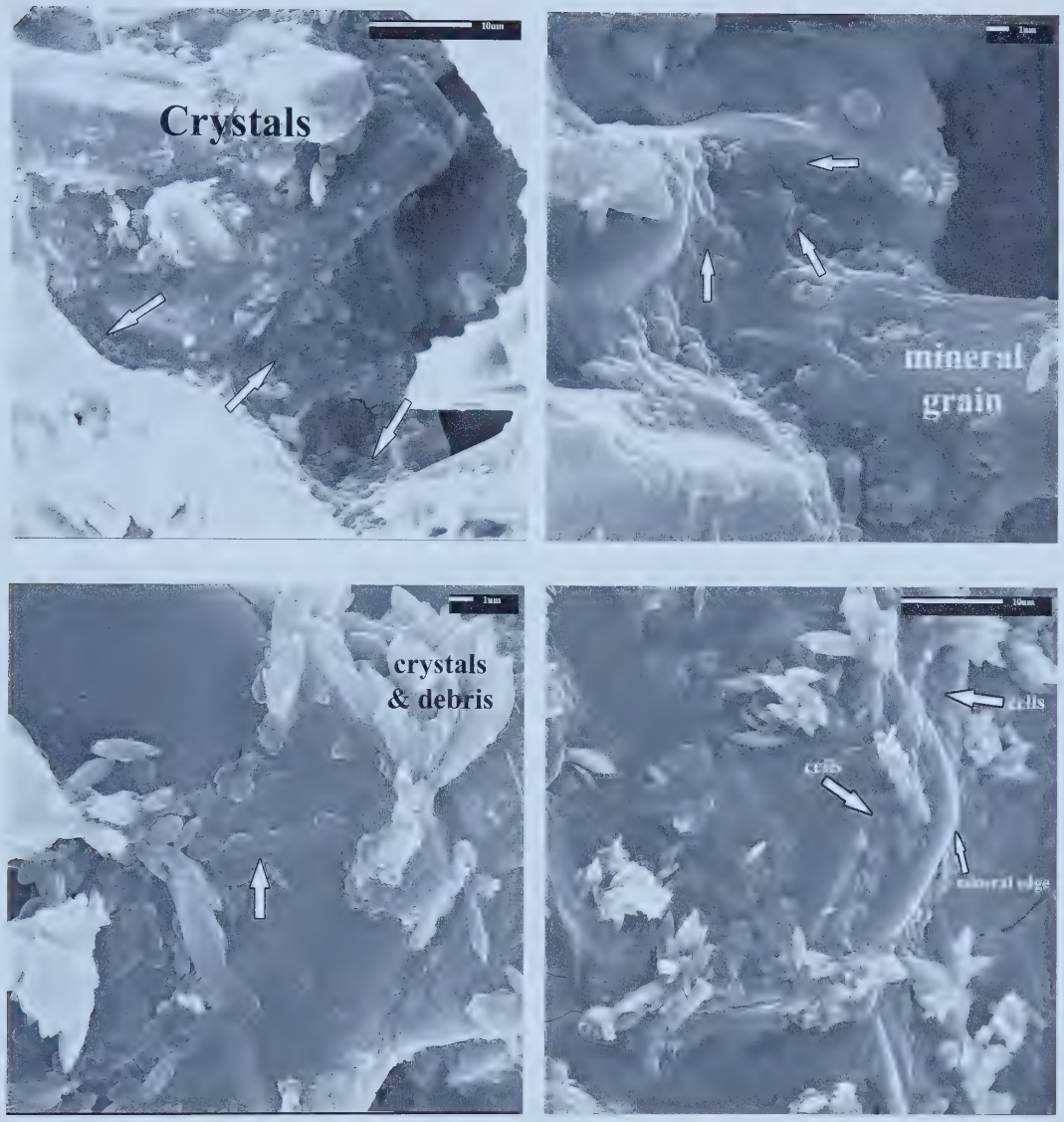

Figure 22: SEM images of cells coating and occupying spaces between mineral grains in sites 'A' and 'B'. Cell colonies are indicated by arrows in all images. The size of individual crystals and inorganic debris is clearly much larger than the cells, which are approximately 1μm in length. The arrow in the bottom left image points to a chain of cells, possibly exhibiting branching in one direction. Scale bars: 1μm (top right and bottom left); 10μm (top left and bottom right).

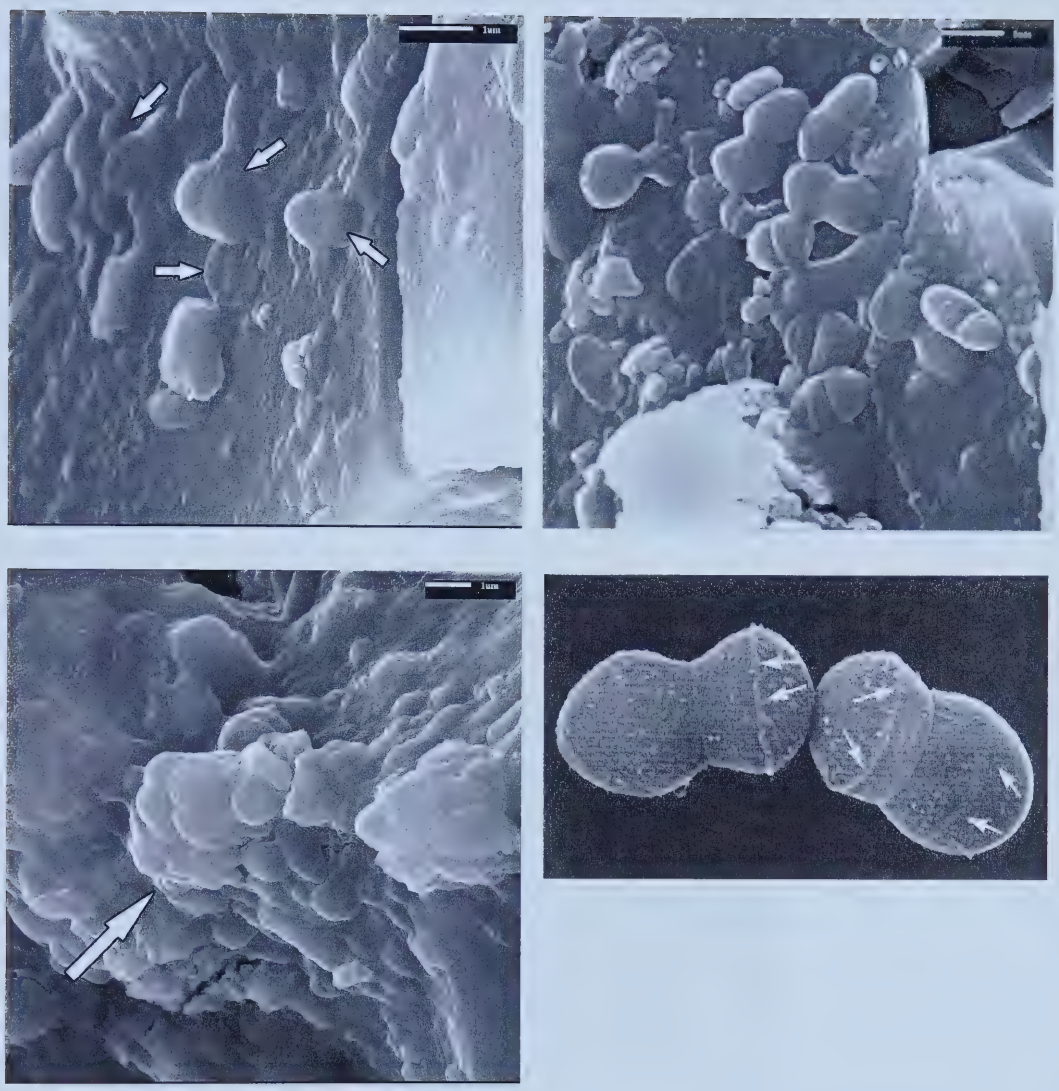

Figure 23: SEM photomicrographs of rods and cocci (indicated by arrows) in chip #2. The cells are attached to mineral surfaces, probably through EPS. Division bridges on some cells are clearly observed in the top two images, indicating that these individuals were in the process of dividing. Bottom right image is from Madigan et al., (1997); arrows point to division bridges formed during synthesis of cell wall on gram-positive bacteria. A cluster of cocci at bottom seems firmly attached to a mineral grain and thickly coated by EPS. Scale bars on all images are 1μm.

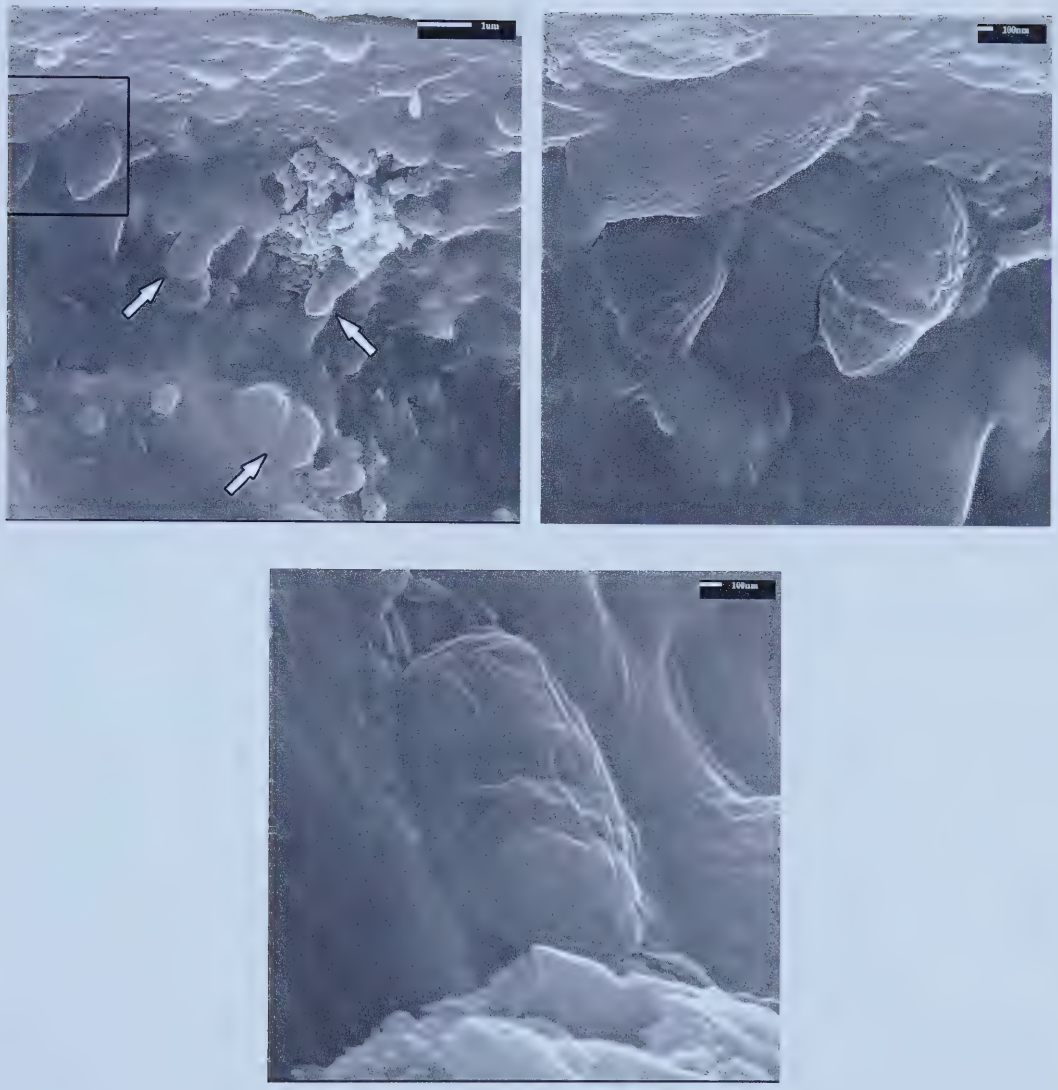

Figure 24: SEM images of microorganisms in chip #2. A bacteria colony (top left); arrows indicate individuals or clusters of rods and cocci. Top right image is the outlined group of rods from the colony in the previous image. A single, shriveled rod is shown in the bottom image; magnification is 40,000x. Scale bars are 1μm (top left); 100 nm (top right and bottom).

cell wall synthesis and which represents the junction between new and old cell wall or peptidoglycan (Madigan et al., 1997b). This demonstrates that the cells were viable prior to iridium coating and SEM imaging. That they are sheltered within generous amounts of EPS and associated biofilms is also unmistakable. It is probable that the microorganisms in both chips are different species but it is also just as likely that the cells have been present for a longer period in chip #2 than those in chip #1.

Another characteristic of chip #1 that seems absent in chip #2 is the cryptocrystalline material. The images show inorganic material is present within cell clusters but crystals in the general area do not have the cryptocrystalline features, even though it has been found on crystals in other areas of the chip. However, whether cryptocrystalline material is lacking in the minerals of the primary sites on chip #2 or the microorganisms themselves totally obscured it, is unknown. One feature discovered on chip #2, not far from site 'A', and seen nowhere else on either chips, appears to be a tunnel or channel that might have been created by microorganisms (Figure 25). Several tunnels are seen to connect inside the main channel, which overall has a coarse, uneven appearance and the appropriate dimensions through which a bacterium would fit (~1x2μm for the smallest, inner tunnel). On closer inspection, the inside appears to be coated with the same type of film that covers all of the cells in this chip, probably EPS and in which, spherical looking features appear entombed (Figure 25*d*). In the basalt, the walls of natural cavities such as deep vesicles, are quite smooth and do not have films, of any type. Unfortunately, EDS analysis could not be done inside the channel but an analysis done just outside the opening shows potassium, titanium and iron are present. Some features (Figure 25*e, f, g*) on the walls of the mineral in which the channel is located have the appearance of microorganisms but are actually the edges of crystals that had been on the verge of crystallizing as the magma cooled. They are enriched in silicate elements, silicon, aluminum, magnesium and oxygen, and are also much smaller than the size commonly accepted for prokaryotic cells.

Fluorescence staining of chip #2 was quite rewarding because cells as well as the act of cell division was imaged. Also, the staining time for this chip was drastically diminished (5 min), substantially improving the contrast between the background and fluorescence signal from the cells. Two or perhaps three cells in the process of dividing

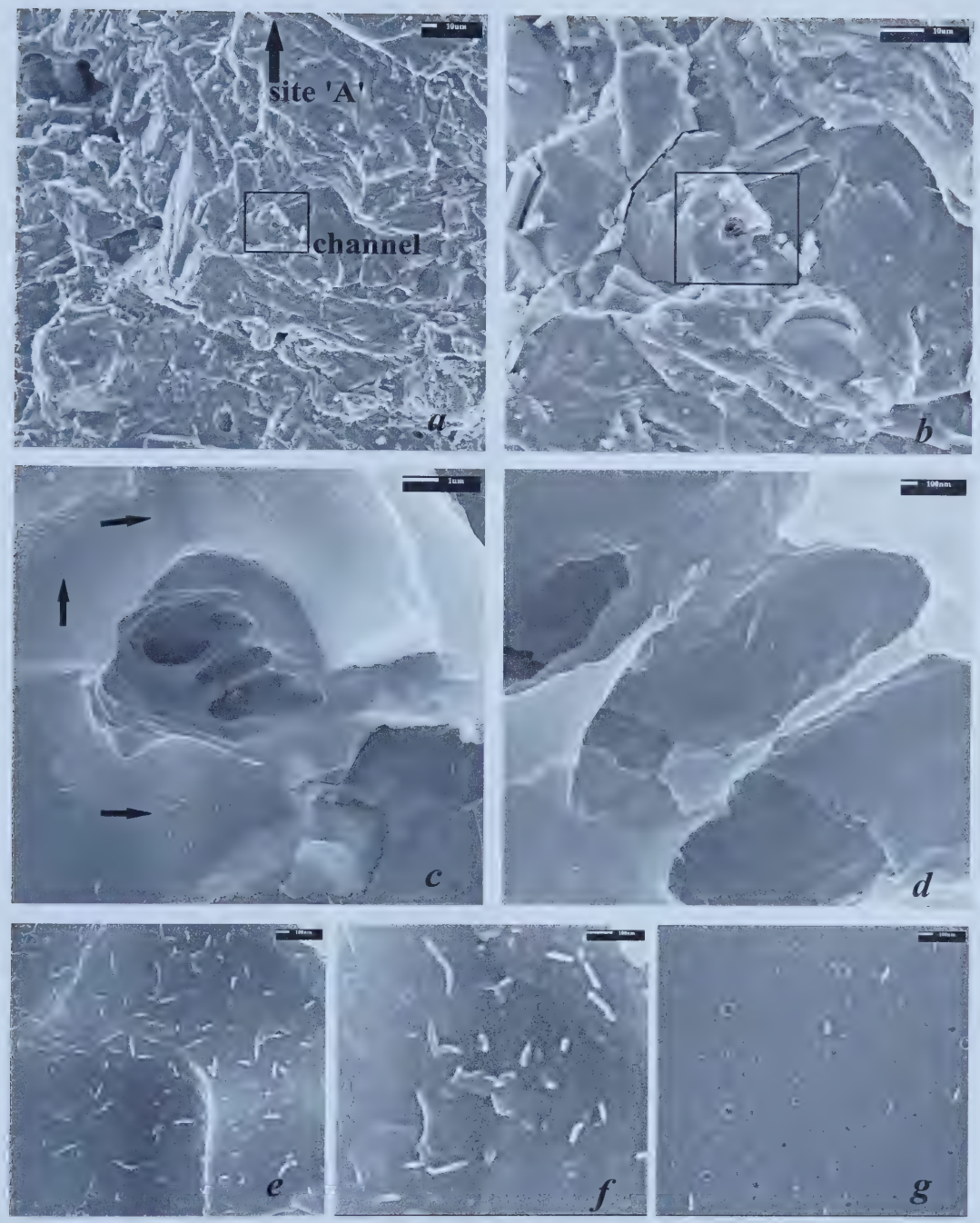

Figure 25: SEM photomicrographs of a possible biogenic tunnel. The tunnel is found in proximity to site 'A' and is outlined in images *a* and *b*. A magnified view of the interior of the tunnel in *d*, shows embedded, spherical features which could be the remains of cellular material covered by a thick layer of EPS. Arrows in *c* point to minerals that were in the process of crystallizing. These seemingly biogenic features are magnified in *e*, *f* and *g* and they illustrate the ease with which abiogenic entities can be mistaken for biogenic elements. Scale bars: 10µm (*a*, *b*); 1µm (*c*); 100nm (*d*, *e*, *f*, *g*).

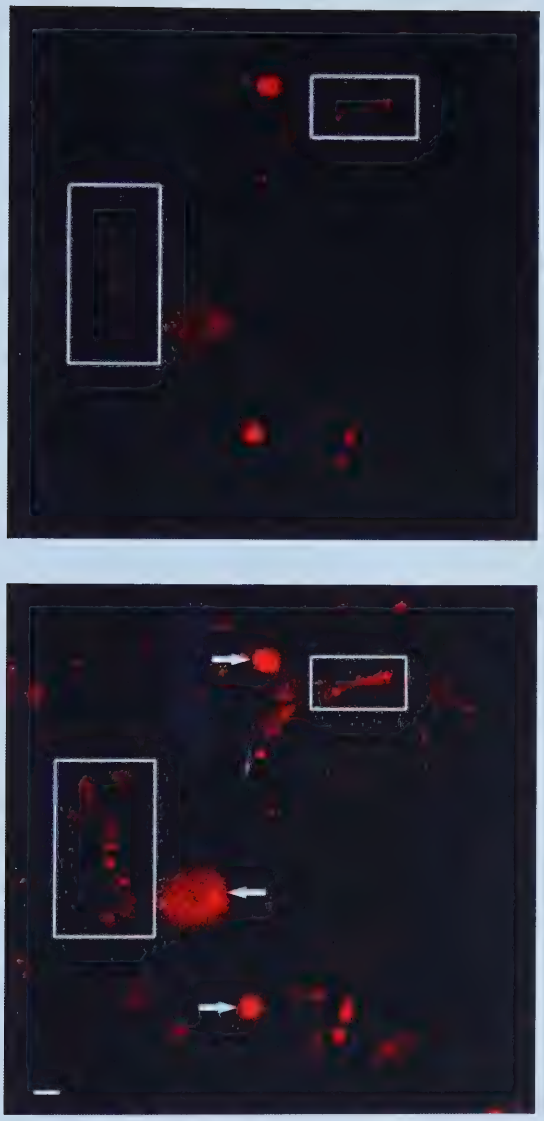

Figure 26: Confocal microscopy fluorescence images from chip #2, site 'A'. Both images are of the same area. Organisms possibly in the process of dividing are outlined; prominent PI concentrations within the cells could be representative of dividing nucleoids. The top image has the background levels of stain color subtracted, which allows the probable signal from the stained nucleoids to be clearly seen. The bottom image has the color adjusted with background levels, allowing the outline of the dividing cells to be seen. Arrows in the bottom image indicate false color artifacts produced during imaging. Scale bar is 2µm and applies to both images.

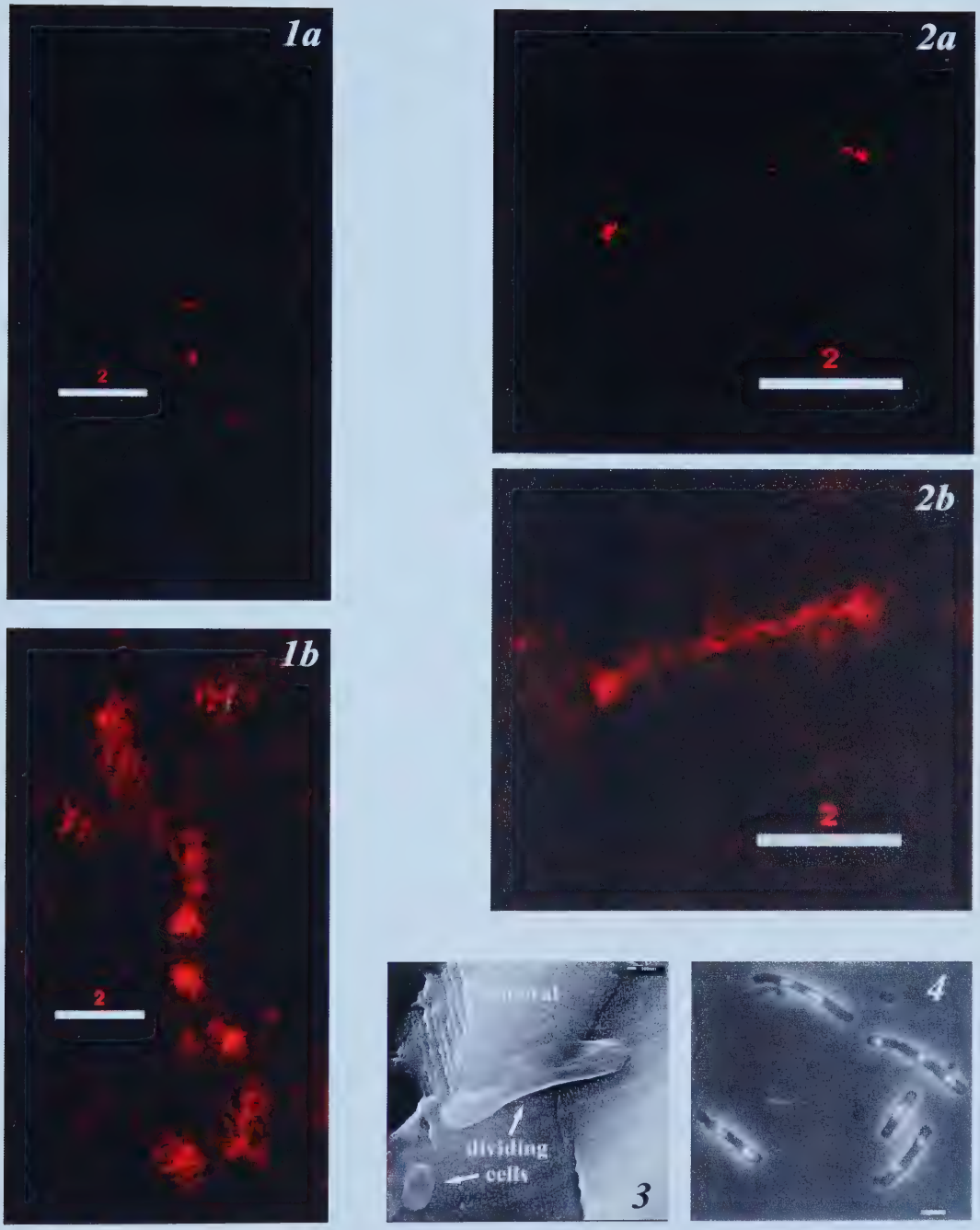

Figure 27: Magnified fluorescence images from Figure 26 of possible dividing microorganisms (*1b* & *2b*). Background is subtracted in top images (*1a* & *2a*), allowing the stained nucleoids to be seen. Image *3* is an SEM example from chip #2 of what the stained organism in *2b* might look like (scale bar is 100nm). Image *4* is from Neidhardt et al. (1990) showing ethidium bromide stained dividing nucleoids of *E. coli* (scale bar is 1μm).

were captured and are presented in Figures 26 and 27. As was the case for chip #1, the images are shown with and without the background. The nuclear region of prokaryotic and eukaryotic cells is considerably different: eukaryotes have a true nucleus, which is a separate membrane-bound structure that houses DNA, a structure that is absent in prokaryotes. A single molecule of DNA, called a chromosome, serves as the nucleus and exists in an essentially unconfined state in prokaryotes. The chromosome however, has a tendency to amass as a more or less distinct structure within the prokaryotic cell and is termed the nucleoid. When a prokaryote divides, the nucleoids separate resulting in distinct individuals with completely replicated genetic material (Madigan et al., 1997b; Neidhardt et al., 1990). It is believed that this process of division was imaged and that the intense fluorescing entities within the supposed outline of cells magnified in Figure 27–*1b* and *2b* are nucleoids. Fluorescing bodies also believed to be cells in the same area of those undergoing division, are shown in Figure 28. Some fluorescence may be due to the stain binding with inorganic debris but the distinct signals remaining after the background has been subtracted, as well as the shape and size of the imaged features would suggest much of the fluorescence is due to the presence of microorganisms. Lastly, imaging of fluorescing cells in this chip was made easier, possibly for two reasons: (1) the cells are more viable, whereas in chip #1 many are dead, dessicated or in the process of dying; (2) imaging at the highest magnification objectives (100x) was possible for this chip but not for chip #1.

It should be mentioned that rock chips of sample 687 were also investigated with the SEM but microorganisms or other evidence of biogenicity was non-existent. This is a curious and interesting find considering sample 687 is much older and a pedogenic or subsurface sample while sample 754 is subaerial and has never been in contact with a soil environment.

Future Work

Geomicrobiology

Finding microorganisms inhabiting the interior of basalts and being able to image them in the process of dividing is an extraordinary but initial step in this work. Larger

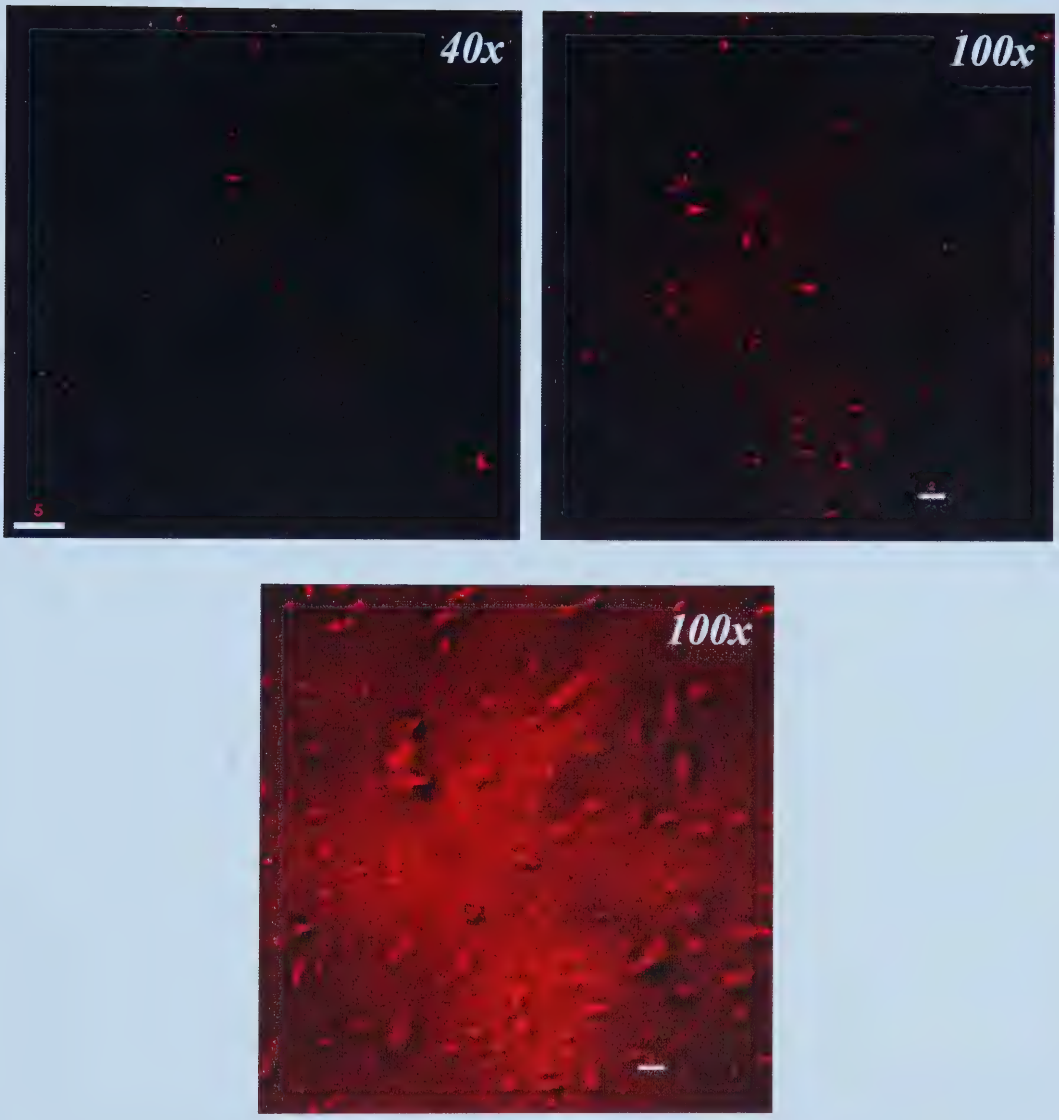

Figure 28: Fluorescence images of another area in site 'A' possibly containing microorganisms. The oil immersion objectives used to take the images, are indicated. Background has been subtracted in top two images and features that might be indicative of microorganisms are observed. The outline of possible cells can also be seen in the bottom image. Scale bars are 5µm (top left) and 2µm (top right & bottom).

and perhaps, more important questions are: (1) what are these organisms – Archaea, Bacteria, eukaryotes? (2) what are they doing to the minerals and are they altering the rock in any way? (3) if they are altering minerals, why are they doing it; for example, is it a means of obtaining energy as in other types of bacteria like chemolithotrophs? (4) what metabolic or chemical process allows them to alter minerals? (5) what allows the organisms to exist inside the basalt, especially in terms of nutrient and water availability? (6) how did the organisms get into the basalt?

Examination of the microorganisms and features in chip #1 suggests the cells are attracted to the cryptocrystalline material but whether they are actually utilizing it for metabolic purposes in order to keep living in the environment they are in, is undetermined. The organisms in both chips are most likely prokaryotic and possibly belong to the evolutionary lineage Bacteria but this is inconclusive and only a speculation, based on the fact that most Archaea are primarily anaerobes and thrive in a variety of extreme conditions (Madigan et al., 1997c), typically where water (fresh water or marine) is abundant. Biofilms and other cellular aggregates are also rarely formed by Archaea (Atlas and Bartha, 1998b). There is no suggestion, at this time, that the microorganisms inhabiting the caliche have any relation to those within the basalt. Apparently the organisms within the caliche may be a type of endolithic lichen; a eukaryote (Garvie et al., 2000). It is almost certain that the microorganisms within the basalt came from the terrestrial environment.

Instrumentation

Additional concerns regarding the techniques used also need to be addressed. For example, nitrogen analysis during element mapping is problematic and raises important questions concerning the quality and accuracy of the data obtained, not just in this study but those that have been previously conducted using the same microprobe and experimental conditions. It has not been determined if the problem is instrumental, for example the particular electron microprobe used in this study, different attachments required depending on the type of analysis to be done (such as a thinner counter window for light elements) or perhaps, the problem is systematic of the type of instrumentation being used for this type of analysis, in other words, the electron microprobe may not be

the ideal instrument for the analysis of nitrogen and other light elements. While instrumental factors, some more than others, might contribute to the overall light element analysis problems, I believe that continuous complications arising from the analysis of nitrogen and sometimes carbon, are due specifically to contamination from the break-down and deposition of carbon from vacuum pump oils. There is a slight possibility that the problems could also be experimental. The samples being analyzed may in fact have no nitrogen or have levels that are below the level of detection but these are minimal compared to the impact of the previous and heretofore, ignored factor.

Steps which I believe are integral and which need to be implemented in future studies to increase the accuracy of results obtained from element mapping include (1) using a carbon-free epoxy, such as sodium metasilicate (Mathez and Delaney, 1981) which removes another source of carbon contamination and the reliance on using chlorine as a detector for commonly used carbon based epoxies; (2) preparing separate standards for geomicrobiological work that are coated with iridium and not carbon, with which the standards used in this work were coated; (3) employing the use of a cold finger or oil-free turbomolecular pumps (Mathez and Delaney, 1981; Cox, 1983) to reduce carbon contamination from the break-down of hydrocarbons from pump oils in the vacuum system of the microprobe. In essence, further work needs to be done in order to improve and optimize the conditions required for precise and accurate light element analysis when using the electron microprobe.

Investigations regarding confocal microscopy and fluorescing staining also need to be considered, especially in regards to its limited use, thus far, in a few geological studies. I believe confocal microscopy has the potential to be a great tool in geomicrobiological work but this will only be accomplished by continued experimentation with the instrument and by undertaking a direct and willful approach to understand the capabilities, limitations and applications of various types of fluorescent probes and more importantly, their performance in different geological materials as well as within the microorganisms that are attached to these materials. For instance, some stains, such as DAPI, have enjoyed extensive use especially by geologists, but whether this is due to its capabilities as a nucleic acid stain, ease of use or some other factor is not known. These aspects however, are not unique to DAPI and it is my belief that its

popularity has more to do with applying what has been the 'norm' in most types of geomicrobiological studies and a general lackadaisical attitude towards exploring and experimenting with different stains.

Conclusions

The aim of this study was to search for and document evidence of biogenicity in two samples of desert basalts from a hot desert environment in Arizona. Three different techniques were employed as biosignatures in order to find life or evidence of life: scanning electron microscopy, electron microprobe element mapping and fluorescence staining with confocal microscopy. These techniques also provided independent and in the case of one sample, corroborating evidence of biogenicity. In addition, a novel method involving fluorescence staining of iridium-coated samples was attempted and shown to work. Remains of organic material is suspected in three channels of pedogenic sample 687 but the evidence at this time is inconclusive and requires further work; however, microorganisms were found in two rock chips of subaerial sample 754. The organisms are most likely prokaryotic and two morphologies, in various life states, are observed. Rods are clearly predominant in both chips and cocci are present but display substantial desiccation in one rock chip. There are variations in cell sizes within each morphology and one chip is rife with dividing rods and significant amounts of EPS and biofilm material. This chip also contains a tunnel structure, which could have been produced by organisms. Despite the tunnel structure, there is no suggestion that the microorganisms are directly altering minerals in any way but they may be utilizing cryptocrystalline material, surrounding many minerals, as a source of nutrients for metabolic processes. Further work is required to establish the identity of the organisms and determine their mode of survival within the basalt. These techniques and the particular environment to which they were applied on Earth, may also serve as a template in the search for present or past life on Mars.

In regards to instrumentation and data obtained, some concerns are noted specifically for element mapping and confocal microscopy. Low concentrations typically

obtained from nitrogen analysis are most likely due to carbon contamination within the instrument but steps can be taken to minimize the problem. This problem has been prevalent but it was not realized that a solution existed until research was undertaken for this thesis. The same contamination can interfere with the analysis of other light elements and therefore, has the potential to significantly impact the accuracy of the data obtained. Confocal microscopy and fluorescence staining are excellent tools for geomicrobiological work but further experimentation is required to fully understand their limitations and potential.

References

Allaby, A., and M. Allaby, (Eds.), *Oxford Concise Dictionary of Earth Sciences*, Oxford University Press, Oxford, 1991.

Anderson, R. T., F. H. Chapelle, and D. R. Lovley, Evidence against hydrogen-based microbial ecosystems in basalt aquifers, *Science*, *281*, 976-977, 1998.

Atlas, R. M., and R. Bartha, Microbial Ecology: Historical Development, in *Microbial Ecology: fundamentals and applications*, 4th edition, pp. 2-17, Benjamin/Cummings, California, 1998a.

Atlas, R. M., and R. Bartha, Microbial Evolution and Biodiversity, in *Microbial Ecology: fundamentals and applications*, 4th edition, pp. 27-54, Benjamin/Cummings, California, 1998b.

Arculus, R. J., and D. A. Gust, Regional Petrology of the San Francisco Volcanic Field, Arizona, USA, *J. Petrol.*, *36*, 827-861, 1995.

Barker, W. W., S. A. Welch, S. Chu, and J. F. Banfield, Experimental observations of the effects of bacteria on aluminosilicate weathering, *Am. Mineral.*, *83*, 1551-1563, 1998.

Baross, J. A., Hydrothermal vents – thermophiles and hyperthermophiles, in *McGraw-Hill Yearbook of Science and Technology*, pp. 180-183, McGraw-Hill, New York, 1998.

Blake, D., M. Schulte, and T. Bunch, Submicroscopic morphological features and mineralogies as biomarkers (abstract), *GSA Annual Meeting*, Denver, CO, 51813, 1999.

Bloomfield, A. L., Chemical, isotopic and petrographic evidence for magma mixing in the San Francisco Volcanic Field, Arizona, *Ph.D. thesis*, The University of Michigan, Ann Arbor, 1990.

Brasier, M. D., O. R. Green, A. P. Jephcoat, A. K. Kleppe, M. J. Van Kranendonk, J. F. Lindsay, A. Steele, and N. V. Grassineau, Questioning the evidence for Earth's oldest fossils, *Nature*, *416*, 76-81, 2002.

Burde, S., L. E. Hersman, B. L. Marrone, J. D. Farmer, and D. S. McKay, Fluorescent staining of microfossils using biological stains (abstract), in *Lunar and Planet. Science, XXX; Papers presented to the Thirtieth lunar and planetary science conference*, Houston, TX, 1999a.

Burde, S., B. L. Marrone, J. D. Farmer, and L. E. Hersman, In-situ detection of DNA in microfossils by fluorescent staining, in *Geological Society of America, 1999 annual meeting*, Denver, CO, 1999b.

Chapelle, F. H., K. O'Neill, P. M. Bradley, B. A. Methe, S. A. Ciufo, L. L. Knobel, and D. R. Lovley, A hydrogen-based subsurface microbial community dominated by methanogens, *Nature, 415*, 312-315, 2002.

Christensen, B. E., and W. G. Characklis, Physical and chemical properties of biofilms, in *Biofilms*, edited by W. G. Characklis and K. C. Marshall, pp. 93-129, Wiley-Interscience, New York, 1990.

Cox, M. G. C., Experimental determination of x-ray intensities, in *Quantitative Electron-Probe Microanalysis*, edited by V. D. Scott and G. Love, pp. 125-146, Ellis Horwood Ltd., England, 1983.

Craig, H., Isotopic standards for carbon and oxygen and correlation factors for mass-spectrometric analysis of carbon dioxide, *Geochim. Cosmochim. Acta., 12*, 133-149, 1957.

Craig, H., Standards for reporting concentrations of deuterium and ^{18}O in natural waters, *Science, 133*, 1702-1703, 1961.

Delaney, J. R., Life on the seafloor and elsewhere in the solar system, *Oceanus, 41*, 10-13, 1998.

D'Hondt, S., S. Rutherford, and A. Spivack, Global patterns of microbial activity in deep-sea sediments, *Eos Trans AGU, F236*, 2000.

Ehrlich, H. L., Introduction, in *Geomicrobiology*, 2nd edition, pp. 1-4, Marcel Dekker, New York, 1990a.

Ehrlich, H. L., The Lithosphere as a Microbial Habitat and The Hydrosphere, in *Geomicrobiology*, 2nd edition, pp. 42-95, Marcel Dekker, New York, 1990b.

Fedo, C. M., and M. J. Whitehouse, Metasomatic origin of quartz-pyroxene rock, Akilia, Greenland, and implications for Earth's earliest life, *Science*, *296*, 1448-1452, 2002.

Fisk, M. R., S. J. Giovannoni, and I. H. Thorseth, Alteration of oceanic volcanic glass: textural evidence of microbial activity, *Science*, *281*, 978-980, 1998.

Fredrickson, J. K., and T. C. Onstott, Microbes deep inside the Earth, *Sci. Am.*, 68-73, 1996.

Friedmann, E. I., Endolithic Microbial life in hot and cold deserts, *Orig. Life 10*, 223-235, 1980.

Furnes, H. and H. Staudigel, Biological mediation in ocean crust alteration: how deep is the deep Biosphere?, *Earth Planet. Sci. Lett.*, *166*, 97-103, 1999.

Furnes, H., K. Muehlenbachs, T. Torsvik, I. H. Thorseth, and O. Tumyr, Microbial fractionation of carbon isotopes in altered basaltic glass from the Atlantic Ocean, Lau Basin and Costa Rica Rift, *Chem. Geol.*, *173*, 313-330, 2001a.

Furnes, H., K. Muehlenbachs, O. Tumyr, T. Torsvik, and C. Xenophontos, Biogenic alteration of volcanic glass from the Troodos ophiolite, Cyprus, *J. Geol. Soc. London*, *158*, 75-84, 2001b.

Gabriel, B. L., Thin Films, in *SEM: A User's Manual for Materials Science,* pp. 149-170, American Society For Metals, Ohio, 1985.

Garvie, L. A. J., F. Bungartz, T. H. Nash, and L. P. Knauth, Caliche Dissolution and Calcite Biomineralization by the Endolithic Lichen Verrucaria rubrocincta Breuss in the Sonoran Desert (abstract), *V. M. Goldschmidt Conference: Journal of Conference Abstarcts* (CD-ROM), *5*, Cambridge Publications, Cambridge, 2000.

Herman, B., Single and multiphoton microscopy, in *Fluorescence Microscopy, Royal Microscopical Society*, *40*, 2nd edition, pp. 89-96, Springer-Verlag, New York, 1998.

Hirsch, P., F. E. W. Eckhardt, and R. J. Palmer Jr., Methods for the study of rock - inhabiting microorganisms – a mini review, *J. Microbiol. Methods, 23*, 143-167, 1995.

Holden, J. F., M. Summit, and J. A. Baross, Thermophilic and hyperthermophilic microorganisms in 3-30 degrees C hydrothermal fluids following a deep-sea volcanic eruption, *FEMS Microbiol. Ecol.*, *25*, 33-41, 1998.

Huber, H., G. Huber, and K. O. Stetter, A modified DAPI fluorescence staining procedure suitable for the visualization of lithotrophic Bacteria, *Syst. Appl. Microbiol.*, *6*, 105-106, 1985.

Huber, H., M. J. Hohn, R. Rachel, T. Fuchs, V. C. Wimmer, and K. O. Stetter, A new phylum of Archaea represented by a nanosized hyperthermophilic symbiont, *Nature, 417*, 63-67, 2002.

Kapuscinski, J., DAPI: a DNA-specific fluorescent probe, *Biotech. & Histochem., 70*, 220-233, 1995.

Karsten, F.H., Introduction to fluorescent probes: Properties, History and Applications, in *Fluorescent and Luminescent Probes for Biological Activity: a practical guide to technology for quantitative real-time analysis*, edited by W. T. Mason, 2nd edition, pp. 17-38, Academic Press, Great Britain, 1999.

Madigan, M. T., J. M. Martinko, and J. Parker, Nutrition and Metabolism, in *Brock Biology of Microorganisms*, 8th edition, pp. 109-144, Prentice-Hall, New Jersey, 1997a.

Madigan, M. T., J. M. Martinko, and J. Parker, Cell Biology, in *Brock Biology of Microorganisms*, 8th edition, pp. 52-105, Prentice-Hall, New Jersey, 1997b.

Madigan, M. T., J. M. Martinko, and J. Parker, Introduction: An overview of microbiology and cell biology, in *Brock Biology of Microorganisms*, 8th edition, pp. 1-20, Prentice-Hall, New Jersey, 1997c.

McCrea, J.M.., On the isotope chemistry of carbonates and a paleotemperature scale, *J. Chem. Phys.*, *18*, 849-857, 1950.

Mathez, E. A., and J. R. Delaney, The nature and distribution of carbon in submarine basalts and peridotite nodules, *Earth Planet. Sci. Lett.*, *56*, 217-231, 1981.

Mittlefehldt, D. W., The latest news from Mars, *Science*, *287*, 1601-1602, 2000.

Neidhardt, F. C., J. L. Ingraham, and M. Schaechter, Structure and Function of Bacterial Cell Parts, in *Physiology of the Bacterial Cell: A Molecular Approach*, pp. 30-59, Sinauer Associates, Inc., Massachusetts, 1990.

Nomenclature Committee of the Royal Microscopical Society, *Royal Microscopical Society Dictionary of Light Microscopy*, Oxford University Press, New York, 1989.

Pedersen, K., S. Ekendahl, E. L. Tullborg, H. Furnes, I. Thorseth, and O. Tumyr, Evidence of ancient life at 207 m depth in a granitic acquifer, *Geology, 25*, 827-830, 1997.

Reysenbach, A. L. and E. Shock, Merging genomes with geochemistry in hydrothermal ecosystems, *Science, 296*, 1077-1082, 2002.

Schlesinger, W. H., The formation of caliche in soils of the Mojave Desert, California, *Geochim. Cosmochim. Acta.*, *49*, 57-66, 1985.

Schopf, J. W., A. B. Kudryavtsev, D. G. Agrestl, T. J. Wdowiak, and A. D. Czaja, Laser-Raman imagery of Earth's earliest fossils, *Nature*, *416*, 73-76, 2002.

Scott, V. D., Wavelength-dispersive x-ray spectrometers, in *Quantitative Electron-Probe Microanalysis*, edited by V. D. Scott and G. Love, pp. 64-79, Ellis Horwood Ltd., England, 1983.

Staudigel, H., A. Yayanos, R. Chastain, G. Davies, E. A. Th. Verdurmen, P. Schiffman, R. Bourcier, and H. De Baar, Biologically mediated dissolution of volcanic glass in seawater, *Earth Planet. Sci. Lett.*, *164*, 233-244, 1998.

Stetter, K.O., Extremophiles and their adaptation to hot environments, *FEBS Lett.*, *452*, 22-25, 1999.

Stevens, T. O., and J. P. McKinley, Lithoautotrophic microbial ecosystems in deep basalt aquifers, *Science*, *270*, 450-454, 1995.

Stolz, J. F., Structure of Microbial Mats and Biofilms, in *Microbial Sediments*, edited by R. E. Riding and S. M. Awramik, pp. 1-6, Springer-Verlag, Heidelberg, 2000.

Summit, M., and J. A. Baross, Thermophilic subseafloor microorganisms from the 1996 North Gorda Ridge eruption, *Deep-Sea Res.*, *45*, 2751-2766, 1998.

Thorseth, I.H., T. Torsvik, H. Furnes, and K. Muehlenbachs, Microbes play an important role in the alteration of oceanic crust, *Chem. Geol.*, *126*, 137-146, 1995.

Tingle, T. N., E. A. Mathez, and M. F. Hochella Jr., Carbonaceous matter in peridotites and basalts studied by XPS, SALI, and LEED, *Geochim. Cosmochim. Acta.*, *55*, 1345-1352, 1991.

Tobin, K. J., T. C. Onstott, M. F. DeFlaun, F. S. Colwell, and J. Fredrickson, In situ imaging of microorganisms in geologic material, *J. Microbiol. Methods, 37*, 201-213, 1999.

Torsvik, T., H. Furnes, K. Muehlenbachs, I. H. Thorseth, and O. Tumyr, Evidence for microbial activity at the glass-alteration interface in oceanic basalts, *Earth Planet. Sci. Lett., 162*, 165-176, 1998.

Westall, F., A. Steele, J. Toporski, M. Walsh, C. Allen, S. Guidry, D. McKay, E. Gibson, and H. Chafetz, Polymeric substances and biofilms as biomarkers in terrestrial materials: Implications for extraterrestrial samples, *J. Geophys. Res., 105*(E10), 24,511-24,527, 2000.

Williams, S. C., Y. Hong, D. C. A. Danavall, H. M. Howard-Jones, D. Gibson, M. E. Frischer, and P. G. Verity, Distinguishing between living and nonliving bacteria: Evaluation of the vital stain propidium iodide and its combined use with molecular probes in aquatic samples, *J. Microbiol. Methods, 32*, 225-236, 1998.

Wingender, J., T. R. Neu, and H. C. Flemming, What are Bacterial Extracellular Polymeric Substances?, in *Microbial Extracellular Polymeric Substances: characterization, structure and function*, edited by J. Wingender, T. R. Neu and H. C. Flemming, pp. 1-15, Springer-Verlag, Heidelberg, 1999.

Wolfaardt, G. M., J. R. Lawrence, and D. R. Korber, Function of EPS, in *Microbial Extracellular Polymeric Substances: characterization, structure and function*, edited by J. Wingender, T. R. Neu and H. C. Flemming, pp. 171-195, Springer-Verlag, Heidelberg, 1999.

Appendix A

Sample 741A

Sample 741A is the third basalt sample obtained from Dr. Knauth and is also from the San Francisco Volcanic Field. The sample is also Pleistocene in age, ~ 175,000-800,000 years old (American stage "Tappan") and was taken from a highly weathered roadcut. It is a pedogenic carbonate sample from a well-defined vertical petrocalcic zone (L. P. Knauth, Arizona State University, personal communication, 2002) and contains only minute areas of basaltic material. As with the other two samples, the basalt in 741A is porphyritic with the same kinds of mineral phases (Table A).

SEM images from an iridium-coated, polished thin section of sample 741A are shown in Figure A. Evidence of biogenic textures and materials were non-existent. Globular features reminiscent of biogenicity were found but are believed to be abiogenic (images *c*, *d*, *e*). The globules are contained within vesicles and are primarily carbonaceous with an approximate size of 10μm. There is a possibility that these features could be associated with organisms inhabiting caliche or from the carbonate soil environment from which the sample was obtained, but this is only a speculation and would require further analysis. A fractured rock chip of sample 741A displayed some of the same globules examined in the thin section but evidence of biogenicity similar to that observed in samples 687 or 754 was not present.

Table A: Major element abundances (wt. %) and probable mineral phases for sample 741A

No.	Na_2O	SiO_2	SO_3	FeO	MgO	Al_2O_3	K_2O	MnO	P_2O_5	Cr_2O_3	CaO	TiO_2	Total	Mineral Phase
101	2.291	47.397	0.032	13.392	4.988	15.845	0.986	0.155	0.240	0.000	7.793	2.949	96.07	glass
102	1.950	47.700	0.012	13.230	4.887	16.123	1.093	0.209	0.324	0.009	7.965	2.964	96.47	glass
103	2.197	47.477	0.041	13.244	4.939	15.842	1.086	0.183	0.256	0.000	7.764	3.071	96.10	glass
104	2.443	47.253	0.027	12.993	4.943	15.714	1.037	0.182	0.298	0.009	8.384	2.991	96.27	glass
105	2.214	46.879	0.036	13.289	4.985	15.796	1.039	0.207	0.319	0.009	8.524	3.013	96.31	glass
106	2.386	47.325	0.045	12.901	5.032	15.806	1.044	0.174	0.342	0.000	8.149	3.094	96.30	glass
107	1.903	47.240	0.034	13.132	4.949	15.923	1.003	0.202	0.349	0.000	8.565	3.025	96.33	glass
108	1.981	47.284	0.022	13.094	4.828	15.744	1.026	0.181	0.317	0.002	8.334	2.866	95.68	glass
109	2.153	47.337	0.038	13.269	4.931	15.805	1.061	0.167	0.258	0.007	7.665	2.930	95.62	glass
110	2.031	47.263	0.023	13.462	4.942	15.664	1.005	0.205	0.298	0.013	7.830	3.039	95.78	glass
111	0.395	39.008	0.030	22.797	29.489	3.398	0.302	0.320	0.000	0.029	1.404	0.703	97.88	olivine
112	0.000	37.072	0.015	20.785	39.069	0.000	0.000	0.233	0.000	0.015	0.284	0.114	97.59	olivine
113	0.037	36.348	0.025	27.334	33.633	0.172	0.025	0.371	0.000	0.007	0.527	0.200	98.68	olivine
114	0.017	37.455	0.021	20.793	39.041	0.000	0.000	0.232	0.000	0.000	0.366	0.098	98.02	olivine
115	0.032	36.768	0.028	20.145	40.455	0.000	0.000	0.202	0.000	0.021	0.219	0.061	97.93	olivine
116	0.007	36.976	0.021	22.945	37.647	0.009	0.004	0.277	0.000	0.008	0.319	0.071	98.28	olivine
117	0.228	39.454	0.039	23.313	32.110	2.315	0.242	0.313	0.078	0.030	0.902	0.517	99.54	olivine
118	0.007	36.570	0.008	20.118	39.795	0.000	0.000	0.261	0.000	0.013	0.222	0.026	97.02	olivine
119	0.003	37.431	0.022	20.258	39.477	0.005	0.007	0.246	0.000	0.001	0.251	0.063	97.76	olivine
120	0.000	37.127	0.014	20.821	39.647	0.210	0.000	0.235	0.000	0.029	0.263	0.091	98.44	olivine
121	0.026	37.182	0.036	20.520	39.258	0.000	0.048	0.187	0.000	0.002	0.262	0.045	97.57	olivine
122	3.543	49.283	0.000	0.885	0.132	29.666	0.150	0.000	0.000	0.000	13.190	0.106	96.96	plagioclase
123	3.695	49.125	0.000	0.962	0.135	29.189	0.158	0.000	0.000	0.000	13.150	0.137	96.55	plagioclase
124	3.670	49.617	0.000	1.100	0.155	28.915	0.175	0.000	0.000	0.000	12.837	0.180	96.65	plagioclase
125	3.436	49.308	0.000	0.937	0.099	29.754	0.179	0.000	0.000	0.000	13.272	0.111	97.10	plagioclase
126	3.920	49.760	0.000	0.782	0.085	28.776	0.196	0.000	0.000	0.000	12.591	0.084	96.19	plagioclase
127	3.765	48.995	0.000	0.985	0.106	29.072	0.156	0.000	0.000	0.000	12.853	0.078	96.01	plagioclase
128	3.396	48.373	0.000	0.786	0.091	29.456	0.162	0.000	0.000	0.000	13.710	0.070	96.04	plagioclase
129	3.613	49.219	0.000	1.015	0.182	28.864	0.204	0.000	0.000	0.000	12.875	0.152	96.12	plagioclase
130	3.738	49.278	0.011	0.835	0.094	28.913	0.181	0.000	0.000	0.000	13.017	0.082	96.15	plagioclase
131	0.000	8.131	0.031	49.597	13.534	11.839	0.038	0.260	0.000	5.625	0.132	8.032	97.22	spinel series
132	0.000	32.134	0.000	25.637	33.782	1.162	0.000	0.210	0.000	0.933	0.227	1.847	95.93	olivine
133	0.106	5.753	0.000	26.858	17.697	30.917	0.000	0.176	0.000	16.454	0.218	1.123	99.30	spinel series
134	0.000	35.882	0.000	22.595	36.664	0.000	0.000	0.219	0.000	0.000	0.164	0.072	95.60	olivine/opx.
135	0.000	36.289	0.000	23.362	36.709	0.000	0.000	0.251	0.000	0.000	0.220	0.046	96.88	olivine/opx.
136	0.000	36.353	0.000	23.612	36.953	0.000	0.000	0.250	0.000	0.000	0.198	0.061	97.43	olivine/opx.
137	0.000	37.591	0.000	15.689	42.476	0.000	0.000	0.122	0.000	0.000	0.014	0.000	95.89	olivine/opx.
138	0.000	37.429	0.000	15.789	42.028	0.000	0.000	0.145	0.000	0.001	0.006	0.000	95.40	olivine/opx.
139	0.000	36.579	0.000	20.802	38.588	0.000	0.000	0.195	0.000	0.000	0.039	0.000	96.20	olivine/opx.
140	0.000	36.278	0.000	20.338	38.624	0.000	0.000	0.205	0.000	0.000	0.077	0.034	95.56	olivine/opx.
141	0.009	36.793	0.000	20.676	38.739	0.006	0.036	0.231	0.000	0.000	0.267	0.082	96.84	olivine/opx.
142	1.427	9.951	0.000	45.725	5.320	11.712	0.347	0.217	0.000	2.921	0.624	20.525	98.77	olivine/spinel
143	0.617	9.086	0.000	45.497	5.723	12.328	0.294	0.218	0.000	2.970	0.620	20.944	98.30	olivine/spinel
144	0.161	2.585	0.035	62.814	5.263	10.502	0.124	0.303	0.000	4.451	0.718	11.113	98.07	olivine/spinel
145	3.620	29.265	0.000	26.040	5.264	12.296	0.149	0.228	0.036	1.641	4.350	8.269	91.16	glass
146	0.091	0.916	0.034	75.007	2.676	2.576	0.161	0.193	0.000	2.721	0.455	5.754	90.58	spinel series
147	0.222	0.912	0.037	62.806	2.661	3.491	0.160	0.153	0.000	2.181	0.341	22.433	95.40	spinel series
148	0.025	7.449	0.000	7.075	0.020	6.507	0.023	0.248	0.000	0.000	14.428	0.047	35.82	?
149	0.031	37.141	0.000	10.907	0.027	24.526	0.033	0.371	0.105	0.000	23.002	0.259	96.40	garnet
150	0.020	37.004	0.000	10.741	0.048	24.559	0.017	0.366	0.064	0.000	22.806	0.241	95.87	garnet
151	0.066	95.117	0.000	0.003	0.000	0.000	0.000	0.017	0.000	0.000	0.085	0.000	95.29	quartz
152	0.001	93.732	0.000	0.000	0.000	0.000	0.000	0.000	0.000	0.000	0.100	0.000	93.83	quartz
153	0.000	26.805	0.000	0.010	0.000	0.000	0.000	0.000	0.000	0.000	0.042	0.000	26.86	?
154	0.085	30.189	0.009	0.835	10.122	2.577	0.062	0.001	0.000	0.000	15.662	0.097	59.64	garnet?
155	0.070	28.281	0.000	0.859	9.632	2.290	0.009	0.017	0.000	0.000	16.096	0.110	57.36	garnet?
156	0.054	36.740	0.000	14.156	0.091	21.421	0.003	0.161	0.000	0.037	23.235	0.025	95.92	garnet
157	0.738	38.715	0.221	18.239	9.886	8.049	0.005	0.279	0.191	0.043	12.292	3.634	92.29	glass
158	0.849	37.104	0.484	19.288	8.950	7.880	0.051	0.177	0.203	0.041	12.108	4.153	91.29	glass
159	0.916	38.340	0.295	18.099	10.651	8.436	0.011	0.190	0.210	0.057	9.873	4.131	91.21	glass
160	0.765	38.201	0.352	17.785	9.966	7.826	0.019	0.351	0.229	0.042	13.403	3.525	92.46	glass
161	0.829	37.124	0.442	19.978	9.123	8.052	0.074	0.136	0.244	0.004	11.640	4.389	92.04	glass
162	0.012	0.005	0.008	36.006	12.362	49.440	0.031	0.183	0.000	0.015	0.048	1.716	99.83	spinel group
163	0.028	0.012	0.008	36.227	12.335	49.352	0.030	0.168	0.000	0.000	0.039	1.754	99.95	spinel group
164	0.051	0.022	0.000	36.290	12.443	49.412	0.032	0.161	0.000	0.000	0.038	1.789	100.24	spinel group
165	0.014	0.005	0.000	35.695	12.725	49.737	0.025	0.155	0.000	0.007	0.027	1.645	100.04	spinel group
166	0.018	0.014	0.000	29.822	14.814	54.992	0.000	0.117	0.000	0.000	0.048	1.193	101.02	spinel group
167	0.043	0.071	0.018	30.321	14.856	54.946	0.007	0.109	0.000	0.000	0.022	1.170	101.56	spinel group
168	0.021	0.020	0.000	31.209	14.462	53.822	0.012	0.121	0.000	0.013	0.014	1.212	100.91	spinel group
169	0.011	0.000	0.000	29.973	14.895	53.367	0.035	0.121	0.000	0.000	0.040	1.037	99.48	spinel group
170	0.060	0.000	0.006	0.292	1.340	0.000	0.013	0.000	0.000	0.000	58.937	0.017	60.67	calcium carbonate
171	0.065	0.000	0.040	0.294	1.192	0.000	0.000	0.000	0.000	0.000	61.283	0.006	62.88	calcium carbonate
172	0.032	0.065	0.014	0.265	1.793	0.057	0.000	0.000	0.000	0.019	59.269	0.032	61.55	calcium carbonate
173	0.050	0.000	0.022	0.256	2.469	0.033	0.000	0.000	0.000	0.037	57.948	0.000	60.82	calcium carbonate
174	1.980	46.112	0.056	13.471	4.651	15.841	1.149	0.167	0.314	0.035	7.896	2.857	94.53	glass

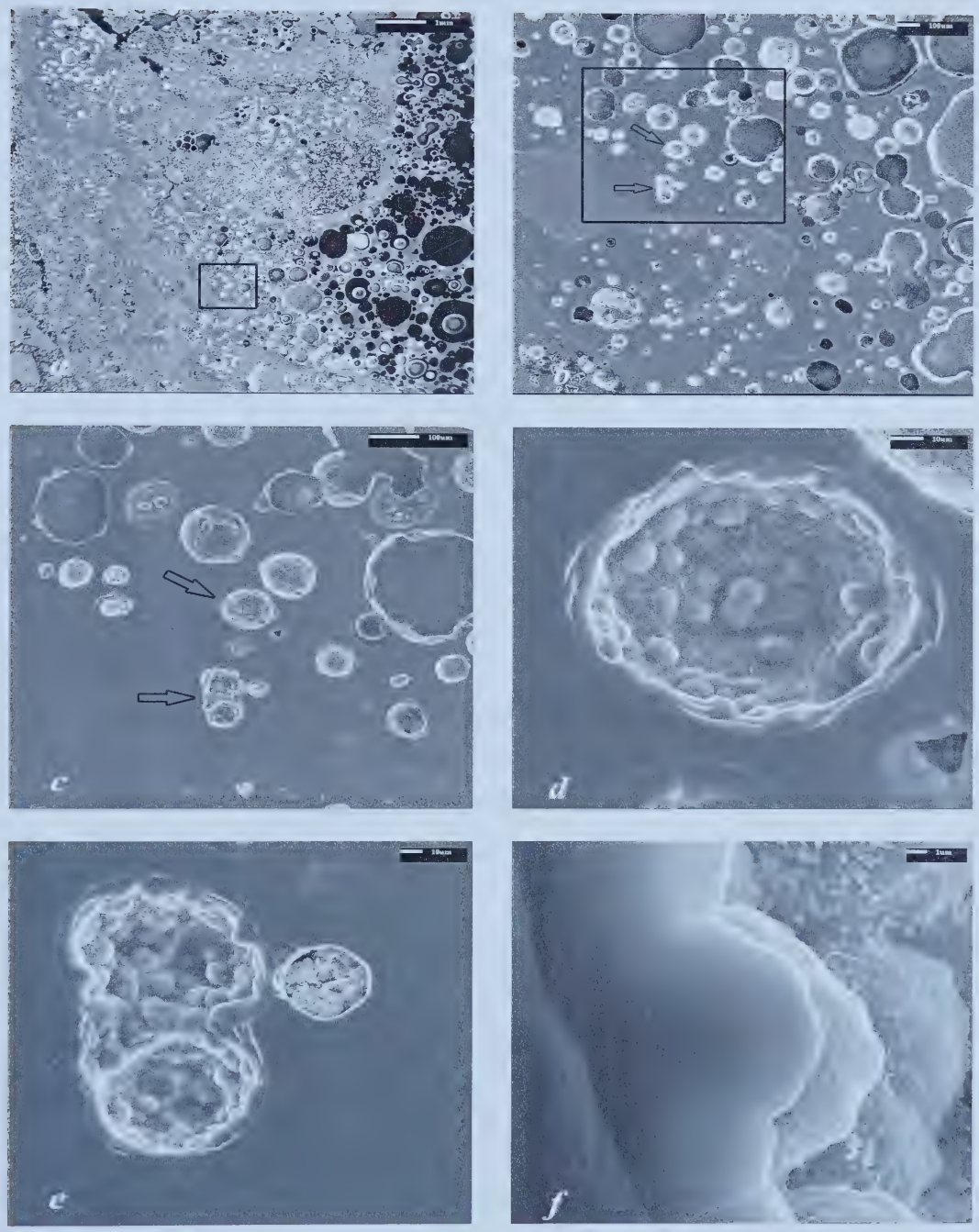

Figure A: SEM photomicrographs of globular features in sample 741A. The spherical globs are housed within vesicles and are not thought to be biogenic in nature. The outlined area and vesicles in images *a* and *b* are magnified and shown in images *c*, *d* and *e*. Image *f* is a cross-section of one of the globs. Scale bars are: 1mm (*a*); 100µm (*b*, *c*); 10µm (*d*, *e*); 1µm (*f*).

Appendix B

Carbon and oxygen isotope result for sample 754

The carbonates in a sample of subaerial 754 were analyzed for carbon and oxygen isotopic composition following the procedure of McCrea (1950). A section was cut from the interior of the main hand specimen and ground into a powder. Approximately 1g was dissolved in 100% phosphoric acid (H_3PO_4) in a warm water bath at approximately 25°C for 24 hours. The CO_2 was extracted under vacuum and immobilized using liquid nitrogen. Analysis of CO_2 was carried out on a Finnegan MAT 252 mass spectrometer. The isotopic data are reported in the usual delta notation with respect to PDB for carbon and SMOW for oxygen (Craig 1957, 1961). The analysis was performed in the stable isotope lab of Dr. Muehlenbachs.

Values of -4.64‰ and 16.90‰ were obtained for $\delta^{13}C$ and $\delta^{18}O$, respectively and are plotted on Figure B, which is copied from Knauth et al., (in review, 2002) and shows the results of caliche isotopic analysis of samples from the SFVF. Two end-members are seen: a subaerial and a pedogenic end-member. The values for basaltic sample 754 plot well outside the range of the other subaerial caliche samples however, this can be viewed as a mixing of CO_2 from atmospheric or inorganic sources and possibly, a biogenic source. The two most important carbon reservoirs on Earth are marine carbonates and biogenic organic matter. The former are isotopically heavy and have a mean $\delta^{13}C$ value of approximately 0‰, while the latter are isotopically light with a mean $\delta^{13}C$ value of about -25‰. Also, mantle carbon has a relatively constant $\delta^{13}C$ value between -5‰ and -7‰. Fractionation due to microbial activity results in a large range of $\delta^{13}C$ values, which can be indicators of both the type of microbe as well as the type of metabolic activity taking place.

Again, further isotopic analysis needs to be conducted and was prevented due to a lack of sample material and access to additional samples.

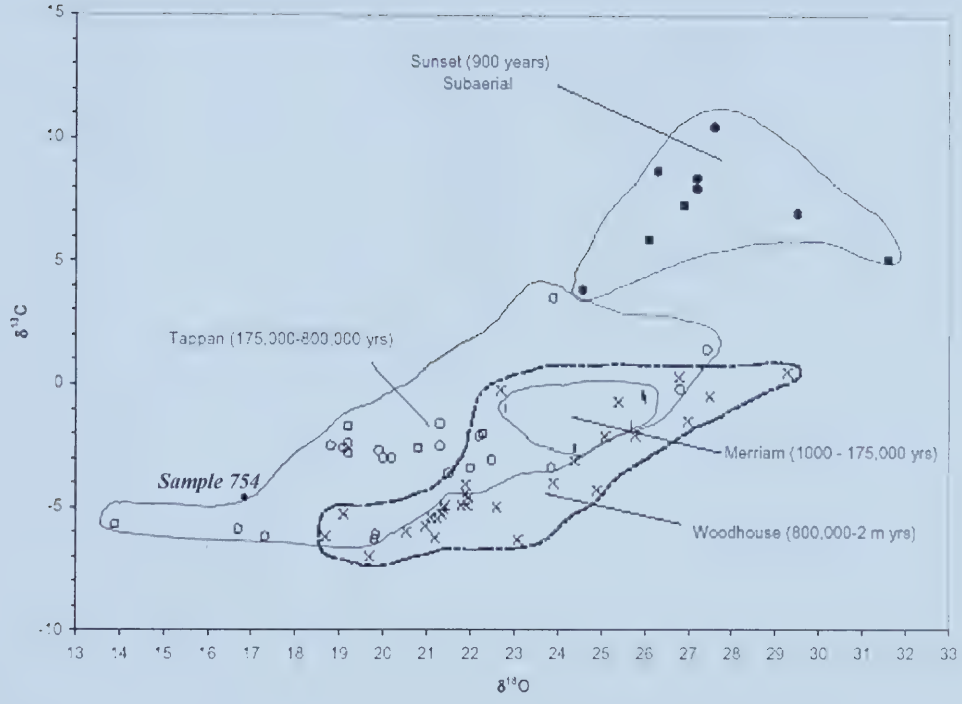

Figure B: Isotopic data for caliche samples from the San Francisco Volcanic Field. The data are from analysis carried out by Knauth et al. (in review, 2002). Subaerial sample 754 plots outside the range of other subaerial caliche samples; however, this might indicate mixing of inorganic and organic sources of CO_2.

University of Alberta Library
0 1620 1720 2191
B45561